Doctoral theses at NTNU, 2022:136

Mishiga Vallabhan K G

Produced water treatment using hydrocyclone

– Theoretical and experimental studies of novel control schemes

Doctoral thesis

NTNU
Norwegian University of Science and Technology
Thesis for the Degree of Philosophiae Doctor
Faculty of Engineering
Department of Mechanical and Industrial Engineering

NTNU
Norwegian University of Science and Technology

Mishiga Vallabhan K G

Produced water treatment using hydrocyclone

– Theoretical and experimental studies of novel control schemes

Thesis for the Degree of Philosophiae Doctor

Trondheim, May 2022

Norwegian University of Science and Technology
Faculty of Engineering
Department of Mechanical and Industrial Engineering

NTNU
Norwegian University of
Science and Technology

NTNU
Norwegian University of Science and Technology

Thesis for the Degree of Philosophiae Doctor

Faculty of Engineering
Department of Mechanical and Industrial Engineering

ISBN 978-82-326-6495-5 (printed ver.)
ISBN 978-82-326-6670-6 (electronic ver.)
ISSN 1503-8181 (printed ver.)
ISSN 2703-8084 (online ver.)

Doctoral theses at NTNU, 2022:136

Printed by NTNU Grafisk senter

To Dillu and Nadu

Preface

This thesis is submitted in partial fulfilment of the requirements for the degree of philosophiae doctor (Ph.D.) at the Norwegian University of Science and Technology (NTNU).

This thesis presents the results of my doctoral studies carried out at the Department of Mechanical and Industrial Engineering (MTP), NTNU, from November 2017 to July 2021. The research is part of Subsea Production and Processing (SUBPRO), a Center for Research-based Innovation (SFI) and is supported by the Research Council of Norway and several major international oil companies and subsea system suppliers. The research was carried out under the guidance of Assoc. Prof. Christian Holden, MTP, NTNU, as the principal supervisor, along with Prof. Sigurd Skogestad, Department of Chemical Engineering, NTNU and Prof. Olav Egeland MTP, NTNU, as co-supervisors.

Acknowledgements

First, I want to express my gratitude to my supervisor, Assoc. Prof. Christian Holden for choosing me as a PhD student and guiding me throughout my study. He believed in me and gave me the freedom to pursue my areas of interest. Christian's extensive knowledge in physics and mathematics (not limited to) motivated me to re-learn many of my concepts and push myself to set new standards. We had to cross many hurdles during the construction of the compact separation lab. However, Christian kept motivating me and reminding me about the light at the end of the tunnel. Thank you Christian!

I want to thank my co-supervisor Prof. Sigurd Skogestad for his valuable inputs and ideas throughout my research. He has always been kind enough to spend time reviewing my papers and many hours of discussions. Each discussion session with him gave me something new to think about and improve upon. His extensive knowledge in process control and his practical approaches in solving a problem has always inspired me.

I would like to thank Prof. Olav Egeland for giving me opportunity to conduct this research at MTP and supporting me for my PhD extension during the pandemic.

I would like to thank lab manager Øyvind Haave for his valuable technical support during the construction and commissioning of the pump system module and for providing a good and safe lab environment to work in. Furthermore, I would like to thank Kristian Linderud Sandmo, workshop engineer, for his help in constructing the test rig. He always tried to prioritize and finish the test rig activities whenever asked for, which helped in completing the test rig on time.

I would like to thank my SUBPRO colleagues Jose, Marcin, Torstein and Sveinung for their collaboration during my research.

I would like to thank my colleague and my office mate Savin for proofreading this thesis and for all the fruitful technical discussions during my PhD study.

I am also grateful to all my colleagues at the Robotics and Automation group at MTP for giving memorable moments of PhD life during lunch breaks, coffee breaks and for few parties that I could make it.

I appreciate the help and coordination received from Gro, Esma and Pål, SUBPRO coordinators, who always made me feel as a part of the SUBPRO family.

I want to thank my friend Jithin, who encouraged me to apply for PhD study. He also made sure that I was motivated throughout my research. All his messages were valuable

when I could not see any light ahead.

I'm deeply indebted to my Achan Gayathri Vallabhan and my Amma Lakshmi Kutty for their support and encouragement to pursue my dreams. Their love, prayers and blessings have been my strength in every step that I took in life. I also would like to thank my sister, Gashmi, for always being a good listener, adviser, and friend.

Finally, I would like to thank the two important persons in my life, Dilshaj, my husband and Nadav, my son. Their unconditional love, understanding, patience and support have been my driving force. There have been days where I felt it was impossible to continue, but Dillu always sat by my side, made me believe in myself and gave that extra push to sail my boat. Thank you, Dillu!. Nadav, you have shown an extreme level of maturity and sacrificed numerous evenings and weekends all these four years. My son, I will always be thankful to you for your understanding.

Summary

Produced-water is a non-lucrative by-product of oil and gas production, and the quantity increases as the field ages. Produced-water is either discharged into the sea or re-injected into the field to enhance pressure. As per the Norwegian Environment Agency, 126.4 million m^3 of produced water was discharged into the Norwegian sea in the year 2020. The discharge of produced water has to meet the OSPAR criteria, where the amount of dispersed oil is limited to 30 mg per litre of discharged water, on a monthly average. In addition, an efficient produced-water (PW) treatment system must meet environmental regulations before discharging the PW to the sea. De-oiling hydrocyclones, compact floatation units (CFUs), or their combination are commonly used for produced water treatment. Maintaining the efficiency of this compact equipment at varying process conditions is always a challenge.

This thesis focuses on de-oiling hydrocyclones, which are commonly used produced-water treatment equipment on the Norwegian Continental Shelf. The compact and light nature of these hydrocyclones, which do not require any additional chemicals or gases to be injected for the operation, makes them attractive for subsea processing.

The main problem with hydrocyclones is the low residence time, which makes them more susceptible to upstream variations such as changes in inlet oil concentration, changes in inflow rate and changes in droplet distribution. Typically, control schemes that use pressure drop ratio (PDR) to control the separation, are implemented to handle these disturbances. However, since this is an indirect way of controlling the hydrocyclones, this option can reduce their efficiency significantly and result in violations of the environmental regulations.

This thesis is divided into two parts; a theoretical analysis part and an experimental analysis part, both with the aim of improving the control aspects of de-oiling hydrocyclones.

In the theoretical analysis part, a control-oriented mathematical model of the hydrocyclones is developed. This model has a static pressure-to-flow relationship which can estimate the flow-rates and the pressures at the outlet of the hydrocyclones when the inlet conditions are known. The separation inside the hydrocyclone is approximated using a polynomial derived from droplet trajectory analysis. A simple mass-balance model is formulated to capture the dynamics, and is used for the control. This model was used

for studying new control schemes for de-oiling hydrocyclones.

In the experimental analysis part of this thesis, a test rig is constructed, with industrial-scale hydrocyclone liners and other auxiliary systems, to support the testing of the novel controllers. The test rig can emulate the first stage gravity separator and generate different disturbances at the inlet of the hydrocyclones installed in the rig. Drawbacks of traditional PDR control schemes were studied at the test rig. Then, new control schemes such as cascade, feed-forward, and direct control schemes were verified at the test rig.

The research carried out during the course of the doctoral studies has been presented as a series of articles in various conferences and journals. These are now grouped together to constitute the body of this thesis.

The second chapter gives the background theory of hydrocyclones and a brief review of the mathematical models of hydrocyclones, their control strategies, constructional details, and features of various experimental test-rigs of hydrocyclones available in the literature. The subsequent chapters cover the theoretical and experimental analysis performed.

Contents

List of figures

Chapter 1

Introduction

Ever-expanding energy needs are demanding more and more oil and gas production. The burning of these fossil fuels, without a doubt, is causing severe environmental damage. Also alarming is the offshore production process of oil and gas, causing severe impact to the ocean environment. Figure 1.1 shows the different sources of pollution from offshore oil and gas production facilities. One of the primary sources of oil pollution during the production is *produced-water*- the water by-product produced by an oil or gas well [11]. Produced-water includes naturally occurring water in the hydrocarbon deposits, and the water which is injected into the reservoir to enhance production. The amount of produced-water increases as the oil fields matures. The daily output of produced-water from all oil and gas fields across the world is $\approx$ 250 million barrels ($\approx$ 39 million m^3), and more than 40 % of it is discharged into the environment [24]. Figure 1.2 shows the historical data and projections of discharge of produced-water on the Norwegian continental-shelf from 1984–2024 [1].

Region-wise regulations are placed by different governmental organisations to reduce the environmental impact caused due to discharge of produced water into the sea. For example, the Norwegian continental shelf (NCS) comes under the regulation of OSPAR and according to the OSPAR criteria, 'produced-water shall contain a maximum of 30 mg of dispersed oil per liter of water discharged, as a weighted monthly average [29].' Thus, the treatment of produced water and regular quality checks of the treatment process is necessary to protect the environment.

An overview of a typical water treatment process in the oil and gas industry, based on the type and the size of contaminating particles is given in [8]. Here, the treatment is divided into three main stages. The first is pre-treatment, where the bulk of oil, gas and coarse particles are removed using dehydration vessels, storage tanks, strainers, de-sanders, etc. This is followed by the primary stage of the main treatment, where tiny droplets and particles are removed using skim tanks and API separators. In the secondary stage, smaller droplets are removed using de-oiling hydrocyclones, compact flotation

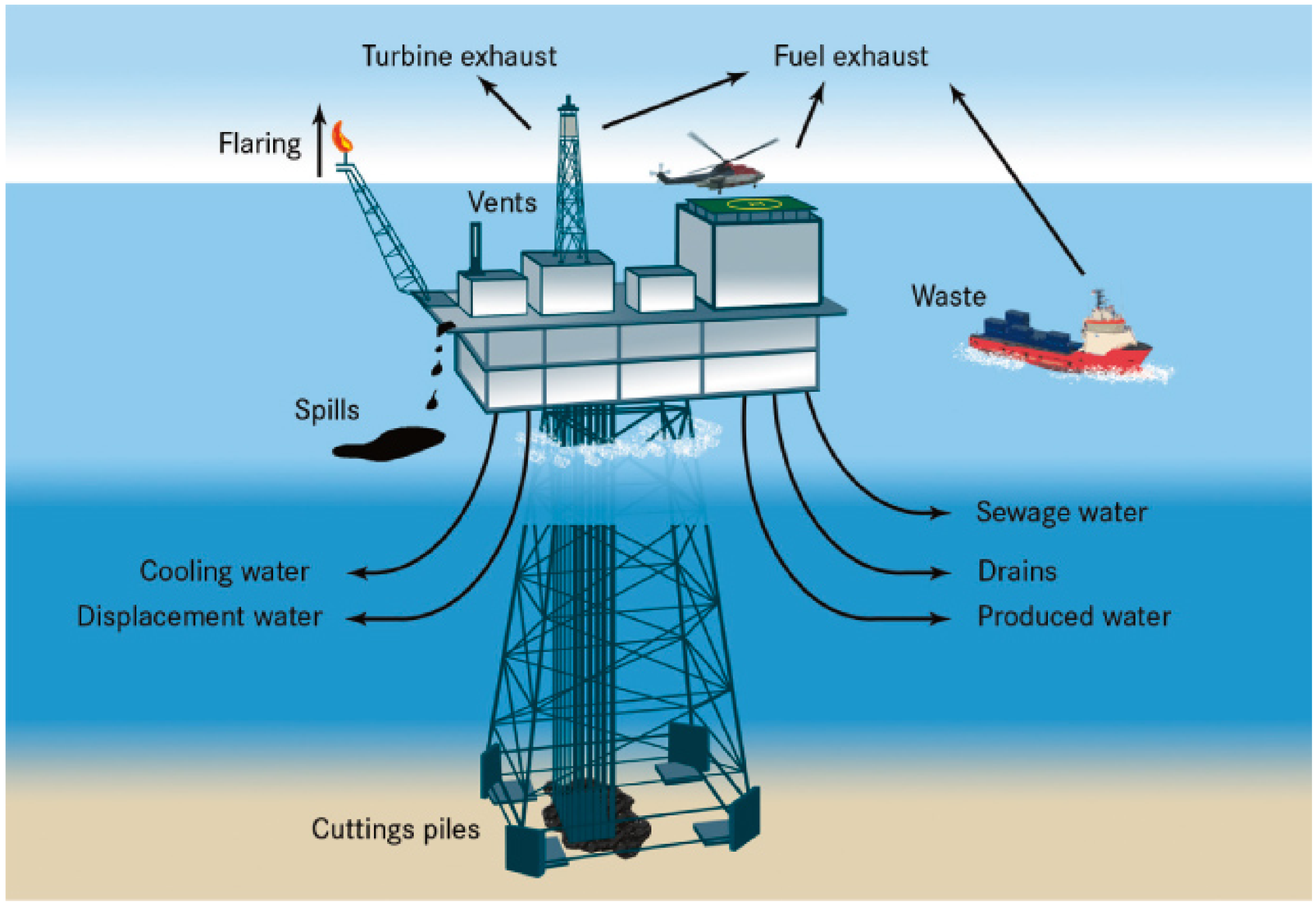

Figure 1.1: Sources of pollution [11].

units, centrifuges, etc. After the secondary stage, dispersed oil content in the produced water goes below the regulation specified by authorities such as OSPAR (30 mg/l). Further polishing can bring the oil concentration levels below 10 mg/l using dual media filters and membranes.

The processing of offshore oil-and-gas can be broadly classified into three categories based on the processing location. The first and most common processing is 'offshore' using fixed platforms, or floaters [10]. The second one is where a tie-back is provided from the seabed to an onshore processing facility [6]. The third and the most recent advancement in the oil and gas industry is 'subsea processing'. Equinor calls these processing facilities 'subsea factories' or 'invisible platforms' [2]. Figure 1.3 shows a pictorial representation of a subsea factory, as envisioned by Equinor. The Marlim field in Brazil is an example of a subsea processing installation at 800 m water depth [28].

The size and type of process equipment depends on the location of processing. An onshore processing plant has the liberty of space and can hence have bigger processing equipment. For offshore processing, equipment size needs to be reduced to fit inside a confined space such as a platform or FPSO. For subsea processing, as shown in Figure 1.3, the equipment needs to be even more compact.

The main task of oil and gas processing facilities is to separate the monetary components, oil and gas, from the remaining fluids, and clean the by-products such as produced water and dispose of/re-use them in adherence with governmental regulations. A typ-

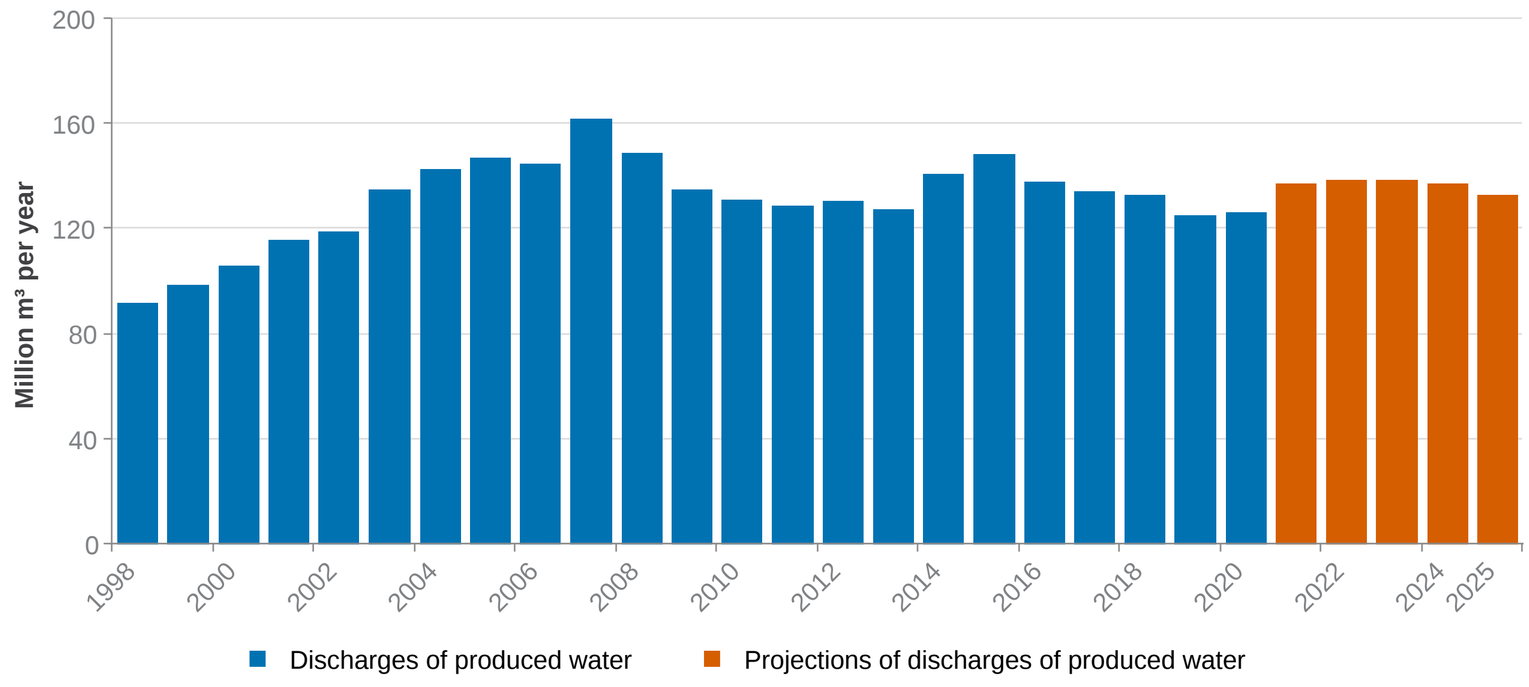

Figure 1.2: Historical data and projection of amount of discharged produced water at the Norwegian continental shelf [1].

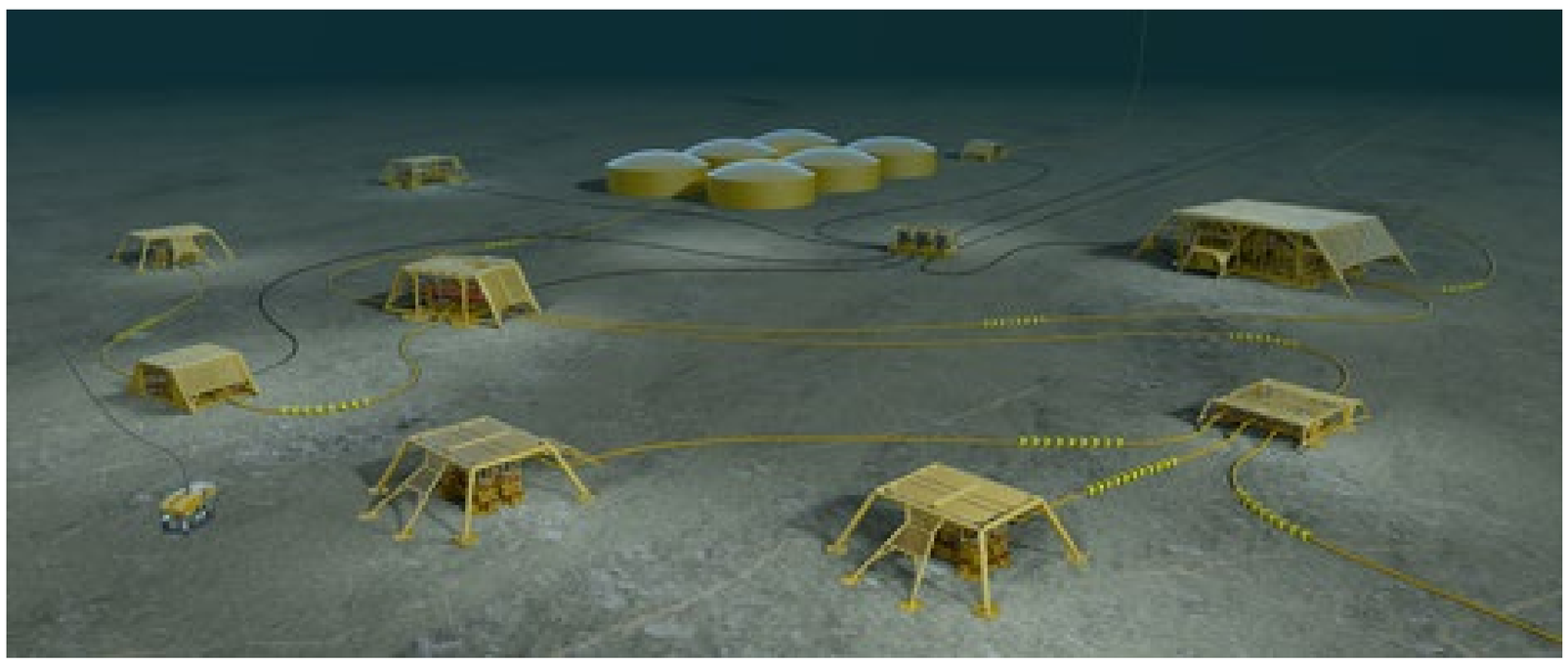

Figure 1.3: Pictorial representation of 'Subsea factory' or 'Invisible Platforms' as envisioned by Equinor.

ical process flow for oil and gas processing in an offshore/onshore facility is shown in Figure 1.4. The fluid from the reservoir comprises of oil, gas and water (and also other solid substances). The reservoir fluid enters the first stage bulk separators (can be more than one), such as gravity separators, which separates out most the oil and gas. The oily water from the first stage is then sent to the produced-water treatment process. Equipment such as de-oiling hydrocyclones or compact flotation units (CFUs) are used for produced-water treatment. Later, the cleaned water can be discharged into the sea if it meets the environmental regulations or re-injected into the reservoir.

Processing at seabed requires more compact separation equipment. Here, bulky gravity separators are replaced with compact pipe separators [28, 32]. The compact nature

of de-oiling hydrocyclones, with no moving parts, make them a good choice for subsea produced-water treatment. A typical process flow of subsea oil and gas processing is shown in Figure 1.5.

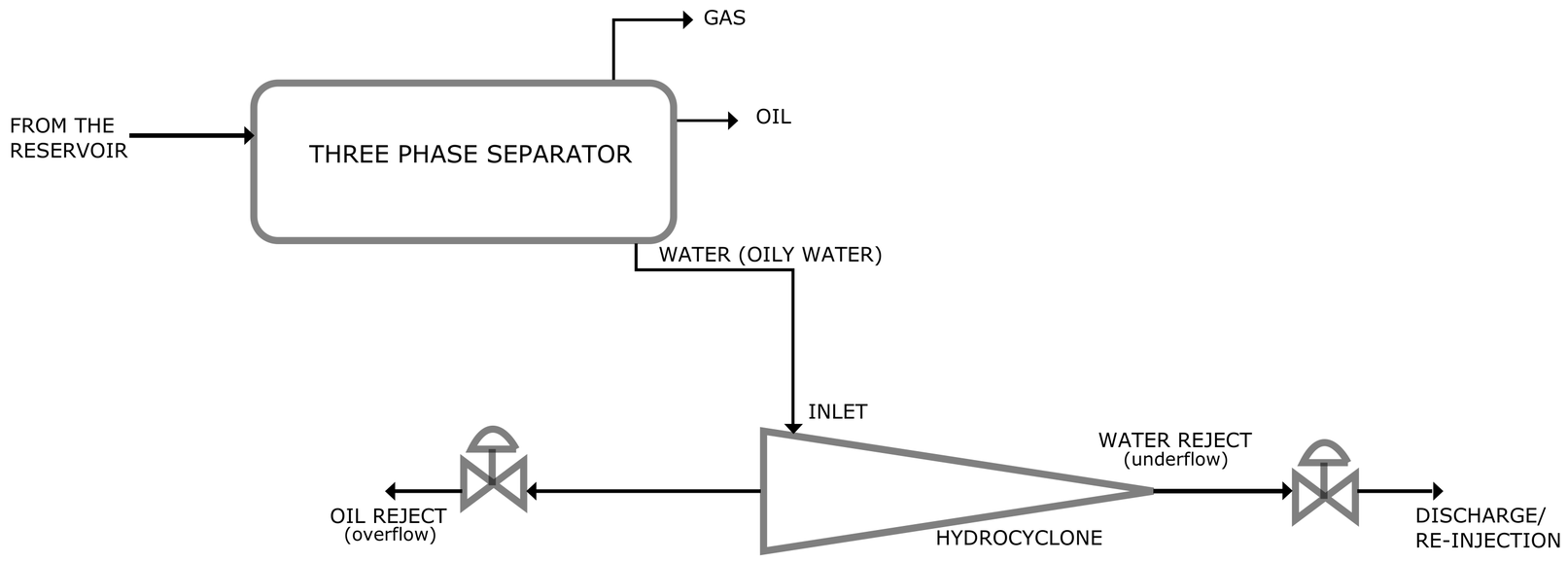

Figure 1.4: Typical topside separation process with a three-phase gravity separator as a first stage separator and de-oiling-hydrocyclones for produced-water treatment.

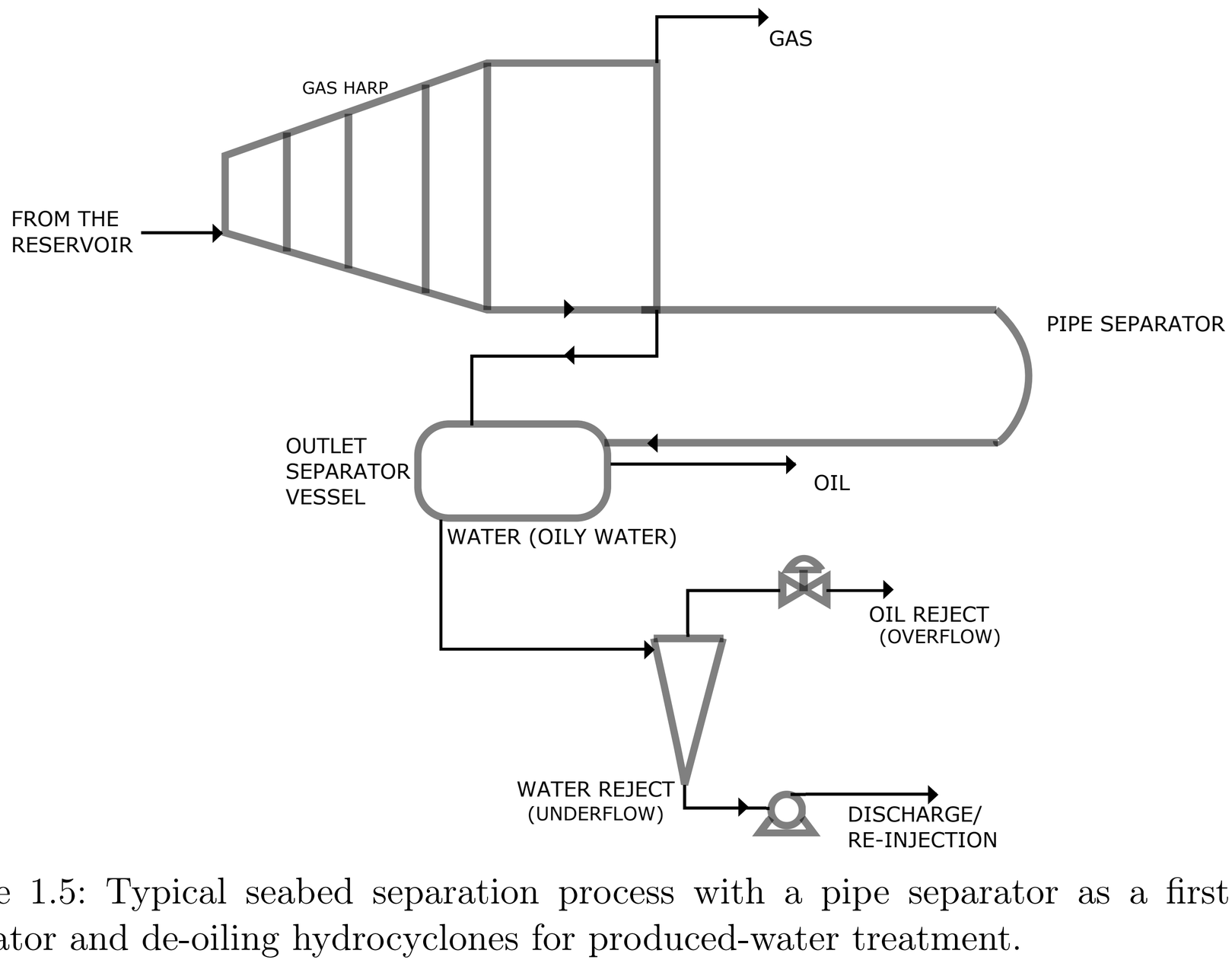

Figure 1.5: Typical seabed separation process with a pipe separator as a first stage separator and de-oiling hydrocyclones for produced-water treatment.

1.1 Motivation

This PhD project is part of the SUBPRO research program that started in the third quarter of 2015. This program's primary focus is to accelerate subsea oil and gas industry innovations in order to increase production with cost-effective and environmental friendly solutions. This project also addresses the present challenges faced in the oil and gas industry, and is performed in close collaboration with the industry partners.

One such problem suggested by the industrial partners was regarding the challenges in maintaining the efficiency of de-oiling hydrocyclones in the produced-water treatment system. Since about 90 % of the Norwegian continental shelf (NCS) process facilities use de-oiling hydrocyclones for produced-water treatment (PWT) [23], maintaining the efficiency of the PWT is critical in reducing the environmental impact caused due to discharge of PW into the sea. A primary objective of this PhD work is to understand the challenges in maintaining efficiency of the de-oiling of hydrocyclones and then, to propose solutions to mitigate or reduce these challenges, thereby contributing to a more significant cause of environmental safety.

The compact nature and low residence times make the control of de-oiling hydrocyclones challenging. The traditional control scheme of hydrocyclones uses an indirect pressure drop ratio (PDR) method to control the separation of hydrocyclones. The PDR control scheme can handle upstream disturbances in the total inflow rate [23, 25]. However, changes in inlet oil concentration and droplet distribution cannot be detected by the PDR control scheme, which reduces the separation efficiency of the hydrocyclones during such scenarios. The changes in inlet oil concentration and droplet distribution may not be drastic in the case of bulk first stage separators at offshore/onshore processing facilities. However, in seabed processing, the first stage separation is more compact with small buffer tanks which can cause more frequent changes in oil concentration and droplet distribution at the inlet of the hydrocyclones. Hence, the need for control algorithms capable of handling these disturbances motivated us to focus the research on developing new control schemes for de-oiling hydrocyclones.

To design and analyse new control algorithms, we need to have models describing the input-output relationship of the system. Many mathematical models are available for de-oiling hydrocyclones where inflow rate, inlet oil concentration, and droplet distribution are the inputs and the output is the separation efficiency. [13, 14, 35] developed different mathematical models to predict the efficiency based on the droplet trajectory analysis of fluids inside a hydrocyclone. [16] presented a control-oriented model for de-oiling hydrocyclones with a swirl element.

In this thesis, we are analysing de-oiling hydrocyclones without a swirl element and this necessitates the development of a control-oriented model to develop new control algorithms. Chapter 3 describes the control-oriented model that we developed in this project work. It is also based on droplet trajectory analysis, but with an additional mass-balance formulation of oil fraction and water fraction at the inlet and the two

outlets of the hydrocyclone, respectively.

Measuring or estimating the oil concentration at the water reject outlet (Figure 1.4) can make the control system design more robust to changes in inlet oil concentration or the droplet distribution. Estimating the oil concentration at the water reject is possible using the developed control-oriented model. Also, the latest advances in sensor technologies have enabled the online measurement of oil-in-water [26, 30]. The online oil-in-water analysers give a direct measure of the separation efficiency of hydrocyclones.

The motivation for building a new experimental test rig was to analyse the effectiveness of an online oil-in-water analyser for controlling the hydrocyclones and testing the new control schemes. The new experimental test rig is equipped with instruments for measuring pressure, flow, and temperature parameters. We have installed online oil-in-water analysers with a stabilising time of 1 s, which can be included in control schemes. Pumps and control valves are connected to the control system which enables autonomous operation. The test rig can emulate the first stage gravity separators and give the correct input to the hydrocyclones. Changes in inflow rate, oil concentration, and oil droplet distribution are the disturbances generated by the test setup.

1.2 The arrangement of this thesis

The remainder of this work is arranged as follows:

Chapter 2 describes the separation theory of hydrocyclones and the different factors that contribute to the separation efficiency of hydrocyclones. It also describes the operational and control philosophy of hydrocyclones followed in the industry. This is followed by a brief literature review pertaining to control and experimental test rigs of hydrocyclones.

Chapter 3 presents articles describing a control-oriented model for de-oiling hydrocyclones. A simple PI controller is used to verify the model and its control properties.

Chapter 4 presents articles describing control schemes and their simulation study. This chapter discusses two simple control schemes: a cascade and a feed-forward controller, and three model-based control schemes: feedback linearization, sliding mode control, and model predictive control.

Chapter 5 presents an article dealing with the construction of the new experimental test setup. It also describes the procedure to generate different disturbances at the inlet of the hydrocyclones, which ensure proper testing and validation of new control schemes.

Chapter 6 presents articles describing the implementation of the three control schemes: a cascade, a feed-forward and a direct feedback at the test rig

Chapter 7 concludes the work done in this thesis and presents some ideas for optimal control of hydrocyclones in the future.

Appendix A presents the details of the experimental setup used in this thesis along with test setup photographs.

Appendix B presents preliminary data collected from the laboratory for calculating the internal separation of hydrocyclones.

Appendix C presents a generic introduction to process control and automation in practical implementation perspective.

1.3 Publications

- Vallabhan K.G. M., Holden, C., and Skogestad, S. (2020). *A First-Principles Approach for Control-Oriented Modeling of De-oiling Hydrocyclones*. Industrial & Engineering Chemistry Research, 59(42), 18937-18950. https://doi.org/10.1021/acs.iecr.0c02859
- Vallabhan K.G. M., Holden, C. *Non-linear control algorithms for de-oiling hydrocyclones*, 2020 28th Mediterranean Conference on Control and Automation (MED), 2020, pp. 85-90.
- Vallabhan K.G. M, Matias, J., and Holden, C. (2021) *Feedforward, cascade and model predictive control algorithms for de-oiling hydrocyclones: Simulation study.* Modeling, Identification and Control, 42(4) pp. 185-195, . https://www.mic-journal.no/ABS/MIC-2021-4-4.asp/
- Vallabhan K. G., Mishiga, Dudek, Marcin, and Holden, Christian. *Experimental Test Setup for Deoiling Hydrocyclones Using Conventional Pressure Drop Ratio Control.* SPE Prod & Oper (2022;): https://doi.org/10.2118/208608-PA.
- VVallabhan K G, Mishiga, Holden, Christian, and Skogestad, Sigurd. *Deoiling Hydrocyclones: An Experimental Study of Novel Control Schemes.* SPE Prod & Oper (2022): https://doi.org/10.2118/209576-PA.

1.4 Contributions

- A control-oriented mathematical model based on first principles was developed for de-oiling hydrocyclones. This model can be used for studying the control properties of hydrocyclones and for developing robust control algorithms to handle different disturbances from upstream systems. The article describing this model is given in Chapter 3.
- The drawbacks of traditional PDR control schemes were analysed theoretically using the model and this is given in Section 4.1. Experimental results to show the drawbacks of traditional PDR control is given in Section 5.1.

- New controllers were developed to mitigate the drawbacks of the traditional PDR controller. Theoretical study of new controllers are given in Chapter 4.
- Three controllers: Cascade, Feedforward and Direct control schemes were validated using experiments. The results of this validation are given in Chapter 6.
- A Pump and tank system module capable of emulating the first stage gravity separator was constructed and commissioned during this PhD study. This test setup can be used as an input system to any produced water treatment equipment. Details of the experimental setup is given in Chapter 5 and in Appendix A.3.

Chapter 2

Background theory

In the year 1968, the need for compact separating devices for the offshore oil and gas industry triggered research in the use of hydrocyclones for liquid-liquid separation; in 1978, the patent for the first liquid-liquid hydrocyclone was filed [33]. Commercial testing of hydrocyclones first happened in 1975 at the Murshim platform [25]. At present, more than 90 % of the NCS uses de-oiling hydrocyclones for produced-water treatment [19].

2.1 Hydrocyclones

A hydrocyclone, or to be more precise a 'hydrocyclone liner', is a passive device with no moving parts. It has one (can be two as well) tangential inlet and two outlets, as shown in Figure 2.1. A hydrocyclone liner has four sections: first, a cylindrical part where the liquid enters; second, a tapered conical section where the fluid is accelerated due to the reduction in the diameter; third, a longer tapered conical section where the majority of the separation occurs, and fourth, a parallel tail section where slower-moving droplets can be recovered.

High-pressure oily water entering the tangential inlet generates a swirling flow pattern inside the hydrocyclone liner. The swirling motion of the fluid generates centrifugal force, which flings out the heavier water particles towards the hydrocyclone walls while the lighter oil particles move towards the center of the cyclone.

The clean water comes out at the water reject (underflow) outlet and the oil-rich stream comes out at the oil reject (overflow) outlet. There exists a reverse flow zone inside the hydrocyclone; upon entering, the oil droplets, reverse their flow direction and comes out through the oil reject outlet thus getting separated (shown in Figure 2.1). Some water will also be present in the reverse flow zone and leave the liner with the overflow. The geometrical structure of a liner comprises of a cylindrical section, followed by two conical sections of reduced diameters and another cylindrical section much longer than rest of the three sections.

According to the pattern revealed by the laser Doppler anemometry in [34], the reverse flow zone extends near the end of the last cylindrical section of the liner. However, maintaining sufficient opening of the oil reject valve prevents the separated oil from coming out through the water reject. The reverse-flow zone is assumed to have the same shape of the hydrocyclone, but with a reduced radius [35].

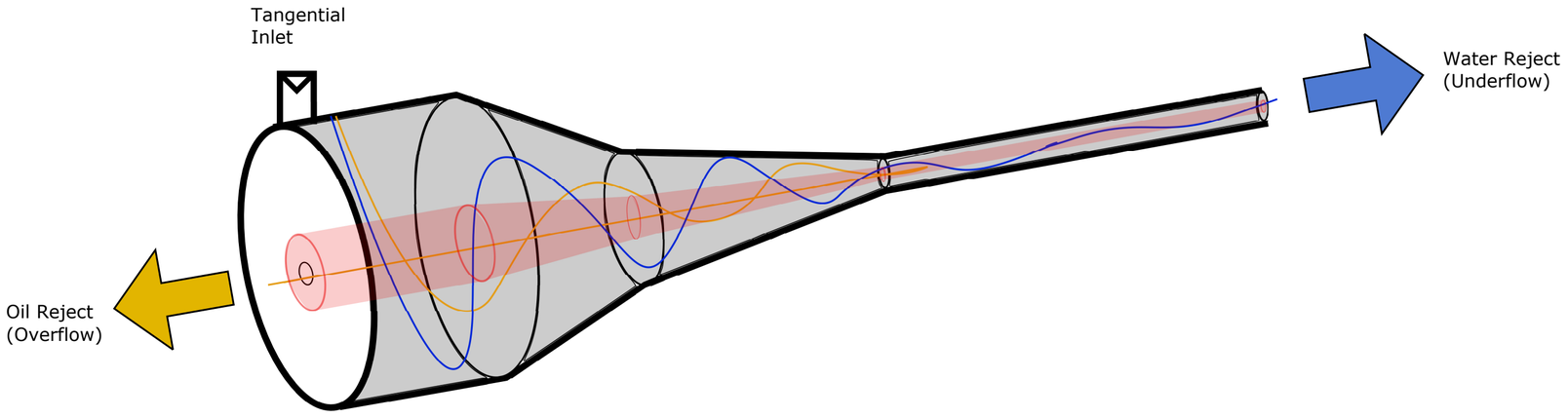

Figure 2.1: Diagrammatic representation of a hydrocyclone liner. Note that radius is greatly exaggerated. Example oil trajectory is yellow, example water trajectory is blue, forward flow zone is gray and reverse-flow zone is red.

The flow inside a hydrocyclone can be described using three velocity components: tangential, axial, and radial. The continuous phase (water) and the dispersed phase (oil) is assumed to have the same velocity profile for axial and tangential components. On the other hand, radial velocity for the dispersed phase has an additional factor due to the drag force experienced by the oil droplets, due to the density difference between the phases. Therefore, the separation inside the hydrocyclone liners can be analysed based on these velocity components.

2.1.1 Tangential velocity

The tangential velocity of hydrocyclone follows a Rankine vortex type behaviour. The velocity near the walls behaves as a free vortex, and velocity towards the centre has a forced vortex behaviour. A simple diagrammatic representation of the free and forced vortex in Rankine vortex is shown in Figure 2.2. Here $v_{\theta 1}$ represents the tangential velocity at the free vortex region and $v_{\theta 2}$ represents the tangential velocity at the free vortex region.

We can define some basic terms for better understanding of the Rankine vortex type behaviour:

- The angular velocity can be expressed in terms of tangential velocity v_θ as

$$\omega = \frac{v_\theta}{r} \ . \tag{2.1}$$

- The moment of inertia I with respect to specific axis of rotation is defined as

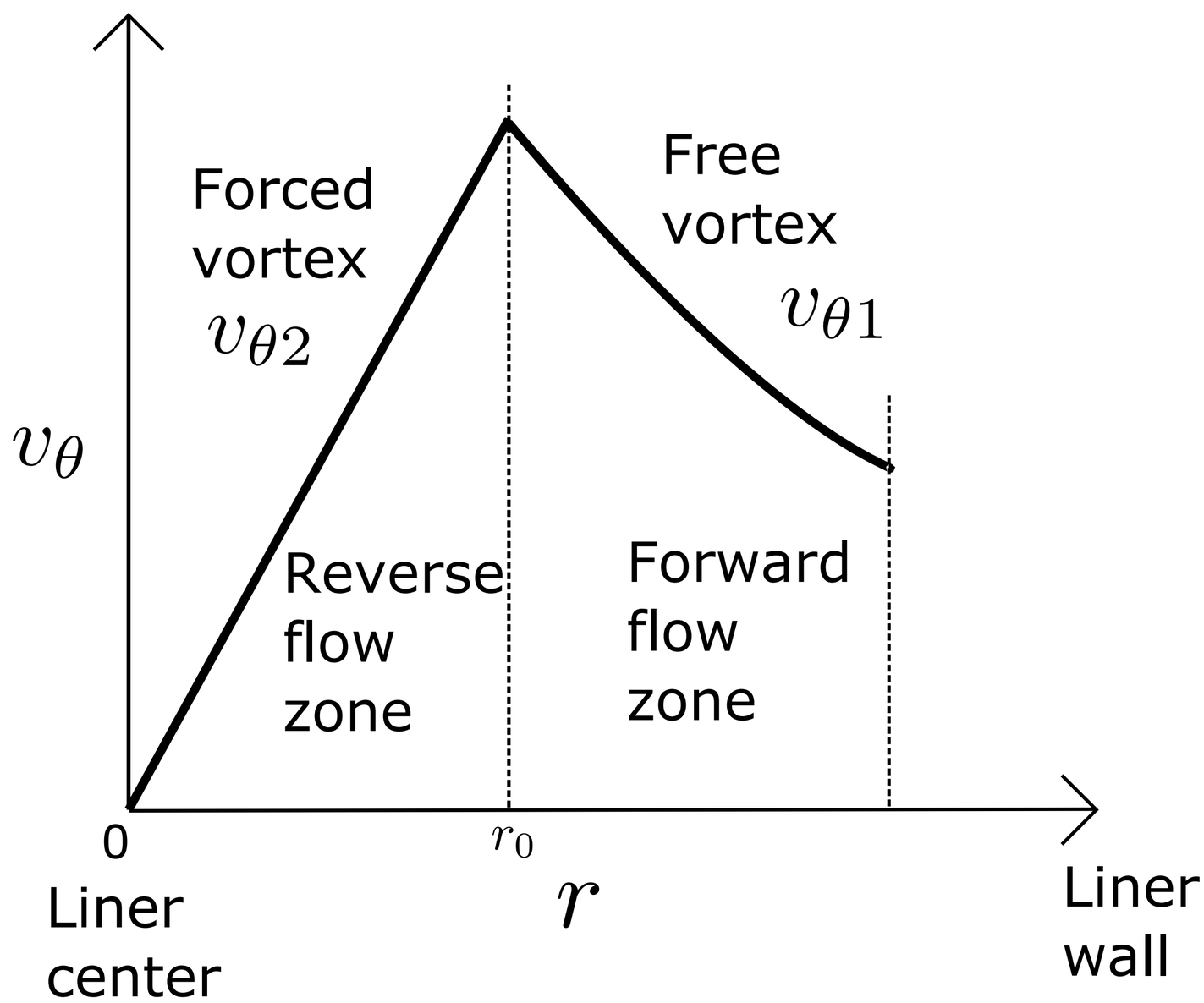

Figure 2.2: Rankine vortex type profile for tangential velocity.

$$I = mr^2 \ , \tag{2.2}$$

where m is the mass and the r is the radial distance of the mass m from the axis of rotation.

- Angular momentum of a rotating object is defined as the product of the moment of inertia I and the angular velocity ω given as

$$L = I\omega = mrv_\theta \ . \tag{2.3}$$

- Then, conservation of angular momentum states that when there is no external torque acting on the system, the angular momentum of the system remains constant.

The conservation of angular momentum applies to the fluid in the free vortex region. We can calculate the velocity of the fluid at any radial position when the initial angular momentum is known. At the inlet of the hydrocyclone, the tangential velocity near the wall will be equal to the inlet velocity [35]. Then, based on the inlet velocity and initial radial position of the fluid, we can calculate the angular momentum as

$$I = \alpha_1 V_{in} R_1 \ . \tag{2.4}$$

Here, α_1 is an empirical factor added to compensate for the lack of perfection at the tangential inlet. As the angular momentum is conserved, we can find the tangential velocity at any radial position r in the free vortex region as

$$\alpha_1 V_{in} R_1 = v_{\theta 1} r = I \ . \tag{2.5}$$

In the forced vortex region the fluid rotates as a solid body with a constant angular velocity,

$$\frac{v_{\theta 2}}{r} = Constant \ . \tag{2.6}$$

Combining the above with (2.1), gives $Constant = \omega$ and ω remains constant in the forced vortex region, so the tangential velocity decreases as the radial position decreases.

Furthermore, the tangential velocity component of the continuous phase $v_{\theta,w}$ and the dispersed oil phase $v_{\theta,o}$ in the free vortex region are assumed to be same. Thus we have

$$v_{\theta 1} = v_{\theta,w} = v_{\theta,o} \ . \tag{2.7}$$

2.1.2 Axial velocity

The axial velocity profile inside the hydrocyclones has two parts: the forward flowing region and the reverse flowing region. A reverse-flow zone exists inside the hydrocyclone, reaching which, the axial flow of the fluid reverses its direction. The radial position at which the axial velocity becomes zero is called a locus of zero axial velocity. The forward flowing region is a part of the free vortex, and the reverse flowing region is a part of the forced vortex region. Figure 2.3 shows a rough sketch of the axial velocity based on the laser Doppler anemometry image shown in [34]. The locus of zero axial velocity, the forward flow region and the reverse flow region are marked in Figure 2.3. In Chapter 3, we calculate the average axial velocity profile of the forward flowing region (marked with pink in Figure 2.3) using the two-dimensional pipe-flow model, where we fix the locus of the zero axial velocity as an empirical constant. The continuity of the axial flow needs to be maintained when droplets moves from one section of the liner to another. This is done by initialising the present section with the last value of the previous section. Equations (11)—(15) in Chapter 3 models the axial flow maintaining continuity between different sections of the liner.

Bram et al. [13], Caldentey et al. [14], Wolbert et al. [35] considered an axial profile as shown in green in Figure 2.3 for their analysis. This profile is mainly valid for the second conical section of a cyclone liner. Wolbert et al. [35] modelled this profile using a polynomial approximation, and the locus of zero axial velocity in this model was fixed based on the experimental data. Caldentey et al. [14] calculated the polynomial constants dynamically, based on boundary conditions such as zero axial velocity near the walls, zero axial velocity at boundaries of the reverse-flow zone, symmetrical axis flow and the

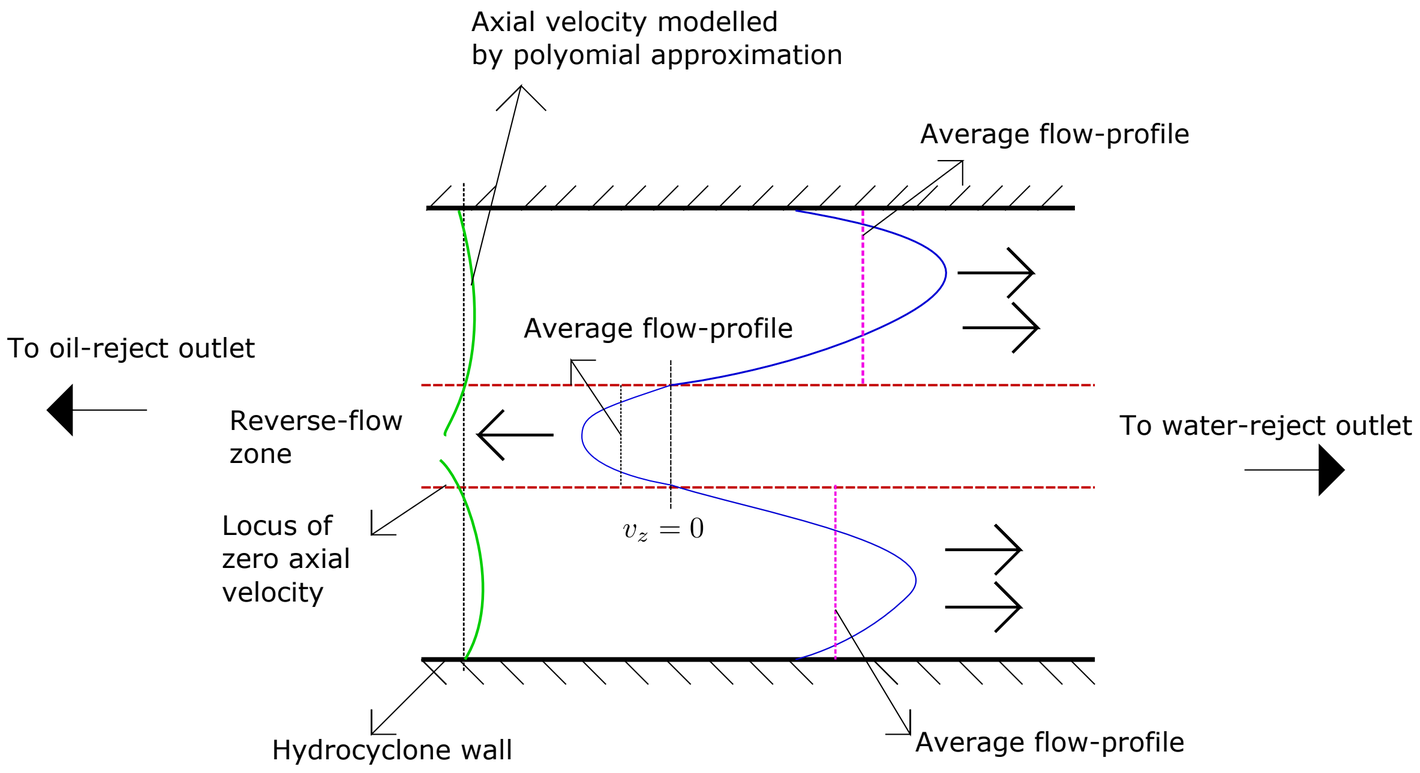

Figure 2.3: Axial velocity profile of flow inside a hydrocyclone.

conservation mass (ignoring the reverse flow). Using these boundary conditions, an axial velocity profile depending on the swirl number S[1] was derived.

Bram et al. [13] modified the polynomial approximation of Caldentey et al. [14], by including an additional boundary condition of reverse flow direction, and updated the polynomial constants. The polynomial approximation model for the axial velocity as given in [13, 14, 35] , with $\hat{r} = \frac{r}{R(z)}$:

$$v_z = V_o(z)(a_o + a_1\hat{r} + a_2\hat{r}^2 + a_3\hat{r}^3) \ . \tag{2.8}$$

$$V_o(z) = \frac{Q_{in}}{\pi R^2(z)}. \tag{2.9}$$

Similar to the tangential velocity, the axial velocity of the continuous phase $v_{z,w}$ and the dispersed phase $v_{z,o}$ are assumed to be the same, and we have

$$v_z = v_{z,w} = v_{z,o} \ . \tag{2.10}$$

2.1.3 Radial velocity

The radial velocity of the hydrocyclone aids the oil droplets in moving towards the center of the cyclone and get separated from continuous phase. The radial velocity of the continuous phase ($v_{r,w}$) needs to satisfy the continuity equation ($\frac{\partial v_z}{\partial z} + \frac{\partial v_r}{\partial r} + \frac{v_r}{r} = 0$). Hence, $v_{r,w}$ will vary with the axial velocity v_z.

[1] Swirl number $S = \frac{\int_0^R r^2 \rho v_r v_z \, dr}{R \int_0^R r^2 \rho v_z \, dr}$ where R is the radius of the pipe [15].

The radial velocity of the dispersed phase ($v_{r,o}$) has an extra component (v_{tr}), called the terminal/settling velocity, due to the drag force and the density difference,

$$v_{r,o} = v_{r,w} + v_{tr} \ . \tag{2.11}$$

Due to the swirling motion inside the cyclone, the oil droplets experience a force F_a caused by the centripetal acceleration, which is much higher in magnitude than gravity, [25], pulling the droplets towards the reverse-flow oil core. Another counteracting frictional force that acts on the droplet is the drag F_d between water and the oil droplets. The frictional force can be expressed in terms of Stokes' drag [35] or quadratic drag [14]. In this thesis we use a quadratic drag for our analysis. The buoyancy force F_b is equivalent to the centripetal force, but in the opposite direction. Figure 2.4 shows the different forces acting on the droplet.

The force due to centripetal acceleration is

$$F_a = m\frac{v_\theta^2}{r} = \frac{\pi}{6}D^3\rho_o\frac{v_\theta^2}{r} \ . \tag{2.12}$$

The force due to quadratic drag is expressed as

$$F_d = \frac{1}{2}C_D\rho_o\pi r^2 v_{tr}^2 \ . \tag{2.13}$$

The force due to buoyancy (displaced weight) is

$$F_b = \frac{\pi}{6}D^3\rho_w\frac{v_\theta^2}{r} \ . \tag{2.14}$$

Here, D is the diameter of the oil droplet, ρ_o and ρ_w are the densities of oil and water, respectively, r is the radial distance of the droplet from the axis of rotation, C_D is the drag coefficient and, v_{tr} is the terminal/settling velocity.

When the terminal velocity is reached, we have

$$F_b - F_a = F_d \tag{2.15}$$

$$\frac{\pi}{6}D^3\rho_w\frac{v_\theta^2}{r} - \frac{\pi}{6}D^3\rho_o\frac{v_\theta^2}{r} = \frac{1}{2}C_D\rho_o\pi r^2 v_{tr}^2 \tag{2.16}$$

$$v_{tr} = \sqrt{\frac{4}{3}\frac{\rho_w - \rho_o}{\rho_o}\frac{v_\theta^2 D}{rC_D}} \ . \tag{2.17}$$

2.1.4 Separation

Two factors that significantly influence the separation of oil from the water inside the hydrocyclones are: the terminal velocity and the residence time. The bigger droplets

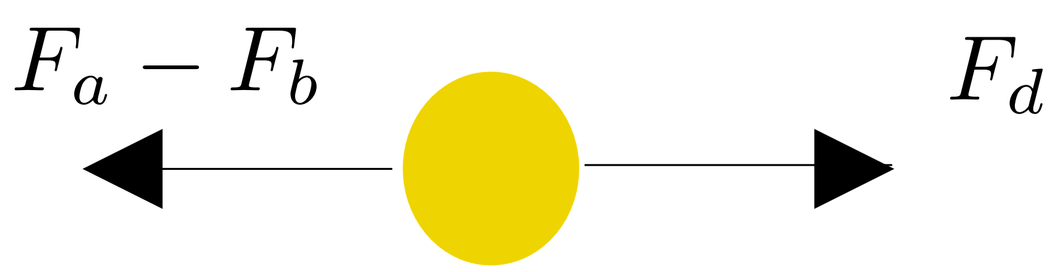

Figure 2.4: Forces acting on an oil droplet inside a hydrocyclone.

experience a higher terminal velocity and reach the reverse-flow zone, and get separated. Furthermore, the droplets getting enough residence time will reach the reverse-flow zone and get separated before exiting the hydrocyclone. Small droplets and droplets with short residence time do not get separated.

Increasing the inflow rate (inlet velocity) increases v_θ, and further increases the terminal velocity. This can help smaller droplets to reach the reverse-flow zone faster, and get separated. However, increasing v_{in} increases the axial velocity v_z, which in turn reduces the residence time of the droplet. As a result, the droplet may not have time to reach the reverse-flow zone before exiting through the water reject. Thus, an increase in the inflow rate has two contradicting effects on separation. Therefore, it is essential to select the correct inflow rate that gives sufficient residence time for the droplets and enough terminal velocity to move towards the reverse-flow zone. (The presence of the long cylindrical section is to extend the residence time, but at some point the losses are too great to maintain swirl and thus separation.)

The separation efficiency of a hydrocyclone is given by

$$\eta = 1 - \frac{\beta_{U,o}}{\beta_{in,o}} \ , \tag{2.18}$$

where $\beta_{U,o}$ is the oil fraction at the water-reject (underflow) and $\beta_{in,o}$ is the inlet oil fraction.

For a specific hydrocyclone, the vendor gives the relationship between separation efficiency and the inflow rate. This relationship gives the minimum inflow rate, $Q_{in,min}$, and the maximum inflow rate, $Q_{in,max}$, between which the hydrocyclone operates at optimum efficiency. Figure 2.5 gives an example of separation efficiency vs. inflow rate. Here, we can see that when the inflow rate is below $Q_{in,min}$, then the tangential velocity is not enough to generate the centripetal acceleration needed for the droplets to move towards the reverse-flow zone. When the inflow rate is above $Q_{in,max}$, then the axial velocity reaches the higher limit and reduces the residence time of the droplets. In this thesis, we are focusing mainly on $\beta_{U,o}$, the oil fraction at the water reject, rather than on the separation efficiency η.

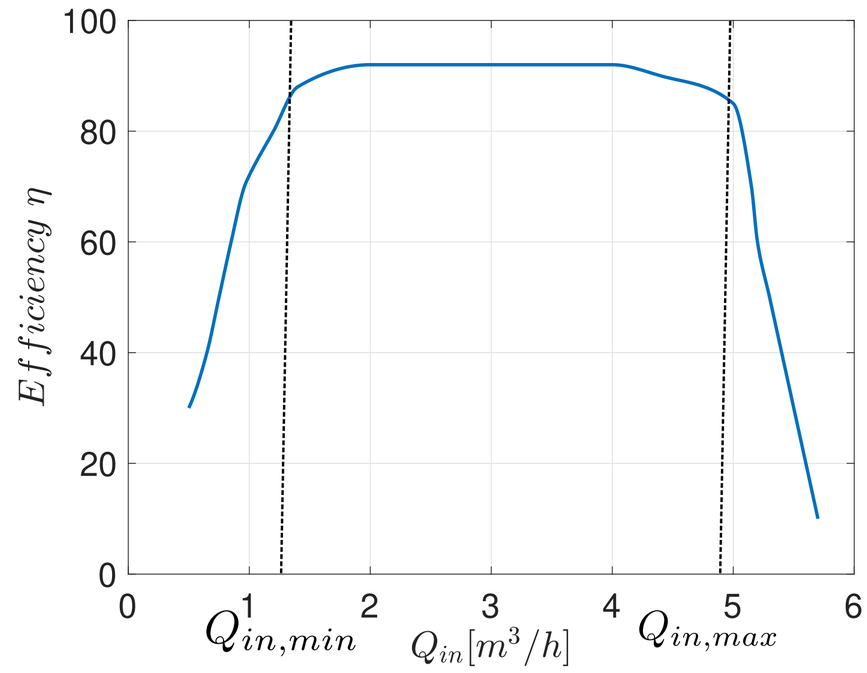

Figure 2.5: Relationship between efficiency and inflow rate of a hydrocyclone [23].

2.1.5 Hydrocyclone liner and chamber

De-oiling hydrocyclones are compact compared to solid-liquid hydrocyclones, and hence, individual hydrocyclones liners are stacked inside a chamber to form a single unit. Figure 2.6 shows the chamber of a hydrocyclone with the liners stacked inside, and Figure 2.7 shows an individual liner. Based on the throughput, the number of in-use liners inside the chamber is increased or decreased.

The trajectory analysis and the separation analysis discussed in the previous section was about the individual hydrocyclone liner. However, the individual hydrocyclone liner and a liner's behaviour inside the chamber, is fundamentally the same. The key difference is that using more liners for the same volumetric flow rate decreases inlet speed V_{in} as the flow is split into multiple liners

2.2 Control of hydrocyclones

Operational control is necessary for operating hydrocyclones at an optimum separation efficiency. The two control schemes used in the industry to achieve this are 'flow rate control' and 'flow split control'.

For example, Figure 2.8 shows a simple P&ID of a typical separation unit, consisting of a first-stage gravity separator and a hydrocyclone with the 'flow rate control' (LIC01) and 'flow split control' (PDRC01) loops. The goal of a flow rate control loop is to maintain an inflow rate in the efficiency plateau (shown in Figure 2.5). Here, the level controller LIC01 controls and maintains the level of the upstream gravity separator by adjusting the water-reject (underflow) valve and thereby maintaining the required inflow rate to the hydrocyclones.

The flow split control helps in maintaining the separation in the hydrocyclones, and

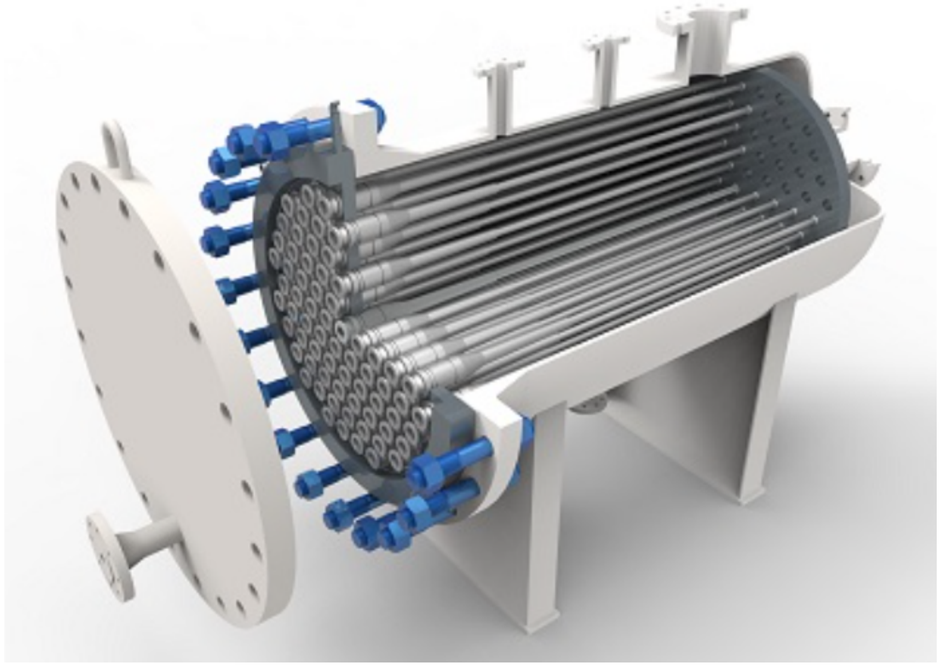

Figure 2.6: Hydrocyclone chamber and the liners placed inside it [9].

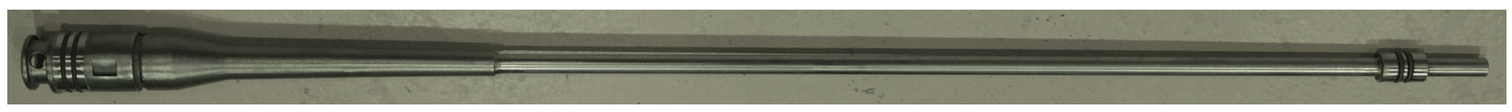

Figure 2.7: Picture of hydrocyclone line from eProess Technologies used at the test rig described in Chapter 5.

also ensures the reverse oil core stability. The term 'flow split', and 'reject ratio' are used interchangeably in literature and is defined as

$$F_s = \frac{Q_o}{Q_{in}} \ , \tag{2.19}$$

where Q_o is the flow rate at the oil reject outlet, and Q_{in} is the inflow rate. The main goal of this control loop is to ensure that the oil concentration at the water reject is meeting environmental regulations. The clean water coming from the hydrocyclones is discharged into the sea, and therefore has to meet the regulations to reduce the environmental footprints. The NCS follows the OSPAR criteria, which has set a performance standard for dispersed oil of 30 mg/l ($\approx$ 30 ppm) of discharged water.

The manipulated variable (MV) in the flow split control loop is the opening of overflow oil reject valve Z_o, and the controlled variable (CV) is the oil concentration at the water reject (underflow) $\beta_{U,o}$. In many cases, there is no measurement available for $\beta_{U,o}$, and hence a flow split F_s is taken as an alternative controlled variable (CV_2). However, the reliable and cheaper pressure measurements made the pressure drop ratio (PDR) a better candidate for the CV_2. Also, [25] calculated a linear relationship between the flow split and the PDR, based on experimental data, giving empirical ground to replace the

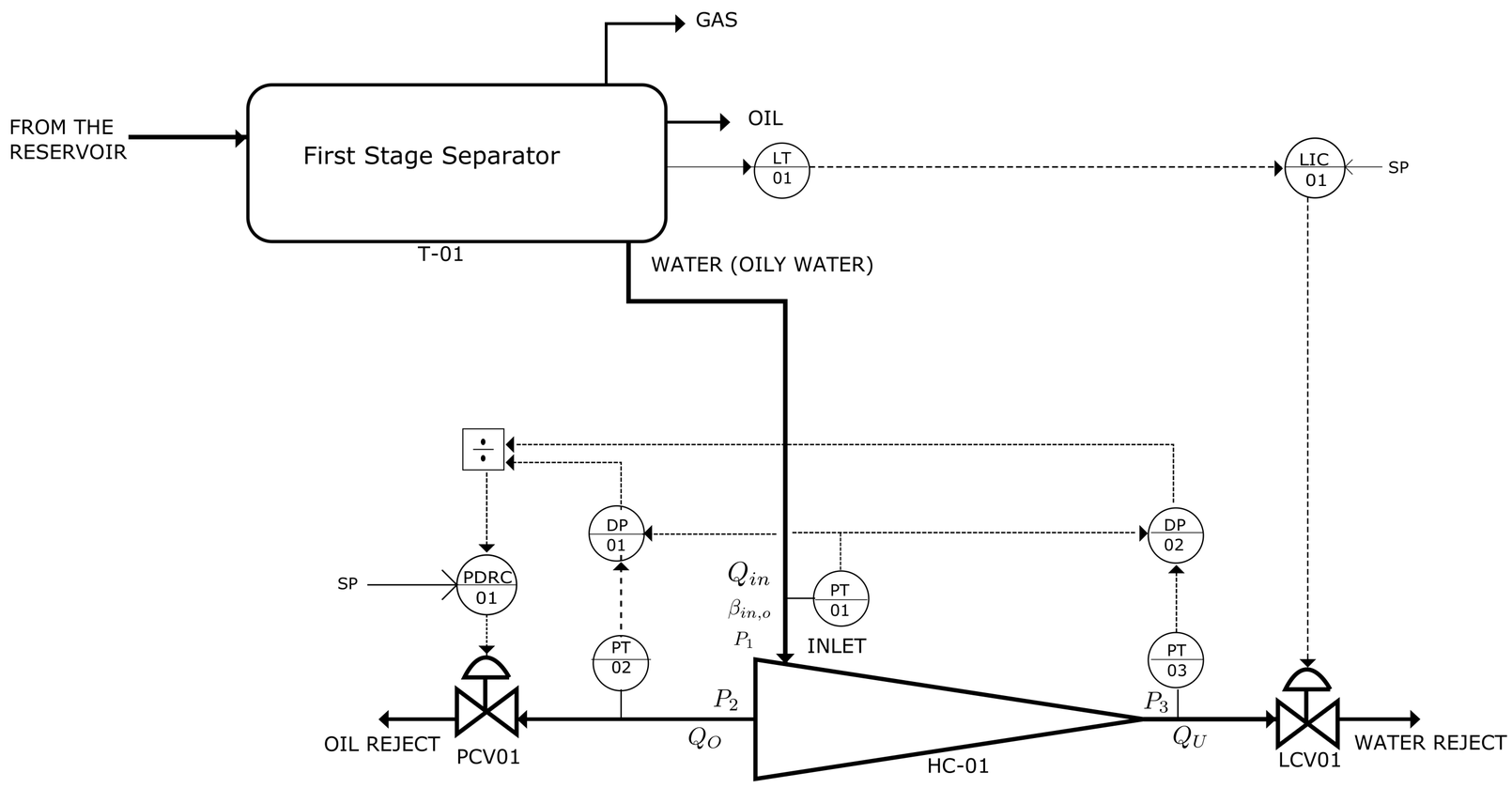

Figure 2.8: Typical control scheme of hydrocyclone representing flow rate and flow split control.

flow split control with PDR control. The PDR can be defined as

$$\text{PDR} = \frac{P_1 - P_2}{P_1 - P_3}\,, \tag{2.20}$$

where P_1, P_2, P_3 are the pressures at the inlet, overflow and underflow, respectively.

It is essential to keep the overflow valve at the right opening to maintain optimum separation. Correct flow split or PDR needs to be given as a setpoint to the controller to maintain a right overflow valve opening. A higher flow split can send more water into the oil reject stream, and takes the water back to the upstream system. Lower flow split increases the oil concentration at the water reject, in case of an increase in inlet oil concentration. Figure 2.9 shows an experimental result showing the relationship between flow split and $\beta_{U,o}$, when there is an increase in the inlet oil concentration. Here, we can see that when the inlet oil concentration is 300 ppm, a flow split of 2.6 % is enough to maintain a $\beta_{U,o}$ of 30 ppm, but when the inlet oil concentration is increased to 550 ppm, then a flow split of 3.8 % is required to keep $\beta_{U,o}$ at 30 ppm. Also note that $\beta_{U,o}$ plateaus beyond a certain F_s.

2.3 Literature review

2.3.1 Mathematical model for hydrocyclones

There are many types of models for liquid-liquid hydrocyclones discussed in the literature. Computational fluid dynamics-based models are instrumental in predicting the

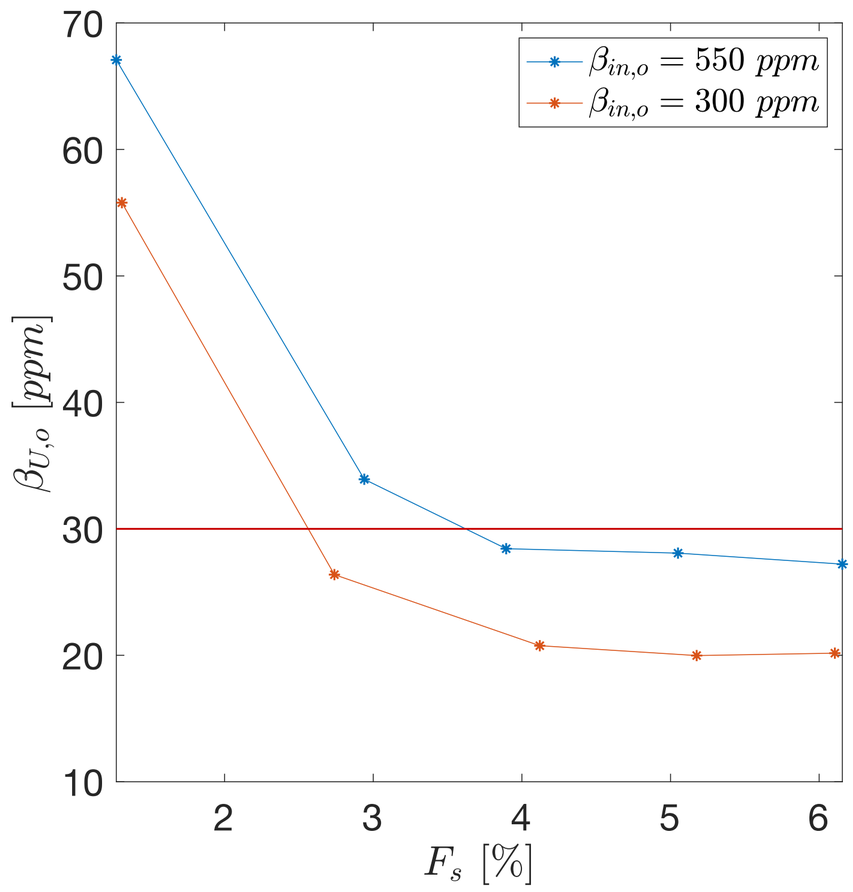

Figure 2.9: Experimental result showing the flow split Vs $\beta_{U,o}$ for two inlet oil concentrations.

flow patterns and separation efficiency, and they are mainly used to improve the design aspects of hydrocyclones. Hargreaves and Silvster [21], Motin [27], and Saidi et al. [31] discussed CFD-based models, and they use these models to enhance the dimensions and structure of hydrocyclones inorder to improve their separation efficiency. In this thesis, we briefly review the simple mechanistic and semi-empirical models available in the literature. These types of models are used in this thesis to develop a control-oriented model for hydrocyclones.

Wolbert et al. [35] developed a droplet trajectory-based model to predict the separation efficiency. Three velocity components — axial, radial and tangential — were used to track oil droplets inside the hydrocyclones. They used the Rankine vortex behaviour to represent the tangential velocity, where the tangential velocity was a function of radial position. Axial velocity (at the low cone section) was defined using a polynomial approximation. The radial position of the locus of zero axial velocity was fixed in this model, as the polynomial constants were empirical values calculated based on experimental data. The radial velocity has two components, one of which was obtained from the continuity equation. The other part was the droplets' settling velocity, which was calculated based on Stokes' law. They calculated the d_{100} diameter (the minimum diameter of a droplet which has a 100 % separation efficiency), found by considering a droplet entering the hydrocyclone at the wall and reaching the locus of zero axial velocity just before the bulk flow leaves the final cylindrical section of the hydrocyclone. They assumed that if this droplet reaches the locus of zero axial velocity, the oil droplet gets separated and

will come out through the oil reject. They also calculated the separation efficiency for a droplet diameter based on the initial position of that droplet, and then the grade efficiency with a known inlet droplet distribution.

Caldentey et al. [14] also proposed a droplet trajectory-based model for predicting the separation efficiency. In the paper, the tangential velocity was expressed as an empirical relationship that relates to the droplet's radial position and the swirl intensity. The axial velocity was defined by a polynomial approximation, where the polynomial constants were calculated based on a set of boundary conditions. With this, the axial velocity profile turned out to be a function of swirl intensity. They obtained the first part of the radial velocity from the continuity equation. Then, they used quadratic drag to express the second part of the radial velocity. In the paper, the pressure drop from inlet to underflow was calculated using Bernoulli's equation. The paper also estimates the separation efficiency for individual droplet size categories, and grade efficiency based on the inlet droplet distribution.

Bram et al. [12] developed a flow resistance model for hydrocyclones to predict the underflow and overflow rates when the upstream pressure of the oil reject valve and the downstream pressure of the water reject valve are known. This flow resistance model was combined with the droplet trajectory model developed by Wolbert et al. [35], and the variation of separation efficiency for changes in overflow and underflow flow was predicted. The flow resistance model also predicted the pressure drop ratio (PDR). Later, Bram et al. [13] modified the droplet trajectory model by considering various boundary conditions as given in Caldentey et al. [14]. One extra boundary condition considered in this paper was to add the volume balance in the reverse flow zone, which was missing in Caldentey et al. [14]. Bram et al. [13] experimentally verified the combined flow resistance and droplet trajectory model for the prediction of separation efficiency. The author also gives a detailed discussion about the experimental setup to validate the model, and the methods to prepare the inlet for the hydrocyclones such that a well-mixed oil-water mixture representing the first stage separation is given to the hydrocyclones. The authors validated the model using the experiments, and the efficiency predicted by the model had a close match with experimental data. However, the inlet droplet distribution of the hydrocyclone was unknown, and the model assumed a droplet distribution with a mean of 15 µm to 20 µm. Hence, as future work the authors suggested model validation using different droplet distributions.

2.3.2 Control

In this section, a brief literature review of hydrocyclones focusing mainly on their control aspect is given.

Meldrum [25] discussed the results from the first commercially tested hydrocyclones at the Murchison platform and the Hutton tension leg platform and different factors influencing the performance of the hydrocyclone. This paper considers the reject ratio

(flow split) and the inflow rate as the two critical means of efficiently controlling the performance of a hydrocyclone over a specific range of operation. Two-phase flow meters were not efficient in measuring the flow split, especially in the presence of gas. Hence, they proposed a pressure drop ratio (PDR) control scheme, which used the pressure drop ratio across oil-reject and water-reject to maintain the required flow split. Meldrum calculated a linear relationship between flow split and PDR experimentally. Later in the paper, he mentions that the relationship between flow split and PDR would not be universal. It depended on the specific field's crude characteristics. This paper also discussed the need to increase the flow split when there is an increase in the oil concentration above a specific range to maintain optimum efficiency.

Husveg et al. [23] studied the performance of de-oiling hydrocyclones for varying inflow rates. First, they experimentally calculated the PDR to achieve the maximum efficiency for an operating inflow rate. Later, they found the relationship between the flow split and the PDR. A PDR of 1.7, mapped to a flow split of 6.5 % to 7 %, was used as a setpoint for the PDR scheme. The hydrocyclone liners with the PDR control scheme were subjected to linear increase, linear decrease and sinusoidal variations in the inflow rate. The experimental results indicated that the PDR control scheme was able to handle the disturbances in the inflow and maintain the efficiency of the hydrocyclones. Inlet oil concentration and droplet distribution were kept constant for their experiment.

Durdevic and Yang [17] considered the upstream gravity separator and the hydrocyclone as a single system, and analysed the interaction of the flow-rate control and the flow-split control. This analysis is relevant when the change in the inflow rate is more drastic, in scenarios such as slugging. They used a level controller to maintain the level of the upstream separator and thereby maintain the required inflow rate. Next, they used a PDR controller for the flow-split control. Experimental results showed that using a simple PID controller for PDR control was ineffective in disturbance rejection (frequent inflow rate changes). In some cases, the oil reject control valve was saturated. Then, a MIMO model for the process was developed and based on that a robust H_∞ controller was designed and tested. The H_∞ controller showed better disturbance rejection and smooth changes in the water reject (underflow) valve in cases of drastic inflow rate changes. Later, Durdevic and Yang [18], analysed the combined system (gravity separator and hydrocyclone) with an oil-in-water measurement at the inlet and water reject of the hydrocyclones. Online measurement helped them directly measure the efficiencies of hydrocyclone when subjected to frequent changes in inflow rate. Also, they compared a simple PID control and a robust H_∞ control scheme for the combined system for the hydrocyclone efficiency. The PID control solution of combined system showed better performance in terms of efficiency while the H_∞ control scheme of the combined system were able to maintain a lower oil concentration at the underflow.

Orlowski et al. [28] described the control system details of the subsea separation system installed at the Marlim Field at a water depth of 870 m. The subsea separation system has a gas harp, a pipe separator, a desander and hydrocyclones. The authors

discuss the practical details of the control scheme for hydrocyclones implemented at the subsea installation. They proposed logic-based controllers with delays and operation bands to keep the flow-split between 2 % to 6 %, instead of a traditional PID based PDR control scheme.

2.3.3 Experimental test rig

In this section, a brief literature review of the different experimental setups for testing the de-oiling hydrocyclones available in literature are given. These setups emulate the first stage gravity separator and generate different inlet disturbances for the hydrocyclones. Changes in inflow rate, oil concentration, and oil droplet distribution are the disturbances that need to be generated by the test setup.

Here, we describe four experimental test rigs, described in Bram et al. [12], Gomez et al. [20], Husveg et al. [23], Young et al. [36]. Proper mixing of oil and water is crucial to get the right droplet distribution, and to get a mixture that represents output from the first-stage separator. Figure 2.10a shows the flow diagram for an inline mixing of oil and water before being fed into the hydrocyclone. Figure 2.10b shows the batch mixing of oil and water in a tank before being fed into the hydrocyclone.

There are different techniques of mixing oil and water inline. Young et al. [36] used a homogeniser with a bypass mixing loop, where the frequency of the homogeniser is adjusted to vary the droplet distribution. Gomez et al. [20] used a static mixer followed by a mixing loop. The desired droplet distribution was achieved by choosing a specific static mixer; passing the mixture through the mixing loop created smaller oil droplets. Husveg et al. [23] used a dynamic water-oil mixer (a pump), and varying the pump speed varied the droplet distribution. Bram et al. [12] mixed oil and water in a tank and created the mixture in batches. The speed of the mixer in the tank was adjusted to create the desired droplet distribution.

In batch and inline test setups, the flow rates of water and oil can be controlled using the variable speed drive connected to the respective pumps. Well-mixed oil and water is sent into the hydrocyclone, and the clean water comes out as water reject (underflow) and the oil-rich stream comes out as oil reject (overflow).

Different measurements such as flow, pressure, and temperature are monitored and logged using suitable data acquisition systems in the test setups. Gomez et al. [20], Young et al. [36] did not implement any control schemes. Bram et al. [12], Husveg et al. [23] implemented a pressure drop ratio (PDR) control scheme to control the oil reject valve PCV01 (Figure 2.10) and to maintain the separation in the hydrocyclones. The underflow (water reject) control valve PCV02 was kept at a constant opening.

A sampling point at the inlet and water reject can be used to measure oil concentration and droplet distribution. Gomez et al. [20], Husveg et al. [23], Young et al. [36] used offline techniques such as IR absorbance for measuring the oil concentration. A light scattering instrument was used to measure the droplet distribution and Dv50. Dv50 is defined as

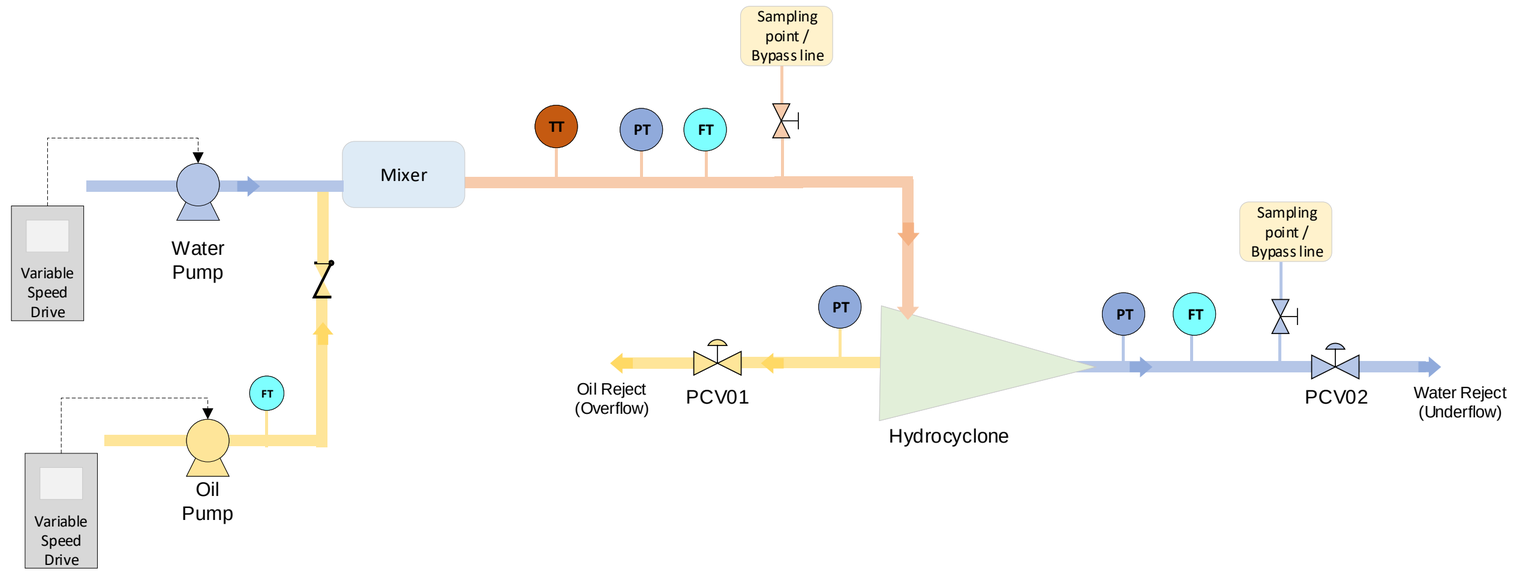

(a) An experimental test rig setup where oil is injected into water line and mixed inline before sending into the hydrocyclone.

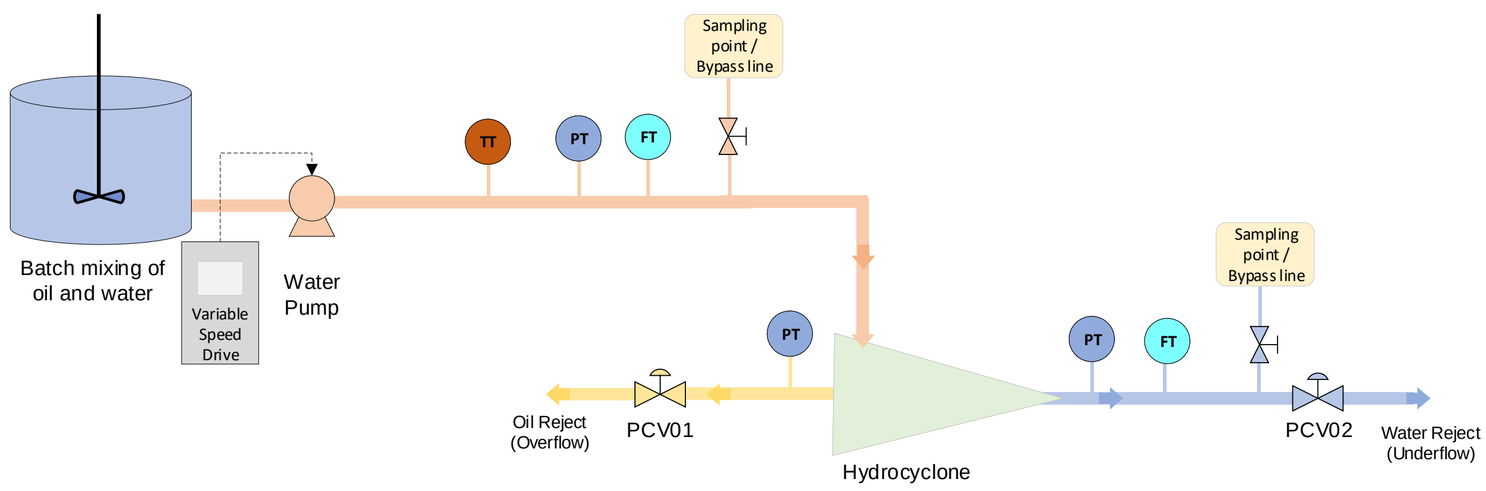

(b) An experimental test rig setup where oil and water is batch mixed and pumped into the hydrocyclone.

Figure 2.10: General test rig setups.

the median (by volume) droplet size; half the droplets are of greater volume and half of lesser volume. In Bram et al. [12], a special side-stream was constructed, parallel to the main pipe line at the main inlet and the water reject. Then, online fluorescence-based oil-in-water analysers were placed in these side-streams to measure the oil concentration. Table 2.1 summarises the key aspects of the various rigs.

2.4 New test rig: constructional and operational details

This section gives the constructional details of the test rig used for the experiments in this thesis. The main goal of this test rig is to test the novel and advanced control schemes for hydrocyclones, which also necessitates the ability to emulate first-stage gravity separators and generate different inlet disturbances to the hydrocyclones. The test rig is also equipped with instrumentation sufficient to test these new control schemes for hydrocyclones, which can be used along with the typical PDR control scheme. A simplified P&ID

Table 2.1: Features of experimental test setup for hydrocyclones available in literature.

Test Setup	**Type of mixer**	**Vary oil conc.**	**Vary droplet dist.**	**Measure oil conc.**	**Control system**
[36]	Homogeniser	Online	○ Yes ○ Varying speed of homogeniser	○ Offline measurement ○ Using analytical method (IR analysis)	○ No control system ○ Flows and pressures are logged
[20]	Static mixer	Online	○ Yes ○ Static mixer with a bypass loop is used ○ Varying the duration of the fluid in the bypass loop	○ Offline measurement ○ Infrared spectroscopy	○ No control system ○ Data acquisition of analog signals (flow, pressures temperatures) are done using NI
[23]	Dynamic mixer	Online	○ Yes ○ By varying the speed of dynamic mixer	○ Offline measurement ○ Infracal TOG/TPH Analyser	○ PDR controller ○ Pressures, flows and temperatures are logged and used in control system
[12]	Batch mixing	Batch	○ No ○ Because of batch mixing the distribution remains constant	○ Online side stream measurement ○ TD-4100XDC fluorescence-based	○ PDR controller ○ Pressures, flows and temperatures, oil concentration are logged and used in control system
Present Test Rig	Control Valve	Online	○ Yes ○ Varying the pressure drop across the inlet control valve	○ Online (inline) measurement ○ Ultrasound-based	○ PDR controller ○ Pressures, flows and temperatures, oil concentration are logged and used in control system ○ Possibility to test new control schemes.

of the test rig with a PDR control scheme is shown in Figure 2.11.

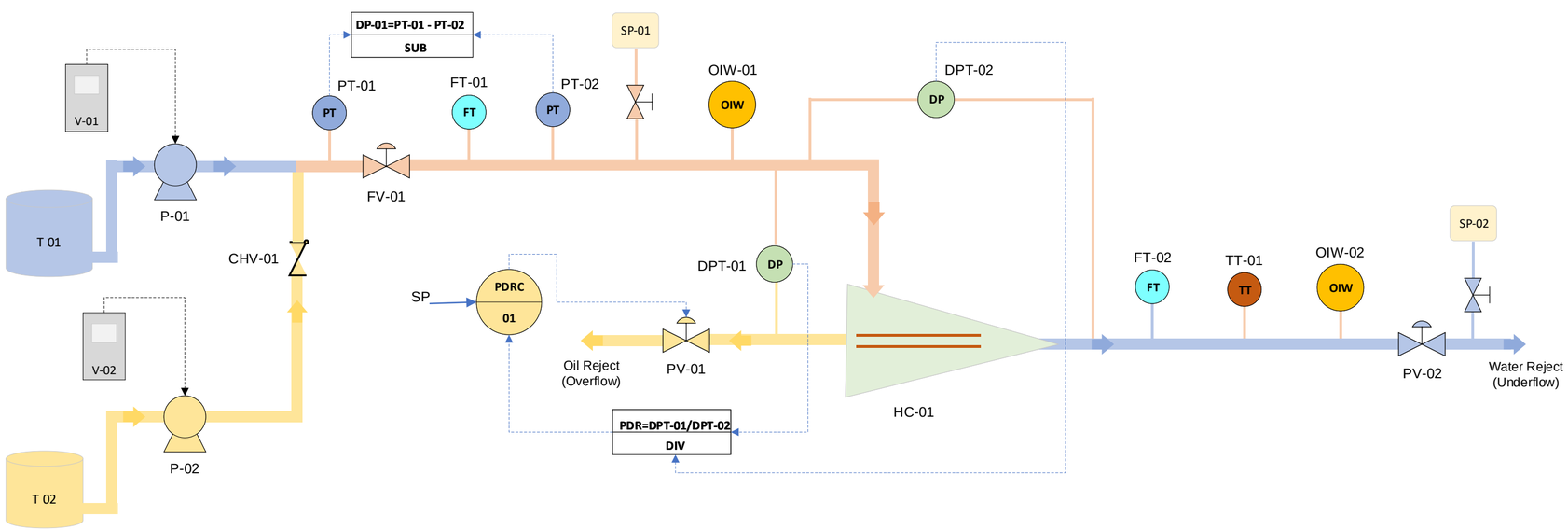

Figure 2.11: Simplified P&ID of the new experimental test rig.

HC-01 in Figure 2.11 represents the hydrocyclones in the test rig. Here we use two DO15 hydrocyclone liners from eProcess Technologies. These two liners are placed parallel in a chamber with a common inlet and two common outlets. The clean oil from the two liners goes into a common oil reject part of the chamber and later taken out through a normal pipe. The cleaner water from the the two liners goes into a common water reject

part of the chamber and later taken out through a normal pipe. According to the data sheet provided by the vendor, a single liner needs a minimum inflow rate of 1.44 m^3/h and can handle a maximum inflow rate of 4.53 m^3/h. As two liners are placed in a chamber, the total inflow rate during the operation has to be greater than 2.88 m^3/h.

The main water reservoir T-01 is a 5000 liter PVC tank with tap water. We use Exxsol D60 for testing, and it is directly pumped from the oil barrel (T-02). The main water line is 1.25 inches and the oil line is 0.25 inches in diameter. A check valve CHV-01 prevents water from entering the oil line. The main water pump P-01 is a centrifugal pump with a rated flow rate of 5 m^3/h and a maximum discharge pressure of 25 bar. The oil pump is a piston pump with a flow dampener to smooth out the pulsating flow. The maximum flow rate of the piston pump is 15 l/h with discharge pressure of 25 bar and 100 strokes/min. The minimum flow rate of the oil pump is 1 l/h. The flow of 1 to 15 l/h enables a variation of inlet oil concentration from 250 to 3000 ppm. The pumps have variable speed drives V-01 (P01) and V-02 (P01), controlled by 4 to 20 mA signal from the control system to regulate the speed. Both of the speed drives also require an additional digital signal to start the pumps, which is also given from the the control system.

The pressure transmitter PT-01 with a pressure range of 0 to 30 bar monitors the discharge pressure of the oil pump. The pressure transmitter PT-02 with a pressure range of 0 to 70 bar monitors the downstream pressure of the FV-01 and the pressure transmitter PT-03 measures the upstream pressure of the FV-01. A Coriolis flowmeter FT-01 measures the total flow (oil and water) and the range of the flowmeter is adjusted to 0 to 5 m^3/h using the optical switch in transmitter's display panel.

A pneumatically operated 1 inch control valve FV-01 is placed after the oil injection point. The pressure-drop DP-01 across FV-01 affects the droplet distribution. The opening and closing of FV-01 can be controlled using a 4 to 20 mA analog signal.

The inlet line and the underflow outlet (water reject) of the hydrocyclone is 2 inch, as most of the flow into the hydrocyclones comes out through the underflow. A pneumatically operated 2 inch control valve PV-02 at the underflow controls the total throughput of the cyclones. The overflow line of the hydrocyclone is 1 inch, and a pneumatically operated 1 inch control valve PV-01 is used to control the separation of the hydrocyclones.

Two differential pressure transmitters DPT-01 and DPT-02 measure the pressure drops across the inlet to overflow and inlet to underflow, respectively. Both of these pressure transmitters are configured in the range of 0 to 8 bar using the switches in their display panel. A magnetic flowmeter FT-02 at the underflow (water reject) is also configured in the range of 0 to 5 m^3/h using the optical switches in the transmitter display panel.

The inlet oil concentration and the water reject oil concentrations can be measured online and offline. Specially designed sampling points SP-01 and SP-02 helps to take out the samples by preserving the droplet distribution. Samples are measured offline using light scattering measurement technique (Mastersizer 3000, Malvern Instruments). Mirmorax ultrasound-based oil-in-water analysers OIW-01 and OIW-02 are used to measure

oil concentration online. These two sensors have a stabilisation time of 1 s, which enables these sensors to be used in the control system.

All the transmitters, control valves and variable speed drives are connected to the LabVIEW programming environment using NI DAQ cards. A graphical user interface is built using LabVIEW to log the data from the instruments and give control signals or manual commands to equipment (valves and pumps). The oil-in-water analyser communicates with the LabVIEW programming environment via MODBUS RTU signals. All the analog signals are sampled at 1000 Hz. Appendix C, describes the practical implementation of the flow split control scheme in the new experimental rig along with different components of process control and automation.

The various articles that present the research done as part of this project follows in the subsequent chapters.

Chapter 3

Control oriented model for de-oiling hydrocyclones

The article presented in this chapter describes a control-oriented model for hydrocyclones, which can help in the development of robust control algorithms for de-oiling hydrocyclones. The model is developed based on first principles and has three parts: a droplet trajectory model for calculating the separation efficiency, a pressure flow model based on Bernoulli's equation for calculating the pressure at the overflow and underflow outlets, and a mass-balance dynamic model for calculating the fraction of oil and water coming out of two outlets.

3.1 A first-principles approach for control-oriented modeling of de-oiling hydrocyclones.

The citation of the published article is given below:

Vallabhan KG, M. V., Holden, C., and Skogestad, S. (2020). *A First-Principles Approach for Control-Oriented Modeling of De-oiling Hydrocyclones*. Industrial & Engineering Chemistry Research, 59(42), 18937-18950. https://doi.org/10.1021/acs.iecr.0c02859

Errata:

Note that Equations (11), (18) and (21)in this paper are incorrect and it needs to be changed to the following

$$v_r(r) = -\frac{U_o}{2}\frac{r}{L}$$

$$v_{r,w}(r) = -\frac{V_o(z)}{2}\frac{r}{L(z)}$$

$$v_{ter}(r) = \sqrt{\frac{4}{3}\frac{\rho_w - \rho_o}{\rho_o}\frac{v_{\theta,w}^2 D}{rC_D}}$$

The postprint version of the paper follows.

3.1. A first-principles approach for control-oriented modeling of de-oiling hydrocyclones.

A First-Principles Approach for Control-Oriented Modeling of De-oiling Hydrocyclones

Mishiga Vallabhan K G,* Christian Holden,* and Sigurd Skogestad*

Cite This: *Ind. Eng. Chem. Res.* 2020, 59, 18937−18950

ABSTRACT: De-oiling hydrocyclones are a promising choice for produced water treatment in the oil and gas industry. The compact nature of hydrocylones makes them suitable for offshore and subsea installations. The commitment toward reduction in environmental footprint makes it a necessity to maintain the efficiency of the produced water treatment system (hydrocyclones) under all plant scenarios. A mathematical model for de-oiling hydrocyclones can help to develop robust control algorithms to handle the uncertainties and to maintain high efficiency. In this paper, a simple first-principle model is developed for hydrocyclones. A pressure-flow relationship is derived using Bernoulli's equation, a droplet trajectory analysis is done for calculating the separation, and a dynamic mass balance is used for control purposes. A simple PI control algorithm tuned using the SIMC tuning rules is used to verify the model and its control properties.

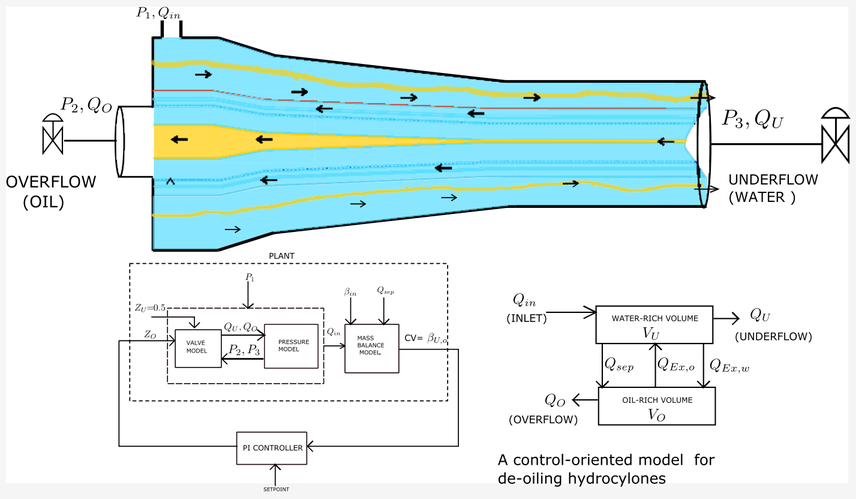

A control-oriented model for de-oiling hydrocyclones

INTRODUCTION

Produced water is a common waste product in oil and gas production. The amount of produced water typically increases with the age of the oil field. Two common methods for produced water treatment are reinjection into the reservoir and discharge to the sea. Reinjection of produced water increases the reservoir pressure and hence may enhance recovery. Discharge of produced water to sea has to meet local governmental regulations. The Norwegian continental shelf comes under the regulation of the OSPAR commission, which has set a limit of 30 mg/L of oil (approximately 30 ppm) in produced water discharged to the sea.[1] Hydrocyclones, compact floatation units (CFUs), and membrane filters are equipment used for produced water treatment.

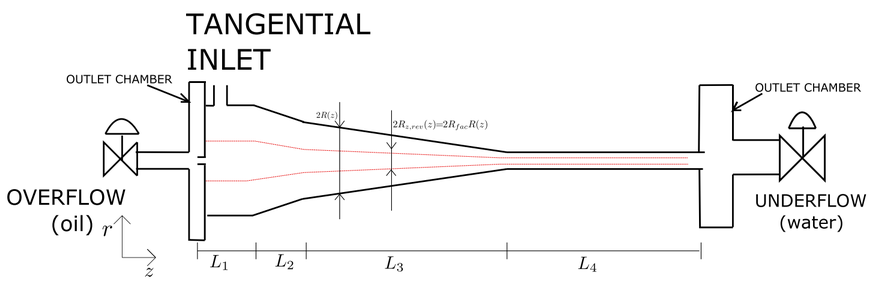

Figure 1. Hydrocyclone liner connected to two outlet chambers (not drawn to scale). The red lines represent the reverse-flow zone.

Almost 90% of the offshore produced water treatment facilities are based on hydrocyclone technology.[2] Simple, lightweight, compact nature of hydrocyclones along with low maintenance costs makes it attractive for the subsea environment as well. The Brazilian Marlim field at 870 m water depth has subsea oil−water separation with a hydrocyclone for produced water treatment.[3,4] This is the only one currently in use subsea.

Since the 1800s, hydrocyclones have been the most popular separation technology in the mining and mineral industry.[5] Later, the oil and drilling industry used simple and rugged cyclone devices for sand separation from oil, drilling mud, and other fluids. In the 1970s, trials began on the possibility of using hydrocyclones to separate oil−water mixtures. By modifying certain geometry and design parameters, the conventional hydrocyclones achieved adequate separation of oil−water mixtures.

The first experimental results were given in ref 6, and in that paper, it is mentioned that the efficiency of cyclones largely depends on the oil droplet size. Design guidelines and advantages and disadvantages of de-oiling hydrocyclones used in offshore platforms are given in ref 7. Details about the

Received: June 8, 2020
Revised: September 23, 2020
Accepted: September 25, 2020
Published: September 25, 2020

https://dx.doi.org/10.1021/acs.iecr.0c02859
Ind. Eng. Chem. Res. 2020, 59, 18937−18950

construction and principle of operation of the first full-scale commercial de-oiling hydrocyclone are given in ref 8. Reference 9 gives details about factors such as separation efficiency, feed characteristics (inflow rate, oil water ratio, etc.), pressure drop, and operation.

There are two different types of de-oiling hydrocyclones: one has a swirl element inside the cyclone (called inline hydrocyclones), whereas the one studied in this paper is without a swirl element. A control-oriented modeling of an inline hydrocyclone is given by ref 10.

This paper focuses on hydrocyclones without a swirl element as shown in Figure 1. The geometry itself induces swirling in these types of cyclones. There have been numerous studies on modeling of de-oiling hydrocyclones without a swirl element. A model to calculate the efficiency of liquid−liquid hydrocyclones based on droplet trajectories is presented in ref 11, where the three velocity components (tangential, axial, and radial) are used for trajectory analysis. Later, ref 12 developed a mechanistic model for liquid−liquid hydrocyclones where the separation efficiency is determined based on swirl intensity and droplet trajectory analysis. They also present a model to predict the pressure drop from the inlet to the underflow outlet. Most recently, CFD-based studies on the velocity distribution and separation performance have become popular, for example, refs 13 and 14.

Most of the models developed for de-oiling hydrocyclones, for example, CFD models, are too complicated and not suitable from a control perspective. One approach for control-oriented modeling of a hydrocyclone is given in ref 15, where experimental data was used to derive transfer function models. Later, ref 16 developed a gray-box model based on flow resistance and droplet trajectory analysis for determining the separation efficiency of hydrocyclones. However, more simple first principles-based models have not been investigated. In this paper, a control-oriented model for a hydrocyclone is derived by combining droplet trajectory analysis, pressure-flow relationships, and a dynamic mass-balance model.

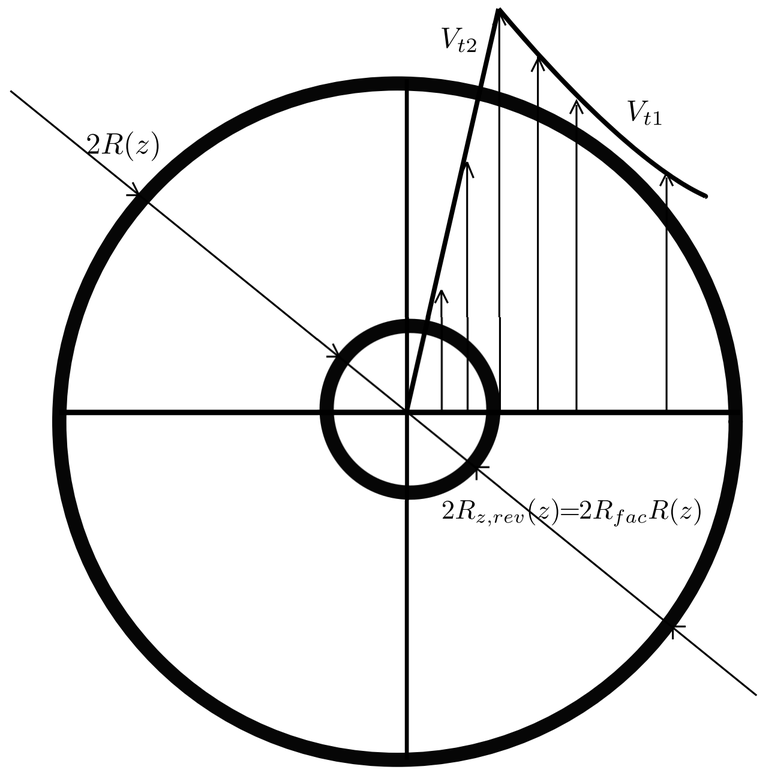

Figure 2. Tangential velocity profile inside a hydrocyclone liner.

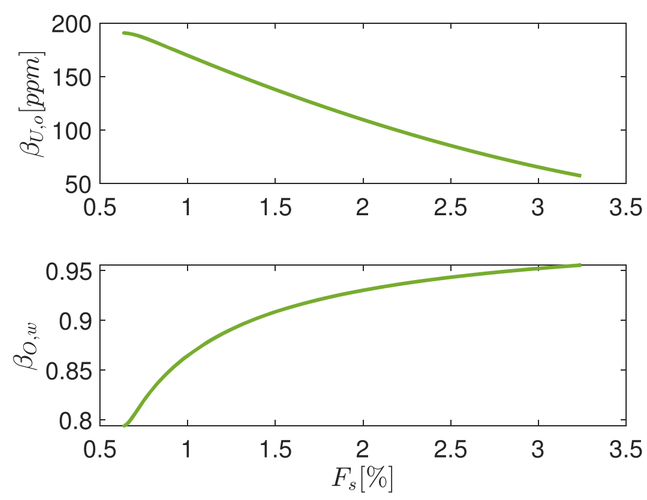

Figure 3. Variation of oil in underflow and water in overflow with flow split. The figure was obtained using the model presented later in this paper (here $\beta_{in,\ o}$=1500 ppm).

■ HYDROCYCLONE MODELING: INTRODUCTION

De-oiling hydrocyclones have a cluster of cyclone liners, which can be added or removed in order to meet flow rate requirements. Each liner has a tangential inlet and two outlets (see Figure 1). The heavy purified water comes out through the underflow outlet, and the lighter oil-rich stream comes out through the overflow outlet. The outflows from all of the liners enter into the two outlet chambers at the overflow and underflow ends. Figure 1 shows a single liner connected to two outlet chambers.

A hydrocyclone liner has four sections: first, a cylindrical part where the liquid enters; second, a tapered conical section where the fluid is accelerated due to the reduction in the diameter; third, a longer tapered conical section where the majority of the separation occurs; and fourth, a parallel tail section where slower-moving droplets can be recovered.

Separation occurs due to centrifugal forces, which are much larger in magnitude than the ones in a conventional gravity-based separator.[8] The tangential inlet section aids in generating the centrifugal force, and the narrowing section of hydrocyclones further accelerates the fluid. The low-density oil droplets move toward the center of the cyclone and form the reverse oil core, which exits at the overflow outlet. At the same time, the higher-density water is pushed toward the walls of the cyclone and carried away as the continuous phase to the underflow outlet.

There exists a reverse-flow zone inside a hydrocyclone liner. The oil droplets entering the reverse-flow zone get separated from the continuous phase and form an oil-rich reverse core at the center of the cyclone liner.

According to ref 12, the location of the reverse-flow zone depends on the swirl intensity. Thus, it is a function of cyclone geometry, the mean axial velocity, and the tangential velocity. In ref 11, the reverse-flow zone is calculated based on the axial velocity profile, which varies with the sections of the hydrocyclone. Hence, we can say that depending on the sections L_1 to L_4 (in Figure 1), the size of the reverse-flow zone varies. Also, while, the reverse-flow zone extends to the underflow,[7] oil present in the reverse-flow zone does not go out through the underflow outlet:

$$R_{z,rev}(z) = R_{fac}(z)R(z) \tag{1}$$

where $R(z)$ is the radius of hydrocyclone at different axial positions z. From refs 12 and 11 , we can say the factor R_{fac} has four different values at four sections L_1, L_2, L_3, and L_4. As the separation mainly takes place in L_3 and L_4, we assume two values for R_{fac}, i.e., $R_{fac,1}$ when it is in sections L_1 to L_3 and $R_{fac,2}$ when it is

https://dx.doi.org/10.1021/acs.iecr.0c02859
Ind. Eng. Chem. Res. 2020, 59, 18937−18950

in L_4 where $1 > R_{fac,1} > R_{fac,2}$. $R_{fac,1}$ and $R_{fac,2}$ are tuning parameters in the model, and we will use values of 0.3714 and 0.27.

The flow pattern inside a hydrocyclone can be described using three velocity components: tangential (θ), axial (z), and radial (r). The tangential velocity shows a Rankine vortex-type rotational behavior as shown in Figure 2.[11] Starting from the hydrocyclone wall, the velocity increases and reaches a maximum. The point where the tangential velocity reaches its maximum is the starting point of the reverse-flow zone for the axial velocity.[12] This is called a locus of zero axial velocity. Further away from this point, the tangential velocity starts to decrease and it approaches zero at the center of the hydrocyclone. The radial velocity distribution depends on the Stokes drag.

A hydrocyclone separates inlet feed into two products, so there are two operational quantities of interest: the fraction of oil in the underflow (water reject), $\beta_{U,\,o}$ (which is our main concern), and the fraction of water in the overflow (oil reject), $\beta_{O,\,w}$. Reference 7 defines the separation in terms of two parameters. One is the separation efficiency, defined as

$$\eta = 1 - \frac{\beta_{U,o}}{\beta_{\text{in},o}} \tag{2}$$

where $\beta_{U,\,o}$ and $\beta_{in,\,o}$ are the fraction of oil in the underflow and the inlet, respectively. Here, the subscript o denotes oil, U denotes underflow, and O denotes overflow.

The second parameter is the flow split, defined as

$$F_s = \frac{Q_O}{Q_{\text{in}}} \tag{3}$$

where Q_O is overflow rate and Q_{in} is the inflow rate. A high-performing hydrocyclone should have a high separation efficiency and a small flow split. However, there is a trade-off between the two parameters. This is seen from Figure 3, where we see that to reduce $\beta_{U,\,o}$ to get a high separation efficiency (desired), we need to increase the flow spilt (F_s) (undesired). From the lower plot, we see that an increase in the flow spilt also increases the fraction of water in the overflow. We also see that the overflow ("oil") contains mostly water, about 80−95% in this case.

In this paper, the hydrocyclone modeling is focused on the control aspects. The flow between the inlet and the two outlets is modeled based on Bernoulli's equation assuming laminar flow (Pressure-Flow Relationship section). The separation and separation efficiency are calculated based on a droplet trajectory model (Oil Droplet Trajectory Analysis and Modeling of Internal Separation sections). The flow and droplet trajectory models are steady-state in nature. Dynamics, which may be required for control purposes, are incorporated in the mass balances by dividing the hydrocyclone into two main control volumes (Dynamic Mass-Balance Model section).

■ PRESSURE-FLOW RELATIONSHIP

This section derives a static relationship between pressures (P_1, P_2, P_3) and volumetric flow rates (Q_U, Q_O) (marked in Figure 4a) assuming:

A1. The size of the reverse-flow zone is fixed, and the reverse-flow zone extends through the length of the hydrocyclone. In other words, a Rankine vortex flow pattern exists from the inlet to the underflow.

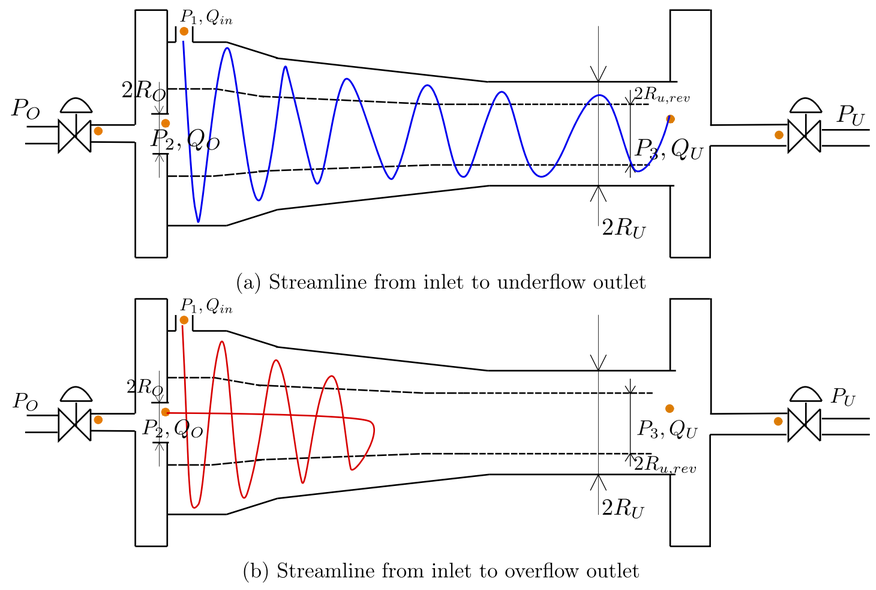

Figure 4. Different streamline considered for calculating the pressure-flow relationship of a hydrocyclone.

Table 1. Parameters Used for Simulation

parameter	value	unit
P_1	6	bar
P_{atm}	1.01325	bar
ρ_O	910	kg/m^3
$\rho_U = \rho_w$	1000	kg/m^3
ρ	989	kg/m^3
R_{in}	0.0035	m
R_O	0.001	m
R_U	0.005	m
V_{HC}	2.0896×10^{-04}	m^3
V_O	5.2239×10^{-07}	m^3
C_D	20	
C_{v1}	5.0671×10^{-05}	m^2
C_{v2}	2.5335×10^{-06}	m^2

A2. The radial velocities at the exit points are negligible.

A3. The frictional losses inside the cyclones are neglected in Bernoulli's equation.

First, consider a water streamline between a point at the tangential inlet and a point at the underflow. This is marked in blue in Figure 4a. Then, from Bernoulli's equation, with no friction loss (Assumption A3), we get:

$$P_1 + \frac{\rho}{2}\left(\frac{Q_{\text{in}}}{A_{\text{in}}}\right)^2 = P_3 + \text{KE}_{\text{Uz}} + \text{KE}_{U\theta}$$

Here, KE_{Uz} is the kinetic energy contributed by the axial velocity of the fluid we have

$$\text{KE}_{\text{Uz}} = \frac{\rho_U}{2}\left(\frac{Q_U}{A_U}\right)^2$$

where A_U is the underflow cross-sectional area and Q_U is the underflow volumetric flow rate. The kinetic energy contributed by the tangential velocity is given $\text{KE}_{U\theta}$. The tangential velocity profile at the underflow is a combination of free and forced vortexes. The detailed derivation of the $\text{KE}_{U\theta}$ is given in Appendix A. Inserting into Bernoulli's equation gives

$$P_1 + \frac{\rho}{2}\left(\frac{Q_{\text{in}}}{A_{\text{in}}}\right)^2 = P_3 + \frac{\rho_U}{2}\left(\frac{Q_U}{A_U}\right)^2 + \frac{5}{4}\frac{\rho_U}{R_U^2}\frac{(\alpha_1 Q_{\text{in}} R_1)^2}{\pi^2 R_{\text{in}}^4} \tag{4}$$

https://dx.doi.org/10.1021/acs.iecr.0c02859
Ind. Eng. Chem. Res. 2020, 59, 18937−18950

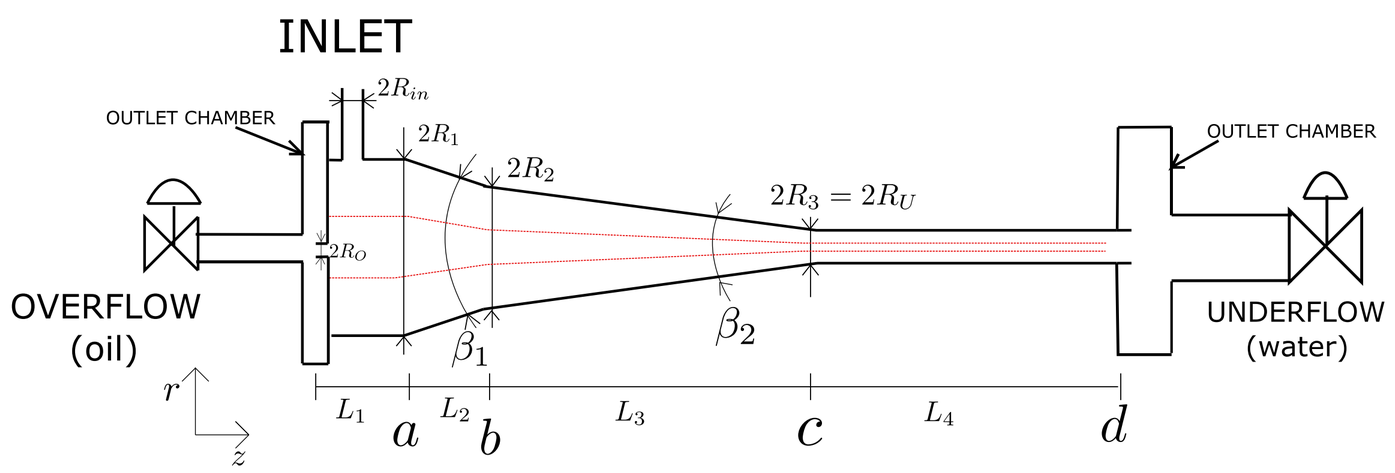

$R_1 = 0.02\text{m}$ $L_1 = 0.04\text{m}$ $\beta_1 = 20°$
$R_2 = 0.01\text{m}$ $L_2 = 0.0567\text{m}$ $\beta_2 = 1.5°$
$R_3 = 0.005\text{m}$ $L_3 = 0.3820\text{m}$
$R_O = 0.001\text{m}$ $L_4 = 0.4\text{m}$

Figure 5. Geometrical details of a hydrocyclone liner used in the model (not drawn to scale).

Next, a second oil streamline is considered between a point at the tangential inlet and a point at the overflow as shown by a red line in Figure 4b. From Bernoulli's equation and Assumption A3, we get

$$P_1 + \frac{\rho}{2}\left(\frac{Q_{\text{in}}}{A_{\text{in}}}\right)^2 = P_2 + \text{KE}_{\text{Oz}} + \text{KE}_{O\theta}$$

where the kinetic energy in the axial direction is

$$\text{KE}_{\text{Oz}} = \frac{\rho_O}{2}\left(\frac{Q_O}{A_O}\right)^2$$

The tangential velocity profile at the overflow has only forced vortex, and hence the forced velocity component contributes to the kinetic energy $\text{KE}_{O\theta}$. The detailed derivation for this term is given in Appendix B. The Bernoulli's equation can then be rewritten as

$$P_1 + \frac{\rho}{2}\left(\frac{Q_{\text{in}}}{A_{\text{in}}}\right)^2 = P_2 + \frac{\rho_O}{2}\left(\frac{Q_O}{A_O}\right)^2 + \frac{\rho_O}{4}\frac{(\alpha_1 Q_{\text{in}} R_1)^2}{(\pi R_{\text{in}}^2)^2 R_{U,rev}^4} R_O^2 \tag{5}$$

Next, consider the pressure at two exits of the liner, thus can be modeled using a standard valve equation for turbulent flow. This gives

$$Q_U = C_{v1} Z_U \sqrt{\frac{2(P_3 - P_U)}{\rho_U}} \tag{6}$$

$$Q_O = C_{v2} Z_O \sqrt{\frac{2(P_2 - P_O)}{\rho_O}} \tag{7}$$

Here, C_{v1} and C_{v2} are the valve constants of the underflow and overflow valves (incorporating frictional losses), P_2 is the pressure at the overflow outlet, P_3 is the pressure at the underflow outlet, $Z_U \in [0,1]$ and $Z_O \in [0,1]$ are the valve positions, and ρ_U and ρ_O are the densities of liquid at the underflow and overflow outlets, respectively. P_O is the downstream pressure of the overflow valve, and P_U is the downstream pressure of the underflow valve . This paper assumes that P_O and P_U are known and equal to the atmospheric pressure (P_{atm}).

Finally, from the overall mass balance:

$$Q_{\text{in}} = Q_O + Q_U \tag{8}$$

In the five (eqs 4−8), there are six unknowns (Q_{in}, P_1, Q_O, P_2, Q_U, P_3). TThen, either the inlet flow Q_{in} or the inlet pressure P_1 is assumed as a known boundary condition and the other unknowns can be found by solving the equations.

As an example, consider that we know P_1 = 600 kPa and the valve positions are $Z_U = Z_O = 0.4$. Then with data in Table 1, we get, P_2 = 470 kPa, P_3 = 539 kPa, $\frac{\rho}{2}\left(\frac{Q_{\text{in}}}{A_{\text{in}}}\right)^2$ = 132 kPa, Q_O = 2.88 × −5 m^3/s, $Q_U = 5.99 \times 10^{-4}$ m^3/s, KE_{Uz} = 29 kPa, $\text{KE}_{U\theta}$ = 163 kPa, KE_{Oz} = 38 kPa, and $\text{KE}_{O\theta}$ = 224 kPa.

OIL DROPLET TRAJECTORY ANALYSIS

The separation efficiency of the hydrocyclone depends on the centrifugal force acting on the two fluid components (oil and water) and the frictional (drag) force acting on the dispersed oil particles. We divide our analysis into two parts: continuous phase (water) and dispersed oil phase. Two simplifying assumptions for this analysis are as follows:

A4. Axisymmetric flow.
A5. The tangential velocity is not zero at the walls.

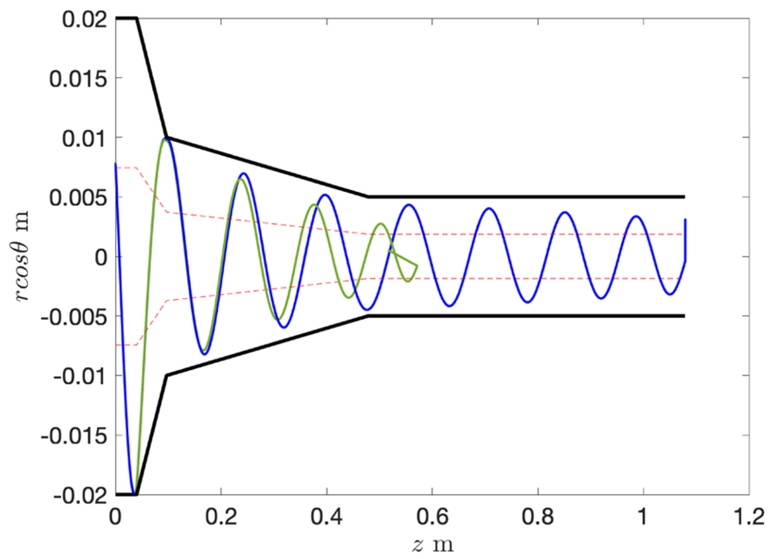

Figure 6. Simulated trajectory of 50 μm oil droplet (green), which is separated as its enters the reverse-flow zone (marked in red), and 5 μm (blue), which is not separated and comes out as underflow. The black marking represents the walls of the hydrocyclone. The picture shows a two-dimensional view of the simulation, and this is why the green line does not reverse immediately when it crosses the red line.

https://dx.doi.org/10.1021/acs.iecr.0c02859
Ind. Eng. Chem. Res. 2020, 59, 18937−18950

Continuous Phase (Water). The three velocity components of the continuous water phase are the tangential velocity $v_{\theta,\,w}$, the axial velocity $v_{z,\,w}$, and the radial velocity $v_{r,\,w}$. Here, the subscript w denotes the water phase, whereas we will use o to denote the oil phase.

Tangential Velocity. The tangential velocity profile inside the hydrocyclone exhibits a Rankine vortex-type behavior (as shown in Figure 2), where the free vortex occurs near the cyclone wall and the forced vortex occurs near the axis of the hydrocyclone.[11,12] Hence, the tangential velocity is a function of radial position; the velocity decreases as the radial position increases in the free-vortex region, and in the forced-vortex region, the velocity increases as the radial position increases. Then, based on the conservation of angular momentum, the following expression holds for the tangential velocity:

$$v_{\theta,w}(r)r^n = \text{constant}$$

Here, $v_{\theta,\,w}(r)$ is the tangential velocity at the radial position r. The value of n varies between -1 (forced vortex) and 1 (free vortex). As most of the separation takes place near the semi-free vortex region,[11] we will for simplicity use one value for n, in the region from 0.5 to 0.9.[11] The constant can be found from the known inlet velocity and inlet radius.

A tuning factor $\alpha_1 \leq 1$ is introduced to enable the calculation of the tangential velocity of the fluid at any given radial position based on the inlet velocity v_{in} and the radius of the first cylindrical part of the cyclone R_1 (see Figure 5). Hence, the tangential velocity is given as

$$v_{\theta,w}(r)r^n = \alpha_1 v_{\text{in}} R_1^n = \alpha_1 \frac{Q_{\text{in}}}{A_{\text{in}}} R_1^n \tag{9}$$

Axial Velocity. The axial velocity of the fluid in the low cone section is given as a polynomial approximation in refs 12 and 11. In our paper, the axial velocity of the continuous phase is modeled as a flow through a pipe of changing diameter. A standard flow model for a two-dimensional converging nozzle is[17]

$$v_z(z) = U_0\left(1 + \frac{z}{L}\right) \tag{10}$$

$$v_r(r) = -U_0\frac{r}{L} \tag{11}$$

Here, v_z is the axial velocity, v_r is the radial velocity, L is the length of the converging nozzle, and U_0 is the initial axial velocity. With this simple flow model, the axial velocity profile of a hydrocyclone is given below:

$$v_{z,w}(z) = V_0(z)\left(1 + \frac{z - Z}{L(z)}\right) \tag{12}$$

$$L(z) = \begin{cases} \infty & \text{if } z \leq a \\ L_2 & \text{if } a < z \leq b \\ L_3 & \text{if } b < z \leq c \\ \infty & \text{if } c < z \leq d \end{cases} \tag{13}$$

$$V_0(z) = \begin{cases} V_0 & \text{if } z \leq a \\ V_0 & \text{if } a < z \leq b \\ V_0\left(1 + \dfrac{(b-a)}{L_2}\right) & \text{if } b < z \leq c \\ V_0\left(1 + \dfrac{(b-a)}{L_2}\right)\left(1 + \dfrac{(c-b)}{L_3}\right) & \text{if } c < z \leq d \end{cases} \tag{14}$$

$$Z = \begin{cases} 0 & \text{if } z \leq a \\ a & \text{if } a < z \leq b \\ b & \text{if } b < z \leq c \\ c & \text{if } c < z \leq d \end{cases} \tag{15}$$

$$V_0 = \frac{Q_U}{\pi R_1^2} \tag{16}$$

Here, R_1 is the radius of the first cylindrical part of the hydrocyclone and Q_U is the volumetric flow rate toward the underflow.

The limits used in eqs 13−15 are marked in Figure 5. The axial flow described above is from the inlet to the underflow. However, there is a reverse-flow toward the overflow outlet, and hence the actual axial velocity will be higher than the one described by eq 16 as the total cross-sectional area is slightly smaller. Rewriting the initial velocity after considering the reverse-flow zone with a fixed radius of R_{fac} gives

$$V_0 = \alpha_2 \frac{1}{(1 - R_{fac})^2}\frac{Q_U}{\pi R_1^2} \tag{17}$$

where a tuning parameter $\alpha_2 \geq 1$ has been added to the initial velocity to capture higher tangential velocity at the inlet.

Radial Velocity. From eq 11, the radial velocity of the water is given as

$$v_{r,w}(r, z) = -V_0(z)\left(\frac{r}{L(z)}\right) \tag{18}$$

Dispersed Phase (Oil). The droplet trajectory analysis for the dispersed oil phase is done using the three velocity components $v_{r,\,o}$, $v_{\theta,\,o}$, and $v_{z,\,o}$. The oil tangential velocity $v_{\theta,\,o}$ and the axial velocity $v_{z,\,o}$ are assumed to be same as for the continuous water phase, i.e.

$$v_{\theta,o} = v_{\theta,w} \tag{19}$$

$$v_{z,o} = v_{z,w} \tag{20}$$

In the radial direction, the oil drops move relative to the continuous water phase because of the difference in the centrifugal forces, as given by the density difference $\rho_o - \rho_w$. In addition, the oil droplets have a frictional (drag) force acting on them. In our analysis, we consider this to be a quadratic drag as in ref 12. The combined effect of these forces makes the oil droplets achieve a terminal/settling velocity relative to the water phase, given as

$$v_{ter}(r) = \sqrt{\frac{4}{3}\frac{(\rho_o - \rho_w)}{\rho_o}\frac{v_{\theta,w}^2 D}{rC_D}} \tag{21}$$

https://dx.doi.org/10.1021/acs.iecr.0c02859
Ind. Eng. Chem. Res. 2020, 59, 18937−18950

where D is the diameter of oil droplet, r is the radial position of oil droplet, ρ_o is the density of the oil, ρ_w is the density of water, and C_D is the drag coefficient. Then, the total radial velocity of the dispersed oil phase is given as

$$v_{r,o} = v_{r,w} + v_{ter} \tag{22}$$

Numerical values of the hydrocyclone dimensions used in the simulations are given in Figure 5. Figure 6 shows the simulation of droplet trajectories using eqs 19, 20, 21, and 22. The black color marking in the figure represents the physical boundary of a hydrocyclone liner, the red dashed marking represents the reverse-flow zone. Here, average axial velocity $v_{z,o}$ is primarily used for calculating the residence time of the droplets in the forward-flow zone. The radial velocity $v_{r,o}$ is used for checking the droplets reaching the reverse-flow zone.

Oil droplets that enter the reverse-flow zone are considered to be separated from the water, see the green trajectory in Figure 6, which represents a 50 μm droplet. It is not necessary for our approach to calculate the internal separation (Modeling of Internal Separation section) to track the droplets after entering the reverse-flow zone, Hence, the trajectory in the figure stops abruptly after entering the reverse-flow zone. The blue marking in Figure 6 represents a trajectory of a 5 μm droplet, and this droplet is not separated as it is not able to enter the reverse-flow zone.

The simulation of droplet categories from 5 to 60 μm using trajectory models 19, 20, 21, and 22 resulted in separation of oil droplets greater than 10 μm.

MODELLING OF INTERNAL SEPARATION

In this paper, a droplet trajectory analysis is used for calculating the separation inside the cyclone. Using eqs 19−22, if an oil droplet reaches the reverse-flow zone before exiting through the underflow, then it is assumed to be separated. The separated oil moves toward the oil-rich reverse core and comes out as underflow. However, there can also exist situations where the entire oil-rich core gets filled by oil and the overflow opening is not large enough to take it out; and the excess oil has to come out through the underflow outlet. In the Dynamic Mass-Balance Model section, a simple approach to capture this scenario is described.

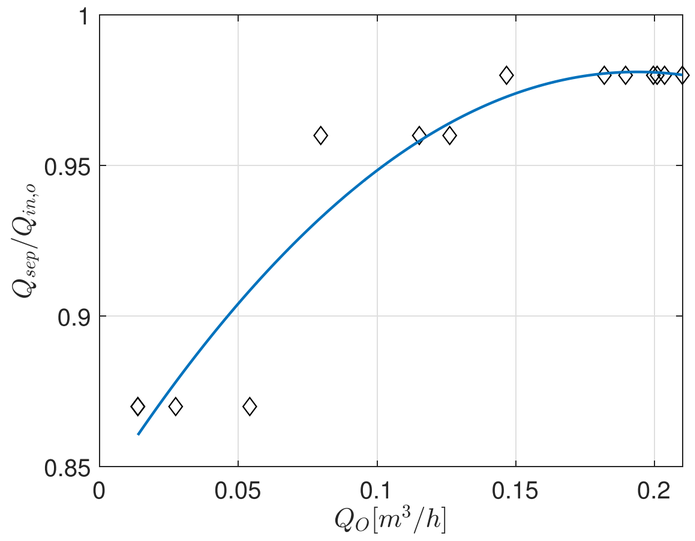

Figure 9. Internal separation $\frac{Q_{sep}}{Q_{in,o}}$ as a function of overflow rate Q_O with fixed underflow valve opening.

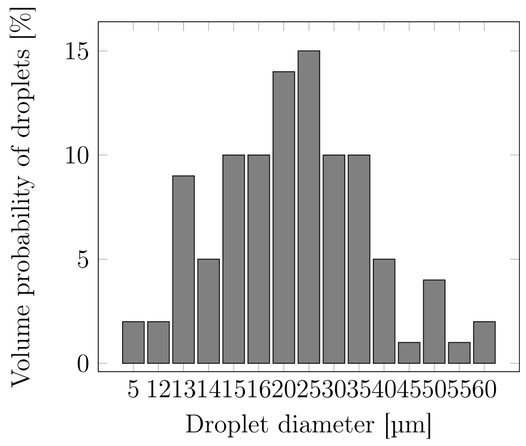

Figure 7. Sample droplet distribution at the inlet of the hydrocyclone.

The oil droplets at the inlet of a hydrocyclone are assumed to range from 5 to 60 μm.[11,18] We will assume that we know the inlet oil droplet distribution.

It is not feasible to simulate all the droplets entering the cyclone one by one (as there are too many), so we simulate a single droplet from each size category and find where it ends up. If the droplet enters the reverse-flow zone before reaching the end of the cyclone, then we assume that all droplets in that category are separated.

We make the following assumptions:

A6. A mixture with 1000 ppm oil with a droplet distribution as shown in Figure 7 enters the hydrocyclone.

A7. Droplets of 15 different diameters: 5 μm, 12 μm, 13 μm, 14 μm, 15 μm, 16 μm, 20 μm, 25 μm, 30 μm, 35 μm, 40 μm, 45 μm, 50 μm, 55 μm, and 60 μm.

A8. All the droplets have the same starting position, and droplet trajectories are tracked using eqs 19−22.

A9. Droplets reaching the reverse-flow zone are separated.

Summing up the volume fraction of droplet categories entering the reverse-flow zone gives the total fraction of the separated droplets. The separation in the hydrocyclone varies with the inflow rate; this can be either due to the variation in residence time or due to the variation of the drag force acting on the oil droplets. It is clear from eq 17 that the axial velocity is influenced by the inflow rate, and thus if the inflow rate is reduced, then the droplets get more residence time and this

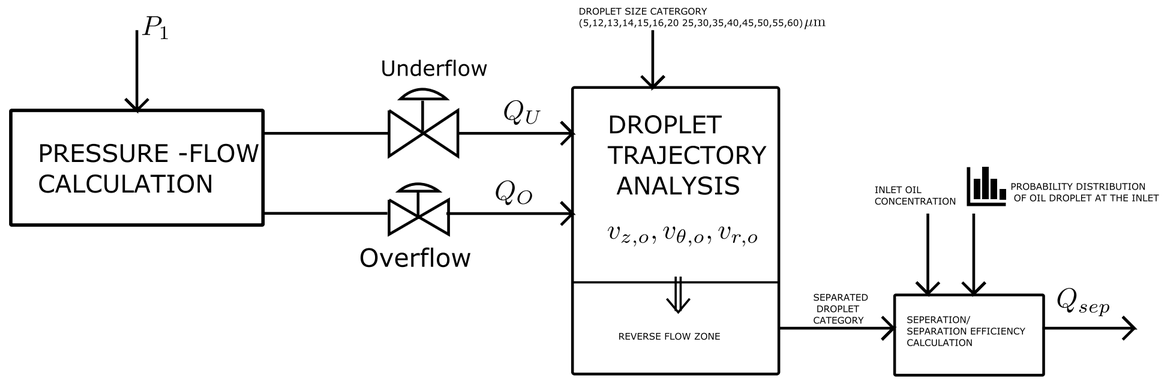

Figure 8. Diagrammatic representation of the calculation of internal separation Q_{sep} (Modeling of Internal Separation section).

https://dx.doi.org/10.1021/acs.iecr.0c02859
Ind. Eng. Chem. Res. 2020, 59, 18937−18950

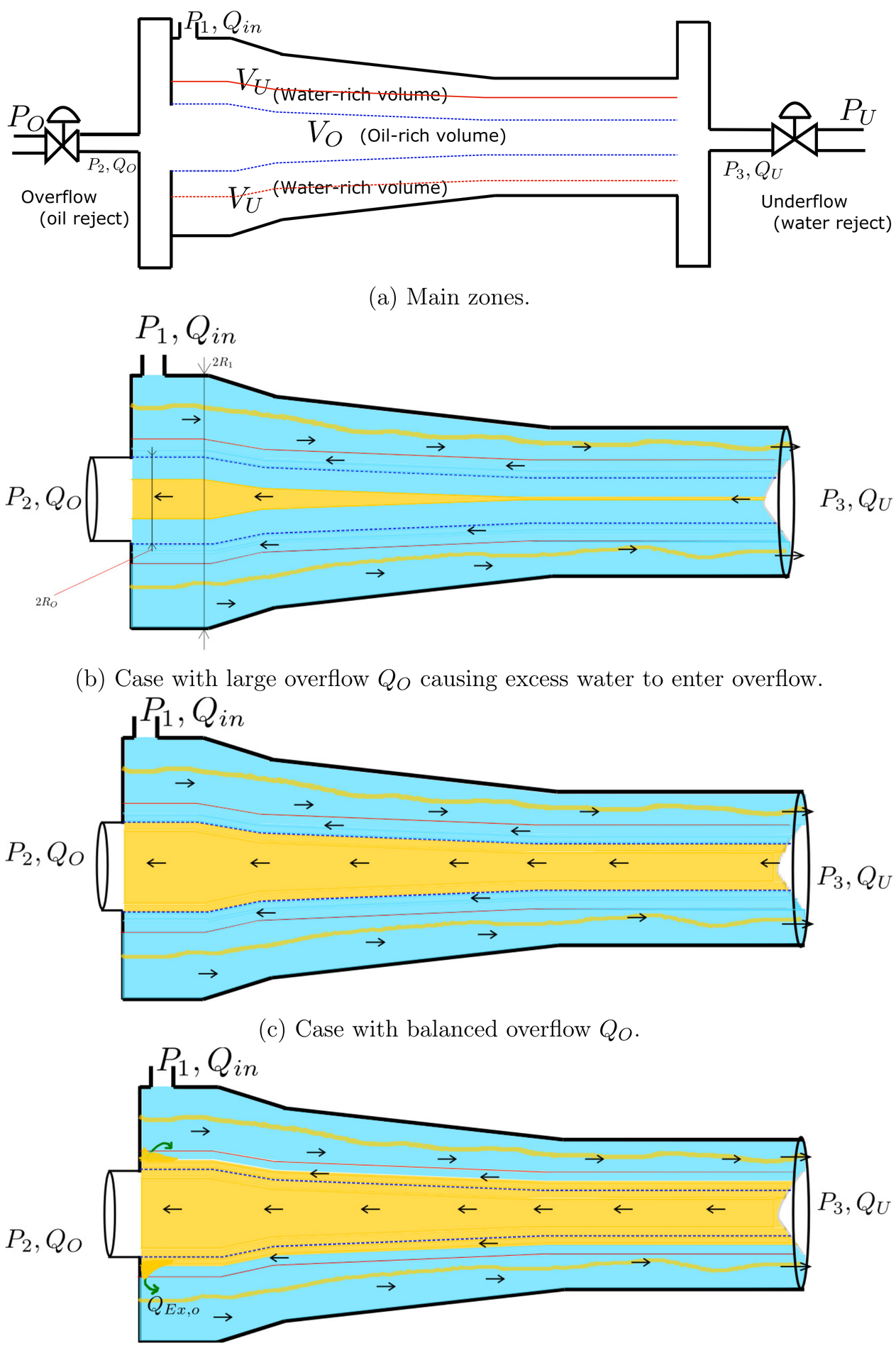

(a) Main zones.

(b) Case with large overflow Q_O causing excess water to enter overflow.

(c) Case with balanced overflow Q_O.

(d) Case when overflow Q_O is too small and excess separated oil returns (green arrows).

Figure 10. Pictorial representation of a hydrocyclone liner. The red lines represent the reverse-flow zone, yellow represents oil, and blue represents water.

increases the separation. However, a decrease in the inflow rate decreases the drag force (from eqs 9 and 22) and this decreases the separation. Hence, these two effects counteract each other, and careful analysis needs to be done based on the region of operation.

The separation can be expressed in terms of volumetric flow as $\frac{Q_{sep}}{Q_{\text{in},o}}$, where Q_{sep} is the volumetric flow rate of the separated oil inside the cyclone and $Q_{in,\ o}$ is the volumetric flow rate of the incoming oil. According to eq 8, the inflow rate of the cyclone can be varied by either changing the overflow rate or the underflow rate. We can vary the overflow rate Q_O with a fixed underflow valve opening to change the inflow rate and calculate the separation. Figure 8 summarizes the method used for calculating the internal separation. We derive an empirical relationship between the overflow rate and $\frac{Q_{sep}}{Q_{\text{in},o}}$, which can be used in a control-oriented model. We use a second-order polynomial approximation:

https://dx.doi.org/10.1021/acs.iecr.0c02859
Ind. Eng. Chem. Res. 2020, 59, 18937−18950

$$\frac{Q_{sep}}{Q_{\text{in},o}} = p_2 Q_O^2 + p_1 Q_O + p_0 \tag{23}$$

To generate the data, the overflow valve opening is changed from 1% to 100% with inlet pressure P_1 at 6 bar, fixed underflow opening at 40%, inlet oil concentration as 1000 ppm, and the droplet distribution as shown in Figure 7. The resulting data are shown by the diamonds in Figure 9. Here, $Q_O = 0.222$ m^3/h corresponds to 100% overflow valve opening. A least-squares curve fit gives $p_2 = -4.821 \times 10^7$, $p_1 = 5190$, and $p_0 = 0.8414$. Here, it is an approximation to consider that the internal separation $\frac{Q_{sep}}{Q_{\text{in},o}}$ depends only on Q_O, but the other factors (e.g., Q_U) affecting the separation are kept constant. The approximation can be expected to be valid with minor changes to these other factors.

■ DYNAMIC MASS-BALANCE MODEL

This section gives a mass-balance control-oriented model of a hydrocyclone. The hydrocyclone is divided into two virtual control volumes. First, the volume V_O at the center of the hydrocyclone is the "oil-rich volume" related to the overflow. This volume is assumed to have the same shape as the hydrocyclone as shown in Figure 10a. A second volume outside V_O is the "water-rich volume", V_U. Most of the V_U is filled with water as the expected inlet oil fraction is less than 5% of the total inflow rate. The total hydrocyclone volume is V_{HC}, and the water-rich volume is thus given as $V_U = V_{HC} - V_O$. V_O is always wholly within the reverse-flow zone, while V_U is predominantly in the forward-flow direction and partially in the reverse-flow zone. V_O and V_U are time-varying, while $V_{HC} = V_U + V_O$ is a constant.

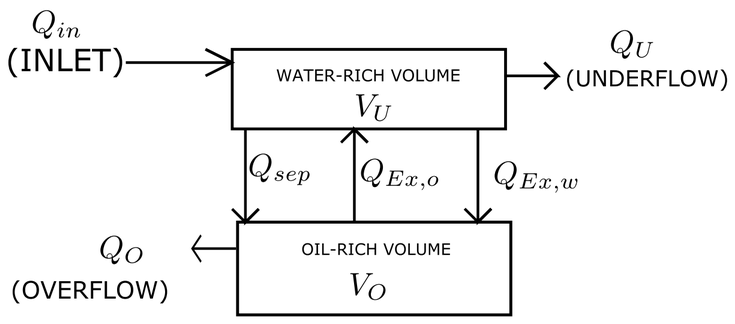

Figure 11. Simplified representation of the model.

Figures 10b–d shows how the separation of oil (yellow) and water (blue) depends on the overflow rate. Note that the hydrocyclone liners and the oil core are magnified in Figure 10 for the purpose of demonstration; in reality, they are longer and thinner. Also, the dimensions of underflow and overflow pipe section and the control valves in Figure 10a are bigger than the underflow and overflow outlets of the hydrocyclone liners. The oil droplets entering the reverse-flow zone (marked by the red color in Figure 10a–d) get separated and move toward the oil-rich volume. The droplets that are not separated remain in the water-rich volume and come out with underflow (the thin yellow line in V_U represents oil droplets that are not separated).

In Figure 10b, the overflow radius is large and the oil-rich volume V_O is not completely filled up by oil. Thus, some excess water ($Q_{Ex,\,w}$) flows from V_U to V_O to fill up the remaining space in V_O. During this period, the overflow outlet will have both water and oil. As the overflow decreases, at some point, the entire V_O is filled with oil as shown in Figure 10c. Further reduction forces separated oil into V_U, and we assume that this separated excess oil flows back to V_U (marked with green arrows in Figure 10d). This excess flow of oil ($Q_{Ex,\,o}$) (back-flow) enters the water-rich volume and comes in the underflow. It is assumed that the back-flow of oil never re-enters the oil-rich volume.

For the mass balance analysis, we consider separately the oil and the water inside the two volumes V_O and V_U and get (see Figure 11)

$$\frac{dV_{O,o}}{dt} = Q_{sep} - Q_{O,o} - Q_{Ex,o} \tag{24}$$

$$\frac{dV_{U,o}}{dt} = Q_{\text{in},o} - Q_{sep} - Q_{U,o} + Q_{Ex,o} \tag{25}$$

$$\frac{dV_{O,w}}{dt} = Q_{Ex,w} - Q_{O,w} \tag{26}$$

$$\frac{dV_{U,w}}{dt} = Q_{\text{in},w} - Q_{Ex,w} - Q_{U,w} \tag{27}$$

Here, $V_{O,\,o}$ is the volume of oil in V_O, $V_{U,\,o}$ is the volume of the oil in V_U, $V_{O,\,w}$ is the volume of water in V_O, $V_{U,\,w}$ is the volume of water in V_U, Q_{sep} is the flowrate of the separated oil entering V_O, $Q_{O,\,o}$ is the flowrate of oil at the overflow, $Q_{U,\,o}$ is the flowrate of oil at the underflow, $Q_{in,\,o}$ is the inflow rate of oil, $Q_{Ex,\,o}$ is the excess flow rate of oil (entering into V_U), $Q_{Ex,\,w}$ is the excess flow of water (entering into V_O), $Q_{O,\,w}$ is the flowrate of water at the overflow, $Q_{U,\,w}$ is the flowrate of water at the underflow, and $Q_{in,\,w}$ is the inflow rate of water.

If $\beta_{in,\,o}$ and Q_{in} are the volume fraction of oil in the feed and the total inflow rate (oil and water), respectively, then

$$Q_{\text{in},o} = \beta_{\text{in},o} Q_{\text{in}} \tag{28}$$

$$Q_{\text{in},w} = (1 - \beta_{\text{in},o}) Q_{\text{in}} \tag{29}$$

The internal separated oil is from eq 23

$$Q_{sep} = Q_{\text{in},o}(p_2 Q_O^2 + p_1 Q_O + p_0) \tag{30}$$

where Q_O is the overflow rate. The volume fractions of oil and water in the two volumes V_O and V_U are defined as

$$\beta_{O,o} = \frac{V_{O,o}}{V_O} \tag{31}$$

$$\beta_{O,w} = 1 - \beta_{O,o} \tag{32}$$

$$\beta_{U,o} = \frac{V_{U,o}}{V_U} \tag{33}$$

$$\beta_{U,w} = 1 - \beta_{U,o} \tag{34}$$

The excess oil entering V_U is

$$Q_{Ex,o} = \begin{cases} Q_{sep} - Q_O, & \text{if } Q_{sep} - Q_O > 0 \\ 0, & \text{otherwise} \end{cases} \tag{35}$$

The excess water entering V_O is

$$Q_{Ex,w} = \begin{cases} Q_O - Q_{sep}, & \text{if } Q_{sep} - Q_O < 0 \\ 0, & \text{otherwise} \end{cases} \tag{36}$$

Assuming for simplicity that the internal volumes V_O and V_U are well mixed so that the compositions in the outflows Q_O and Q_U are the same as inside, we get from definitions 31–34:

https://dx.doi.org/10.1021/acs.iecr.0c02859
Ind. Eng. Chem. Res. 2020, 59, 18937−18950

$$Q_{O,o} = \beta_{O,o} Q_O \tag{37}$$

$$Q_{U,o} = \beta_{U,o} Q_U \tag{38}$$

$$Q_{O,w} = \beta_{O,w} Q_O \tag{39}$$

$$Q_{U,w} = \beta_{U,w} Q_U \tag{40}$$

Rewriting eqs 24−27 in terms of volume fractions gives

$$\frac{d\beta_{O,o}}{dt} = \frac{1}{V_O}(Q_{sep} - \beta_{O,o} Q_O - Q_{Ex,o}) \tag{41}$$

$$\frac{d\beta_{U,o}}{dt} = \frac{1}{V_F}(Q_{in,o} - Q_{sep} - \beta_{U,o} Q_U + Q_{Ex,o}) \tag{42}$$

$$\frac{d\beta_{O,w}}{dt} = \frac{1}{V_O}(Q_{Ex,w} - \beta_{O,w} Q_O) \tag{43}$$

$$\frac{d\beta_{U,w}}{dt} = \frac{1}{V_F}(Q_{in,w} - Q_{Ex,w} - \beta_{U,w} Q_U) \tag{44}$$

The two outlet flows are given from eqs 6 and 7. Here, from eqs 31−34, we can also choose the pair 41−42 or the pair 43−44 as model equations.

■ SUMMARY OF THE MODELS

The model in this paper can be divided into three parts. The first part gives a static relationship between the pressures and the flows using Bernoulli's equations. If we know the inlet pressure and the inlet oil fraction, then the static relationship described in the Pressure-Flow Relationship section (eqs 4−8) gives the two outlet pressures (P_2 and P_3) and the two volumetric outflows (Q_U and Q_O).

The second part of the model is given in the Modeling of Internal Separation section. Here, the separation of oil droplets inside the cyclone liner is determined. A polynomial approximation of the separation as a function of overflow volumetric flow rate for use in the control-oriented model is given in eq 23. The calculation of the separation uses the droplet trajectory analysis described in the Oil Droplet Trajectory Analysis section and the pressure-flow relationship described in the Pressure-Flow Relationship section.

The third part of the model is a control-oriented dynamic mass-balance relationship of the oil fraction inside a hydrocyclone liner, and this is given in the Dynamic Mass-Balance Modelsection, see eqs 41−42. The pressure-flow relationship and the separation are used in the dynamic model for calculating the volumetric flow rate of oil. This dynamic mass-balance relationship gives the fraction of oil and water at the underflow (water) outlet ($\beta_{U,o}$, $\beta_{U,w}$) and the overflow (oil) outlet ($\beta_{O,o}$, $\beta_{O,w}$).

■ VALIDATION OF MODELS

The different parts of models are here validated against experimental data from the literature.

Validation of Pressure-Flow Relationship. The experimental results from ref.8 shows that the pressure drop from the inlet to the underflow (dP_u) is less than that from the inlet to the overflow (dP_o) and increases as the flow rate increases. Figure 12 shows the experimental result (dP_u(Exp) and dP_o(Exp)) from ref 8 and the simulation results (dP_u(Sim) and dP_o(Sim)) of eqs 4−8 in normalized axes. The simulation is done with boundary condition P_1 = 6 bar. From the plots, it can be seen that the behavior of experimental results and the simulation results is similar.

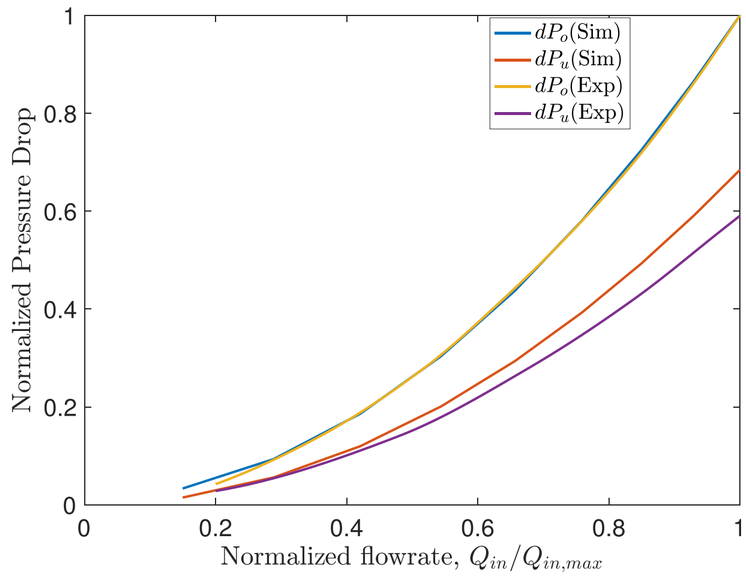

Figure 12. Pressure drop versus flow rate relationship using the experimental results (ref 8) and the simulation results of eqs 4−8.

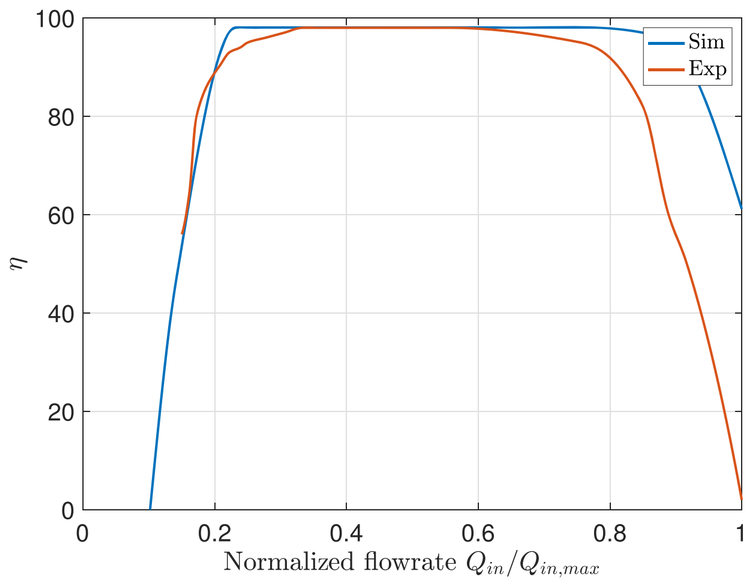

Figure 13. Experimental results (ref 8) and simulation results for efficiency η as a function of Q_{in} of de-oiling hydrocyclone with a constant overflow valve opening.

Validation of Droplet Trajectory Model. The experimental data for the separation efficiency η from ref 8 are shown in Figure 13. The separation efficiency η is defined by eq 2. We use the method described in the Modeling of Internal Separation section and summarized in Figure 8 (i.e., combining the droplet trajectory model and pressure-flow relationship) for calculating the internal separation. Here, the overflow valve is kept constant, the inlet pressure P_1 is set at 6 bar, inlet oil concentration as 1000 ppm, and the droplet distribution as shown in Figure 7. The resulting simulated separation efficiency is also shown in Figure 13. This separation efficiency is calculated using a static model without considering the excess oil flow ($Q_{Ex,o}$). Including this effect would make the efficiency drop more sharply. The separation efficiency increases with flow rate, then it remains constant for certain range of flow rate and then decreases sharply. It can be seen that the simulation results match the behavior of the experimental results.

■ DYNAMIC SIMULATION OF THE MODEL UNDER CLOSED-LOOP CONTROL

For the dynamic simulation, the underflow valve is kept at a fixed opening of 50%. (This value is not an optimal one; further investigation needs to be done to maximize the underflow rate

https://dx.doi.org/10.1021/acs.iecr.0c02859
Ind. Eng. Chem. Res. 2020, 59, 18937−18950

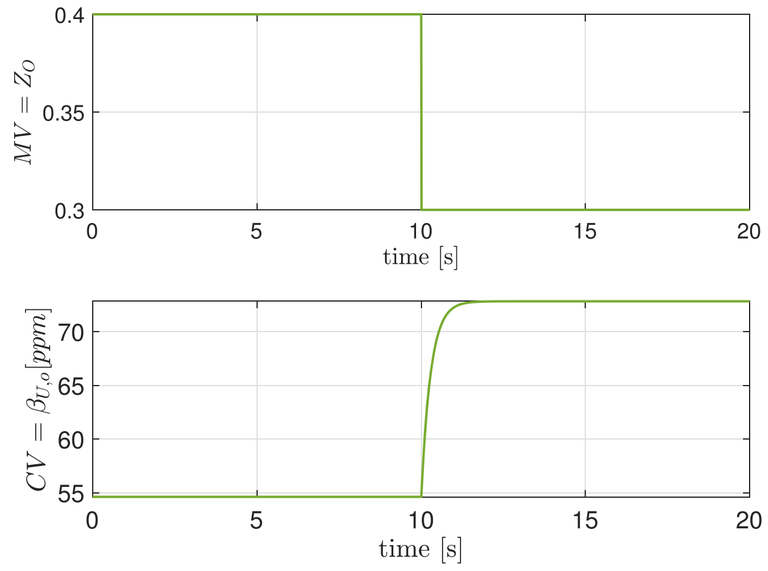

Figure 14. Dynamic effect of MV (Z_O) on the CV ($\beta_{U,\,o}$).

and keeping the oil fraction at the underflow at a minimum.) The overflow valve is used as the manipulated variable (MV) to control the oil in water ($\beta_{U,\,o}$) setpoint of 30 ppm (we assume that 30 ppm ≈ 30 mg/L). We assume that we can measure the oil-in- water concentration $\beta_{U,\,o}$ online (e.g., ref 19). Also, the results from ref 20 are promising in terms of using the oil-in-water sensor for control purposes.

Figure 14 shows the dynamic effect of a step change in the MV (Z_O) on the CV ($\beta_{U,\,o}$). This shows a first-order response with the process gain $k = -1.82 \times 10^{-4}$, process time constant $\tau_1 = 0.28$ s, and time delay $\tau_d = 0.002$ s. If we choose the closed-loop response time $\tau_c = 1.5$ s, then, based on SIMC rules,[21] we have the proportional-integral (PI) controller of the form $K_c\left(1 + \frac{1}{\tau_I s}\right)$, where $K_c = -1012$ and $\tau_I = -0.285$ s.

There are no experimental results to validate the dynamic model in the literature because most of the available data is based on pressure difference ratio (PDR) control and not giving the outlet purity $\beta_{U,\,o}$. Figure 15 shows the block diagram representation of the plant model and the controller used for the simulations. Values of different parameters used in the simulation are listed in Table 1 (we have considered a Colman and Thew's type hydrocyclone liner[11,22]), and the tuning factors used in the simulation are given in Table 2. Here, we take inlet pressure $P_1 = 6$ bar as the boundary condition.

Table 2. Values of Tuning Factors Used in the Model

tuning factor	value
α	0.175
α_2	2.67
n	0.63
$R_{fac,1}$	0.3714
$R_{fac,2}$	0.27

The proposed controller is tested in closed-loop simulations in seven plausible scenarios as shown in Figures 16–. The simulation results are also summarized in Table 3. Note that, in scenarios 1–6, all cases are operating with excess water in the oil overflow as shown in Figure 10b. Scenario 7 operates with excess oil flow to V_U. The results are discussed next.

For Scenario 1, we have an increase in the inlet oil concentration $\beta_{in,\,o}$ from 1000 to 1200 ppm. To separate this additional oil, the centrifugal force has to be increased. An increase in the inflow rate Q_{in} increases the centrifugal force and hence the separation. To increase Q_{in}, we have to increase Q_O (the underflow valve opening Z_U is fixed in the simulation). Indeed, the controller opens the overflow valve and the overflow rate increases; thus, the purity of the underflow outlet is maintained at 30 ppm.

A decrease in the inlet oil concentration (Scenario 2) naturally causes a decrease in the oil concentration in the underflow. The controller reduces the overflow opening to maintain the 30 ppm setpoint.

For Scenario 3, an increase in the underflow valve opening causes a sudden decrease in the overflow rate, which makes the separation less efficient. The controller opens the overflow valve to maintain the 30 ppm setpoint.

In the case where the underflow valve opening is decreased, the underflow rate decreases and causes a sudden increase in the overflow rate (Scenario 4). This improves separation; however, the controller reduces the overflow opening to maintain the 30 ppm setpoint.

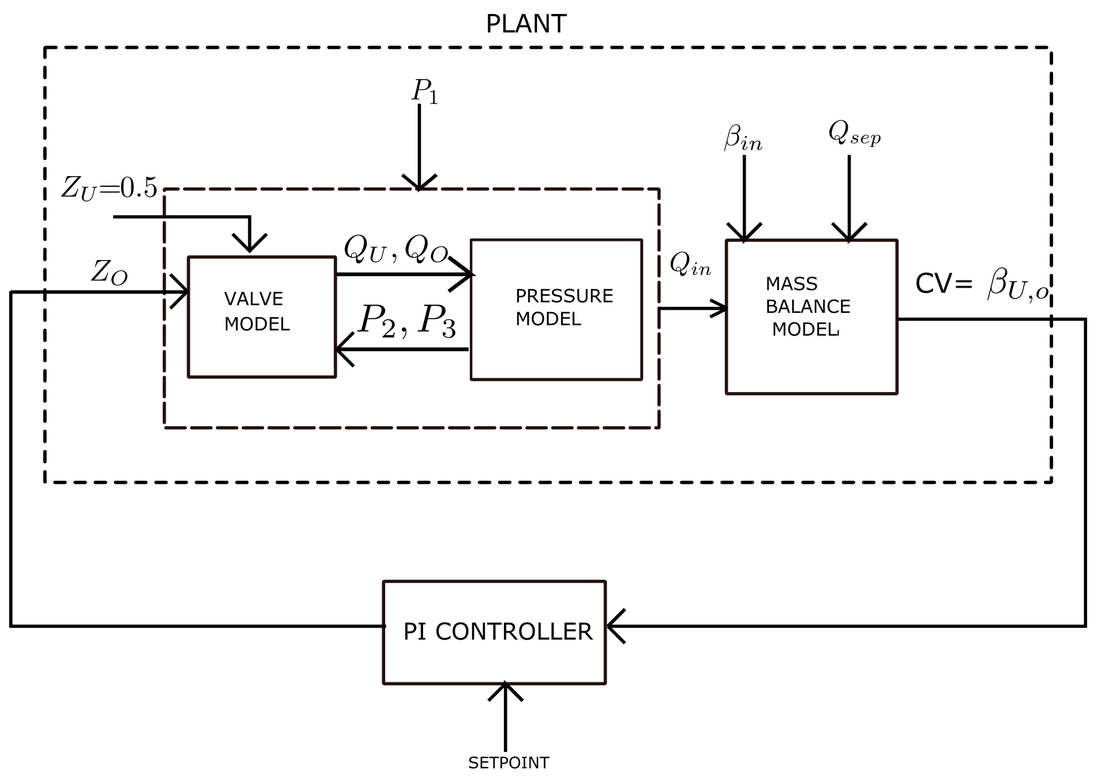

Figure 15. Control structure.

https://dx.doi.org/10.1021/acs.iecr.0c02859
Ind. Eng. Chem. Res. 2020, 59, 18937–18950

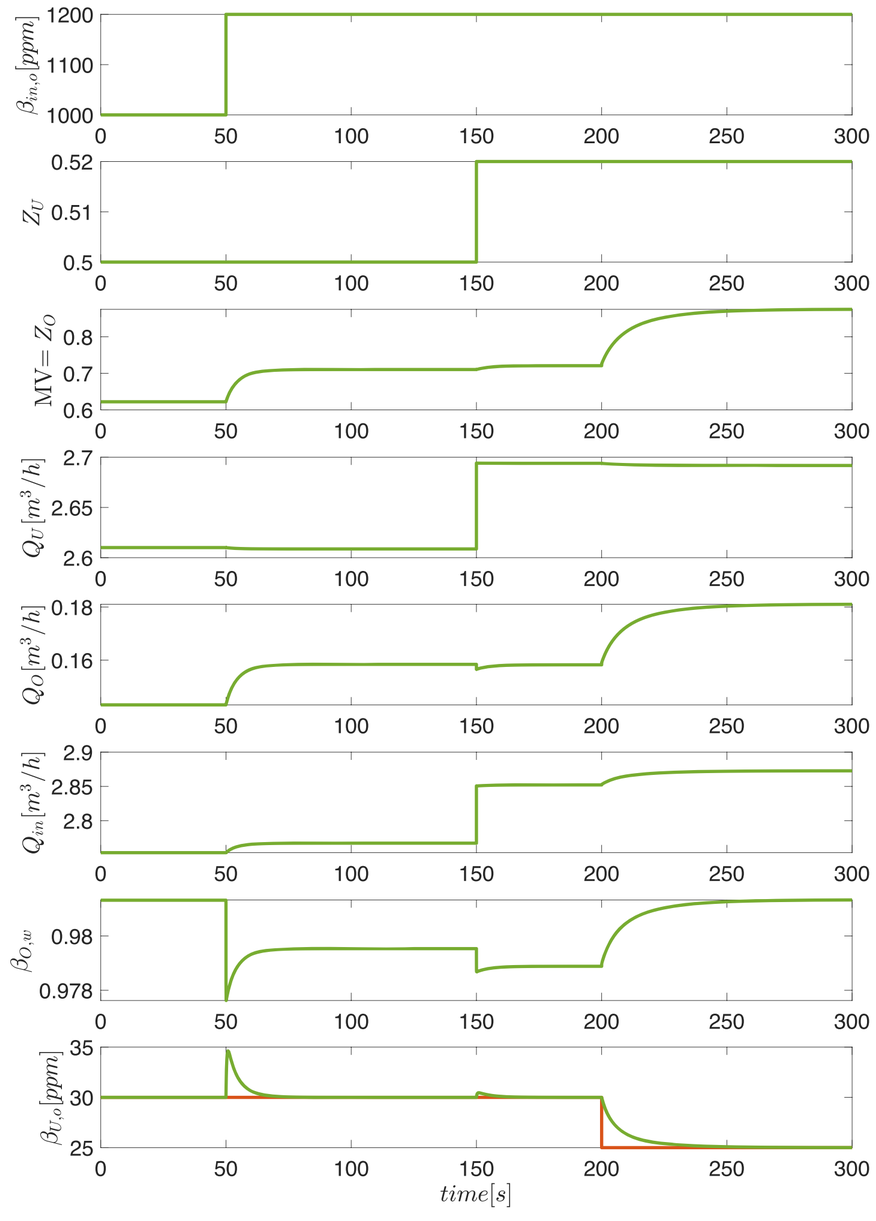

Figure 16. Simulation of control system in Figure 15 for Scenarios 1, 3, and 5; an increase in inlet oil fraction at t = 50, increase in underflow rate at t = 150, and decrease in setpoint at t = 200.

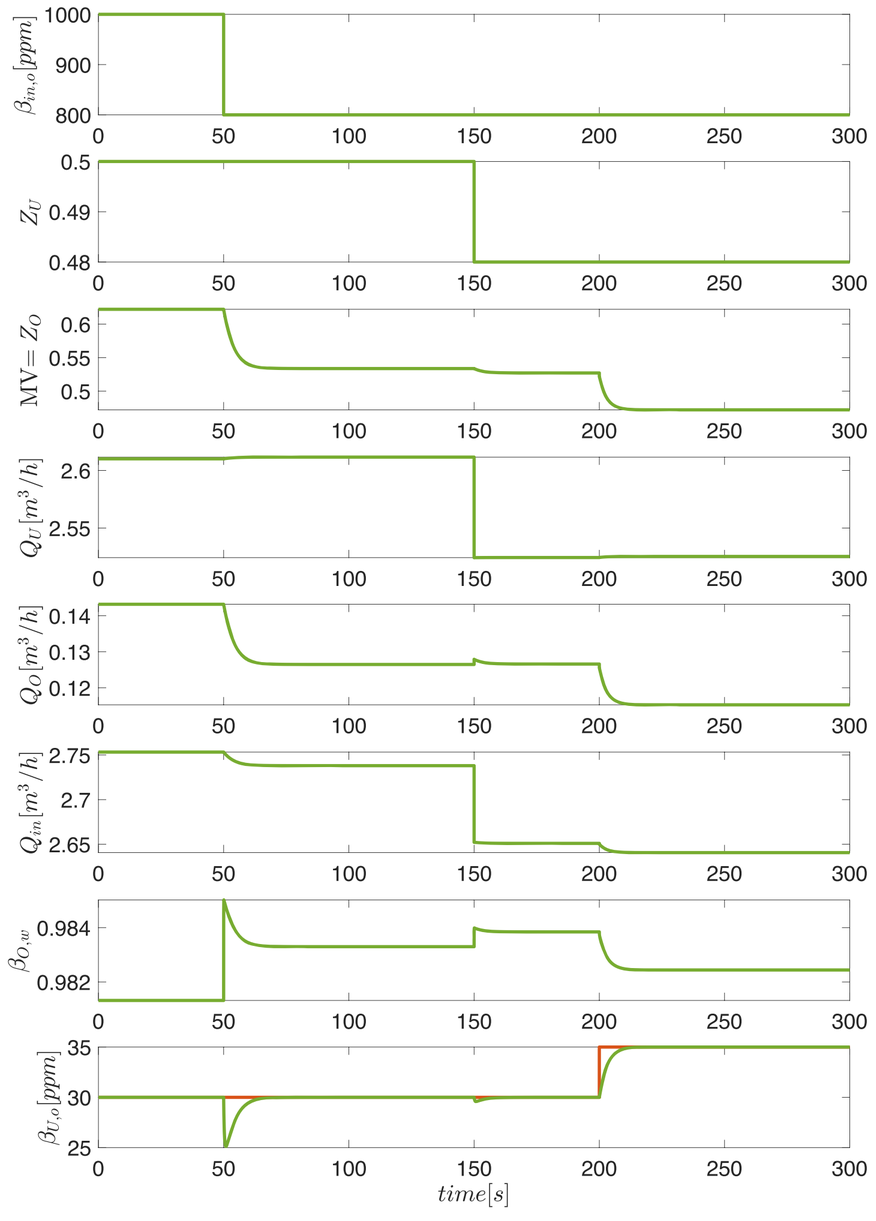

Figure 17. Simulation of control system in Figure 15 for Scenarios 2, 4, and 6 ; a decrease in inlet oil fraction at t = 50, decrease in underflow rate at t = 150, and increase in setpoint at t = 200.

Finally, Scenarios 5 and 6 consider the closed-loop response to a setpoint change. The controller tracks the setpoint change with a response time of 5 s.

In the above simulations, we have no oil back flow ($Q_{Ex,\,o} = 0$). Hence, to test the effect of excess oil flow to V_U, we start the simulation with a setpoint of 100 ppm and later at t = 50 increase the setpoint to 200 ppm. Figure 18 shows the simulation result of this scenario (Scenario 7). Here, the controller closes the overflow valve to attain the setpoint. Due to the small overflow opening, the excess oil flow back to V_U as demonstrated in Figure 10d and the fraction of water $\beta_{O,\,w}$ at the overflow becomes zero.

For Scenario 8, we do an open-loop simulation with the overflow valve at 12% opening and the underflow valve at 50% opening. The inlet oil concentration is increased from 1600 to 15,000 ppm at t = 50. Due to the increase in the inlet oil concentration, more oil flows in to V_O and fraction of water ($\beta_{O,\,w}$) becomes zero. The overflow opening is not large enough to take excess oil. Hence, the oil flow backs to V_U and $Q_{Ex,\,o} > 0$. Figure 19 shows the simulation result of this scenario (Scenario 8).

An industrial control system controls the pressure drop ratio (PDR) to maintain the efficiency of the hydrocyclones. PDR control is an indirect way of achieving the specified criteria. If there is an increase in the inlet oil concentration, then it is required to manually change the setpoint of the PDR controller to maintain the efficiency.[8] One of the future works to improve the PDR control strategy is to adjust the PDR setpoint in a cascade manner. More specifically, we propose to use the oil fraction $\beta_{U,\,o}$ (at the underflow water outlet) as the controlled variable (CV) and the PDR setpoint as the manipulated variable (MV).

■ CONCLUSIONS

A first-principles control-oriented model was developed for a de-oiling hydrocyclone. The development of the model was divided into three main parts: first, a droplet trajectory analysis for calculating the separation; second, a static pressure-flow model; and third, a dynamic mass-balance model. Combining these different gives a dynamic model, which is suitable for process control. In this paper, the proposed model uses the simplified polynomial approximation of the separation. The static models for pressure-flow relationship and the separation efficiency were qualitatively validated against the experimental results from the literature.

A PI controller was implemented to test the derived dynamic model. The simulation results show that the model gives the expected behavior for different scenarios. The goal of the controller was to keep a constant setpoint of 30 ppm oil for $\beta_{U,\,o}$ varying the overflow valve opening.

As a future work, the dynamic model is planned to be validated using experiments in a newly constructed laboratory. The model developed is non-linear in nature, giving opportunities for developing advanced non-linear control algorithms. Another future investigation is to optimize the number of hydrocyclone liners (here we have considered a single liner).

https://dx.doi.org/10.1021/acs.iecr.0c02859
Ind. Eng. Chem. Res. 2020, 59, 18937−18950

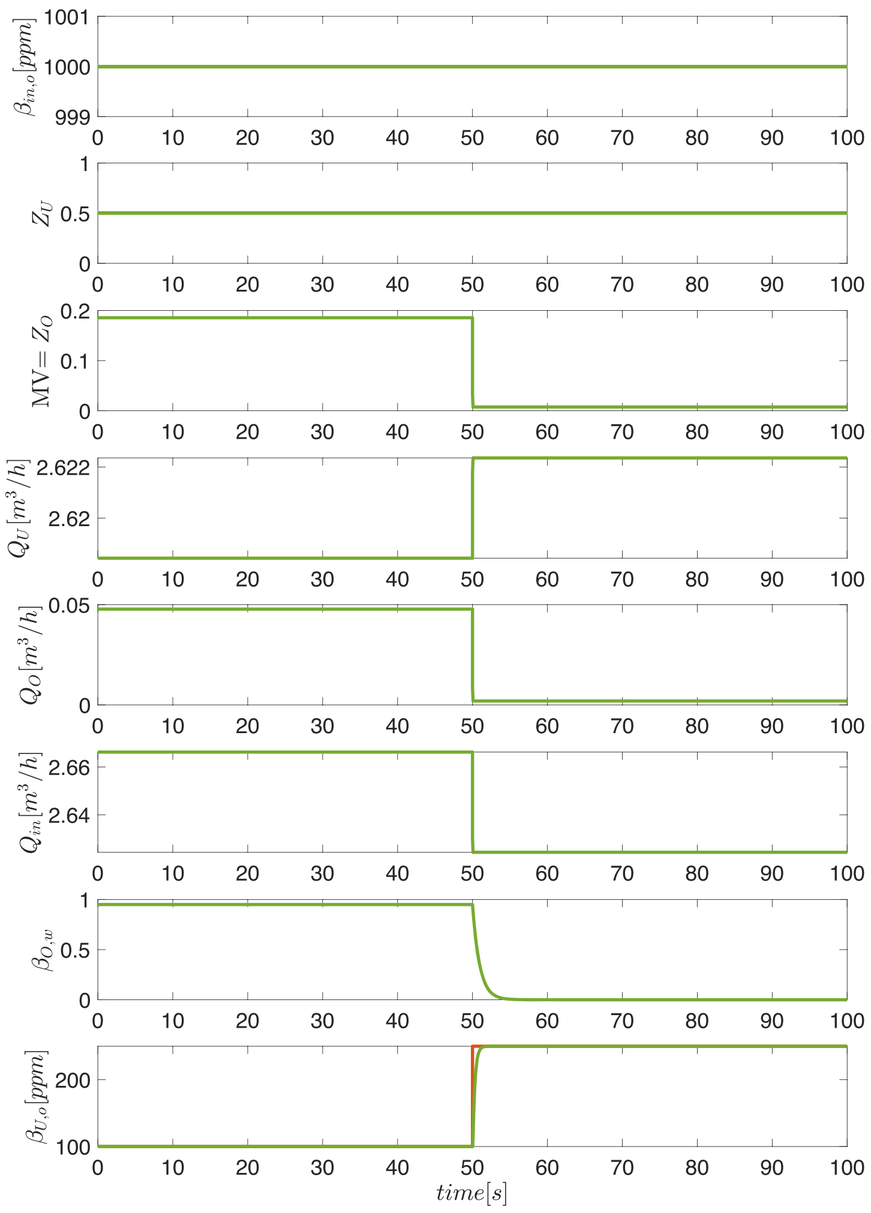

Figure 18. Simulation of Scenario 7; an increase in setpoint from 100 to 200 ppm at t = 50 causing excess oil flow $Q_{Ex,\,o}$ to V_U.

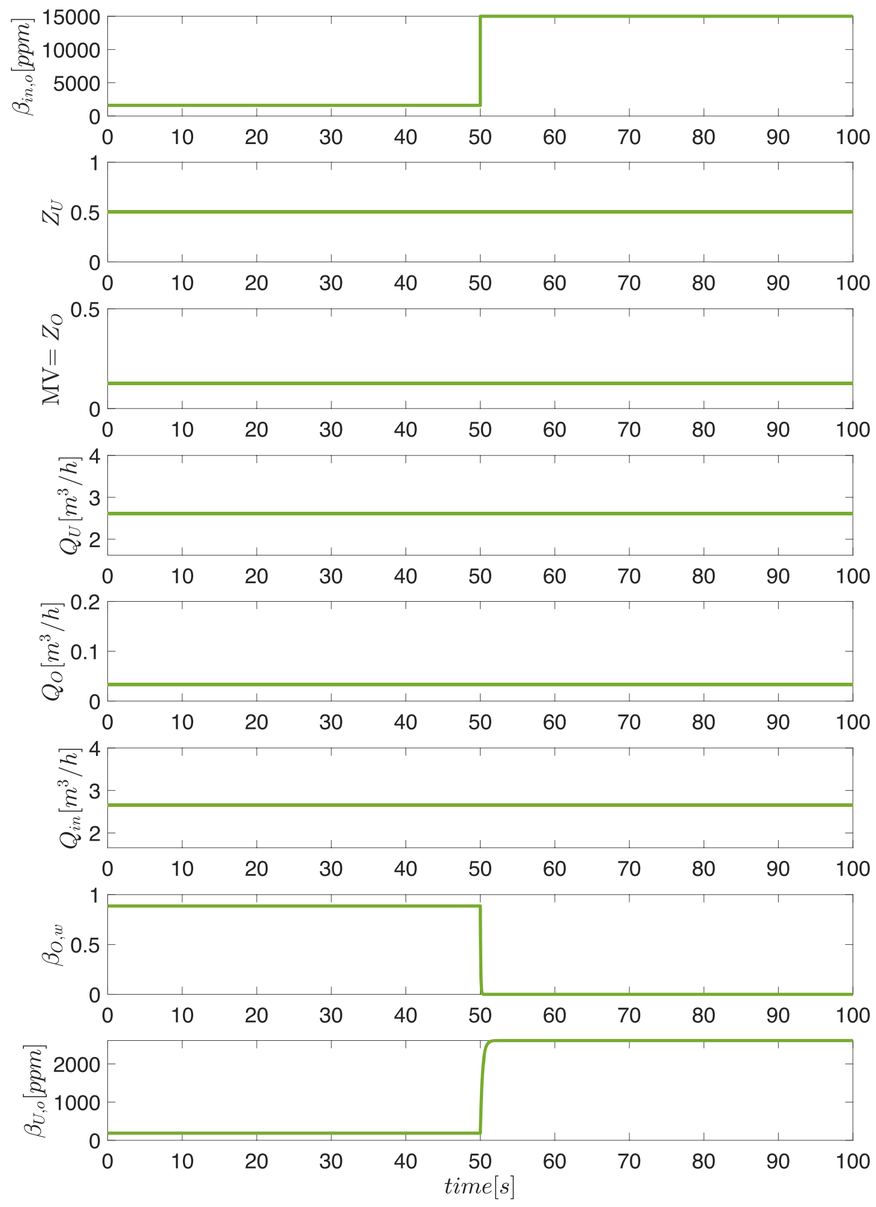

Figure 19. Simulation of Scenario 8; an open-loop simulation where the overflow valve opening is fixed at 12% and the underflow valve opening is fixed at 50% and at t = 50, $\beta_{in,\,o}$ is increased from 1600 to 15,000 ppm causing excess oil flow $Q_{Ex,\,o}$ to V_U.

APPENDIX A: TANGENTIAL KINETIC ENERGY AT THE UNDERFLOW

This appendix gives the derivation of the tangential kinetic energy ($KE_{U\theta}$) at the underflow outlet of a hydrocyclone liner. It is assumed that reverse-flow zone extends to the underflow so that the tangential velocity profile at the underflow will have a Rankine vortex profile as shown in Figure 2. Substituting $R(z)$ = R_U in Figure 2 gives the tangential profile representation at the underflow outlet.

The tangential velocity V_{t1} (shown in Figure 2) of the fluid at the free vortex part is

$$V_{t1} = \frac{a_1}{r} \tag{45}$$

Table 3. Discussion of Simulation Results in Figures 16−19

#	description	behavior of the controller
1	Increase in inlet oil concentration (from 1000 to 1200 ppm).	The controller opens up the overflow control valve and the overflow rate Q_O increases.
2	Decrease in inlet oil concentration (from 1000 to 800 ppm).	Due to the criteria of 30 ppm as a setpoint, the controller reduces the overflow rate to achieve the setpoint.
3	Increase in underflow rate by opening the underflow valve from 50% to 52%.	The controller opens the overflow valve, which increases the overflow rate, which in turn reduces the underflow rate.
4	Decrease in underflow rate by closing the underflow valve from 50% to 48%.	Controller closes the overflow valve to attain the setpoint, though the reduction in ppm at the underflow is a desired scenario.
5	Decrease in setpoint (from 30 to 25 ppm).	The controller tracks the setpoint change with a response time of 5 s.
6	Increase in setpoint (from 30 to 35 ppm).	The controller tracks the setpoint change with a response time of 5 s.
7	A change in setpoint from 100 to 200 ppm to test the excess oil flow to V_U.	To achieve the setpoint of 200 ppm overflow valve closes, the small opening of overflow outlet causes backflow of oil to V_U and $\beta_{O,\,w}$ becomes zero.
8	A change in inlet oil fraction from 1600 to 15,000 ppm to test the excess oil flow to V_U.	The simulation is done in open loop with overflow control valve at 12% opening and underflow control valve at 50% opening. As the overflow opening is not large enough to take out the increase of oil due to change in the inlet oil concentration, the excess oil flows back to V_U, making $Q_{Ex,\,o} > 0$.

https://dx.doi.org/10.1021/acs.iecr.0c02859
Ind. Eng. Chem. Res. 2020, 59, 18937−18950

The tangential velocity V_{t2} (shown in Figure 2) of the fluid at the forced vortex part is

$$V_{t2} = a_2 r \tag{46}$$

Here, r represents the radial distance of the vortex from the center, and a_1 and a_2 are proportionality constants. The computation of constant a_1 can be done using eq 9 where n = 1 and also taking the inlet velocity v_{in} and the radius of the first cylindrical part of the cyclone R_1 as

$$a_1 = \alpha_1 \frac{Q_{in} R_1}{\pi R_{in}^2} \tag{47}$$

Peak tangential velocity occurs at the boundary of the reverse-flow zone as shown in Figure 2, and V_{t1} and V_{t2} are equal at $R_{U,\,rev} = R_{fac,2} R_U$:

$$a_2 R_{U,rev} = \frac{a_1}{R_{U,rev}} \rightarrow a_2 = \frac{a_1}{R_{U,rev}^2} \tag{48}$$

Then, the average kinetic energy contributed by the tangential velocity is given as

$$\begin{aligned} \mathrm{KE}_{U\theta} &= \frac{\rho_U}{2} \frac{1}{A_U} \left[\int_0^{2\pi} \int_{R_{U,rev}}^{R_U} \left(\frac{a_1}{r} \right)^2 \mathrm{d}A \right. \\ &\quad \left. + \int_0^{2\pi} \int_0^{R_{U,rev}} (a_2 r)^2 \mathrm{d}A \right] \\ &= \frac{\rho_U}{2} \frac{2}{R_U^2} \left[\int_{R_{U,rev}}^{R_U} \left(\frac{a_1}{r} \right)^2 r \mathrm{d}r + \int_0^{R_{U,rev}} (a_2 r)^2 r \mathrm{d}r \right] \\ &= \frac{\rho_U}{2} \frac{2}{R_U^2} \left[a_1^2 (\ln(R_U) - \ln(R_{U,rev})) + \frac{a_2^2}{4} R_{U,rev}^4 \right] \\ &= \frac{\rho_U}{2} \frac{2}{R_U^2} \left[a_1^2 (\ln(R_U) - \ln(R_U R_{fac,2})) + \frac{a_2^2}{4} R_{U,rev}^4 \right] \end{aligned}$$

The difference $\ln(R_U) - \ln(R_U R_{fac,2}) \in [0.9,1.3]$ (approximated as 1) when the $R_{fac,2} \in [0.27,0.4]$. Hence

$$\mathrm{KE}_{U\theta} = \frac{5}{4} \frac{\rho_U}{R_U^2} \frac{(\alpha_1 Q_{in} R_1)^2}{\pi^2 R_{in}^4}$$

APPENDIX B: TANGENTIAL KINETIC ENERGY AT THE OVERFLOW

This appendix gives the derivation of the tangential kinetic energy ($\mathrm{KE}_{O\theta}$) at the overflow outlet of a hydrocyclone liner. The tangential velocity at the overflow has only the forced vortex part of the Rankine vortex and hence tangential velocity is given by eq 46. Then, the average kinetic energy contributed by this tangential velocity is given as

$$\begin{aligned} \mathrm{KE}_{O\theta} &= \frac{\rho_O}{2} \frac{1}{A_O} \left[\int_0^{2\pi} \int_0^{R_O} (a_2 r)^2 \mathrm{d}A \right] \\ &= \frac{\rho_O}{R_O^2} \left[\int_0^{R_O} (a_2 r)^2 r \mathrm{d}r \right] = \frac{\rho_O}{R_O^2} \left[\int_0^{R_O} \left(\frac{a_1}{R_{U,rev}^2} \right)^2 r^3 \mathrm{d}r \right] \\ &= \frac{\rho_O}{4} \frac{(\alpha_1 Q_{in} R_1)^2}{(\pi R_{in}^2)^2 R_{U,rev}^4} R_O^2 \end{aligned}$$

AUTHOR INFORMATION

Corresponding Authors

Mishiga Vallabhan K G − *Department of Mechanical and Industrial Engineering, NTNU Norwegian University of Science and Technology, Trondheim 7491, Norway;* orcid.org/0000-0002-5722-0851; Email: mishiga.vallabhan@ntnu.no

Christian Holden − *Department of Mechanical and Industrial Engineering, NTNU Norwegian University of Science and Technology, Trondheim 7491, Norway;* Email: christian.holden@ntnu.no

Sigurd Skogestad − *Department of Chemical Engineering, NTNU Norwegian University of Science and Technology, Trondheim 7481, Norway;* Email: sigurd.skogestad@ntnu.no

Complete contact information is available at: https://pubs.acs.org/10.1021/acs.iecr.0c02859

Notes

The authors declare no competing financial interest.

ACKNOWLEDGMENTS

This project is supported by the Norwegian Research Council, industrial partners, and NTNU under the Subsea Production and Processing (SUBPRO) SFI program.

REFERENCES

(1) OSPAR *Discharges, OSPAR convention*; 2001https://www.ospar.org/work-areas/oic/discharges, (accessed Sep 23, 2020).

(2) Georgie, W. J. *Effective and Holistic Approach to produced Water Management for Offshore Operation*; Offshore Technology Conference: Houston, Texas, 2002; 13.

(3) Orlowski, R.; Euphemio, M. L. L.; Euphemio, M. L.; Andrade, C. A.; Guedes, F.; da Silva, L. C. T.; Pestana, R. G.; de Cerqueira, G.; Lourenço, I.; Pivari, A.; Witka, A.; Folhadella, H.; Pacheco, L.; Kronemberger, S.; Vilela, J. *Marlim 3 Phase Subsea Separation System - Challenges and Solutions for the Subsea Separation Station to Cope with Process Requirements*; Offshore Technology Conference: Houston, Texas, USA, 2012; 11.

(4) Pereira, R. M.; de Campos, M. C. M. M.; de Oliveira, D. A.; de Souza, R. d. S. A.; Filho, M. M. C.; Orlowski, R.; Duarte, D. G.; Raposo, G. M.; Lillebrekke, C.; Ljungquist, D.; Carvalho, A.; Fares, M. *SS: Marlim 3 Phase Subsea Separation System: Controls Design Incorporating Dynamic Simulation Work*; Offshore Technology Conference: Houston, Texas, USA, 2012; 13.

(5) Svarovsky, L.; Thew, M. *Hydrocyclones: analysis and applications*; Springer Science & Business Media: 2013; *12*.

(6) Colman, D.; Thew, M.; Corney, D. Hydrocyclones for oil/water separation. In *Int. Conf. on Hydrocyclones*; 1980; 143−165.

(7) Thew, M. Hydrocyclone redesign for liquid-liquid separation. *Chem. Eng. (London)* **1986**, 17−23.

(8) Meldrum, N. Hydrocyclones: A Solution to Produced-Water Treatment. *SPE Prod. Eng.* **1988**, *3*, 669−676.

(9) Thew, M. *Encyclopedia of Separation Science*; Elsevier: 20004; 1480−1490.

(10) Das, T.; Jäschke, J. Modeling and control of an inline deoiling hydrocyclone. In *3rd IFAC Workshop on Automatic Control in Offshore Oil and Gas Production OOGP*; 2018, *51*, 138−143.

(11) Wolbert, D.; Ma, B.-F.; Aurelle, Y.; Seureau, J. Efficiency estimation of liquid-liquid Hydrocyclones using trajectory analysis. *AIChE J.* **1995**, *41*, 1395−1402.

(12) Caldentey, J.; Gomez, C.; Wang, S.; Gomez, L.; Mohan, R.; Shoham, O. Oil/water separation in liquid/liquid hydrocyclones (LLHC): Part 2-Mechanistic modeling. *SPE J.* **2002**, *7*, 362−372.

(13) Motin, A. Theoretical and numerical study of swirling flow separation devices for oilwater mixtures. Ph.D. thesis, Michigan State University, 2015.

(14) Kharoua, N.; Khezzar, L.; Nemouchi, Z. CFD Simulation of Liquid-Liquid Hydrocyclone: Oil/Water Application. In *Fluids Engineering Division Summer Meeting*; 2009; 2085−2094.
(15) Durdevic, P.; Pedersen, S.; Bram, M.; Hansen, D.; Hassan, A.; Yang, Z. Control oriented modeling of a de-oiling hydrocyclone. In *17th IFAC Symposium on System Identification SYSID* 2015; *48*, 291−296.
(16) Bram, M. V.; Hansen, L.; Hansen, D. S.; Yang, Z. Hydrocyclone Separation Efficiency Modeled by Flow Resistances and Droplet Trajectories. In *3rd IFAC Workshop on Automatic Control in Offshore Oil and Gas Production*; 2018, *51*, 132−137.
(17) White, F. *Fluid Mechanics; McGraw-Hill series in mechanical engineering*; McGrawHill: 2011; *4*, 283.
(18) Young, G. A. B.; Wakley, W. D.; Taggart, D. L.; Andrews, S. L.; Worrell, J. R. Oil-water separation using hydrocyclones: An experimental search for optimum dimensions. *J. Pet. Sci. Eng.* **1994**, *11*, 37−50.
(19) Mirmorax *Oil-in-water analyzer*; https://mirmorax.com/oil-in-water-analyzer/, (accessed Sep 23, 2020).
(20) Durdevic, P.; Raju, C.; Bram, M.; Hansen, D.; Yang, Z. Dynamic Oil-in-Water Concentration Acquisition on a Pilot-Scaled Offshore Water-Oil Separation Facility. *Sensors* **2017**, *17*, 124.
(21) Skogestad, S. Simple analytic rules for model reduction and PID controller tuning. *J. Process Control* **2003**, *13*, 291−309.
(22) Gomez, C.; Caldentey, J.; Wang, S.; Gomez, L.; Mohan, R.; Shoham, O. Oil/water separation in liquid/liquid hydrocyclones (LLHC): Part 1-Experimental investigation. *Spe J.* **2002**, *7*, 353−372.

https://dx.doi.org/10.1021/acs.iecr.0c02859
Ind. Eng. Chem. Res. 2020, 59, 18937−18950

Chapter 4

Model-based and simple controllers

In this chapter we discuss new control schemes for de-oiling hydrocyclones which can improve the separation and regulates the oil concentration of the underflow (water reject) to 30 ppm. A simulation study of these controllers is done in this chapter. Here, we propose two simple control schemes, which act as supervisory layer to the traditional PDR control: a cascade control scheme and a feed-forward control scheme. Three model-based controllers were also derived for the hydrocyclones, based on the control-oriented model in Chapter 3: a model predictive controller, a feedback linearization controller and a sliding mode controller. All three model- based control schemes assume that the oil concentration at the underflow and the overflow can be measured.

4.1 Feedforward, cascade and model predictive control algorithms for de-oiling hydrocyclones.

The citation of the published article is given below:

Vallabhan K.G. M, Matias, J., and Holden, C. (2021) *Feedforward, cascade and model predictive control algorithms for de-oiling hydrocyclones: Simulation study.* Modelling, Identification and Control, 42(4) pp. 185-195, . https://www.mic-journal.no/ABS/MIC-2021-4-4.asp/

The preprint version of the paper follows.

Feedforward, cascade and model predictive control algorithms for de-oiling hydrocyclones: Simulation Study.

Mishiga Vallabhan K G [1] Jose Matias [2] Christian Holden [1]

[1] *Department of Mechanical and Industrial Engineering, Norwegian University of Science and Technology, N-7491 Trondheim, Norway. E-mail:*{mishiga.vallabhan,christian.holden}@ntnu.no

[2] *Department of Chemical Engineering, Norwegian University of Science and Technology, N-7491 Trondheim, Norway. E-mail:* {jose.o.a.matias}@ntnu.no

Abstract

Maintaining the efficiency of the produced-water treatment system is important for the oil and gas industry, especially taking into consideration the environmental impact caused of the produced-water. De-oiling hydrocyclones are one of the most common type of equipment used in the produced-water treatment system. The low residence time of this device makes it difficult for a control system to maintain efficiencies at different plant disturbances. In this paper, a control-oriented hydrocyclone model with a traditional pressure drop ratio (PDR) controller is analysed, and the inability of the PDR controller to maintain the efficiency when increasing the inlet concentration is shown experimentally as well as in simulation. Then, we propose three control schemes for dealing with this issue: a feed-forward, a feed-back/cascade and a model predictive controller. We show in simulation that all proposed schemes are able to improve and maintain the efficiency of hydrocyclones considering the upstream disturbances, such as variations in inlet oil concentrations and inflow rates. We also discuss the characteristics of the three methods and propose guidelines for choosing the appropriate scheme based on the available resources at the industrial site (such as measurements, hardware and software at hand).

Keywords: De-oiling hydrocyclones, Control Schemes, Simulation

1 Introduction

The treatment of produced-water (naturally occurring water that comes out of the ground along with oil and water) is an inevitable process in oil and gas production facilities. In Norway, for example, nearly 160×10^6 m^3 of this waste stream are discharged annually, which corresponds to a potential release of 1900 tonnes of crude oil to sea (Beyer et al., 2019). Traditionally, the produced-water is re-injected into the well. However, the constant increase of the wastewater volumes and the associated costs make this choice debatable. On the other hand, the water can be discharged into the sea if the oil is separated beforehand. Processes such as membrane filtration, compact flotation units and separation through hydrocyclones can be used for this end. The challenge then becomes guaranteeing that they operate efficiently, complying with the requirements set out in local regulations.

Among the disposal alternatives, hydrocyclones are specially suited for offshore sites. They are compact, light, and do not require any additional chemicals or gases to be injected for the operation. Moreover, they have already been successfully implemented in subsea below 800 m (Orlowski et al., 2012). The main problem

http://dx.doi.org/10.4173/doi:10.4173/

with this alternative is the hydrocyclones low residence times, which makes them more susceptible to upstream variations such as frequent changes in inlet oil concentration, inflow rate, etc. Typically, control schemes that use pressure drop ratio (PDR) to control the separation are implemented to reject these disturbances. Since this is an indirect way of controlling the hydrocyclones, this option can reduce their efficiency significantly and result in violations of the environmental requirements.

In this paper, we propose three new control schemes that take into consideration disturbances such as inlet oil concentration and inflow rate. Two of the proposed approaches, one based on feed-forward and another on feedback/cascade schemes, automatically adjust the setpoint of the PDR controller based on the current disturbance. The third one uses model predictive control to minimize the variation of underflow concentration from a reference value. We also discuss the pros and cons of the alternatives and provide an assessment of the possible implementation issues.

1.1 Previous work

The control aspects of hydrocyclones have been gaining more and more focus in recent years. A control-oriented approach based on transfer functions models using experimental data from a test rig was developed by Durdevic et al. (2015). Then, a grey box static model to calculate the separation efficiency of hydrocyclones based on flow resistance and droplet trajectory was developed by Bram et al. (2018). A control-oriented model for de-oiling hydrocyclone with a swirl element was developed by Das and Jäschke (2018). In Bram et al. (2020), a virtual flow resistance model with an extended trajectory model was developed and performance of hydrocyclone was compared using the model and experimental data from a scaled pilot plant. A first-principles model for de-oiling hydrocyclones based on pressure-flow relationship, separation efficiency and dynamic mass balance was developed by Vallabhan et al. (2020).

Husveg et al. (2007) studied the performance of hydrocyclones to varying inflow rates and emphasised that adequate operational control of hydrocyclone is necessary to maintain efficiency. Considering a first stage gravity separator and a hydrocyclone as a single plant, a robust control strategy was proposed by Durdevic and Yang (2018) and a model predictive control was proposed by Hansen et al. (2018). Later, nonlinear model based control algorithms to improve the efficiency of hydrocyclones were proposed by Vallabhan and Holden (2020).

When the hydrocyclones are connected to bulky first stage gravity separators, the rate of change of disturbances at the inlet of hydrocyclones are expected to be less frequent and of relatively low amplitude. However, when we move towards compact separation at subsea, e.g., Marlim fields in Brazil (Pereira et al., 2012), pipe separators are used upstream of the hydrocyclones. Due to the compactness of this type of separators, the hydrocyclones will be subjected to frequent changes in inlet oil concentration, oil droplet distributions, inflow rates etc. Consequently, the dynamics are faster and difficult to control. The existing control schemes for hydrocyclones uses an indirect pressure drop ratio to control the separation of hydrocyclones. PDR control scheme works well if the disturbance is in the inflow rate of the hydrocyclones as it gets reflected in the pressure drop. However, the PDR control scheme cannot detect the changes such as inlet oil concentration and inlet oil distribution. Hence, it is necessary to address these variations when we are designing a control system for hydrocyclones (produced-water treatment) subsea.

2 Hydrocyclone model

This section gives a brief description of the hydrocyclone model that is used as the "true" system for studying the different control schemes proposed in this paper. The model is based on Vallabhan et al. (2020). A simplified diagram of a hydrocyclone liner and a block diagram representation of a control-oriented model for hydrocyclone is shown in Figure 1.

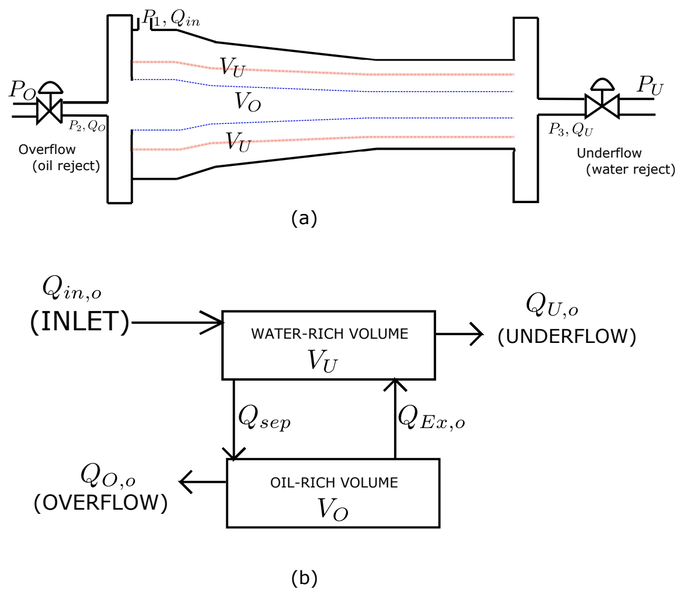

Figure 1: Simplified diagram of a hydrocyclone liner representing the 'oil-rich volume' (V_O) and the 'water-rich volume' (V_U) (shown in (a)) and a block diagram representation of a control-oriented model making use (V_O) and (V_U) (shown in (b))

We divide the hydrocyclone liners into two volumes: one is the 'oil-rich volume' (V_O) and the other is the

'water-rich volume' (V_U). The oil droplets entering the reverse-flow zone (between the red lines in Figure 1) go to the oil-rich volume and leave the system at the overflow outlet. The remaining oil in the water-rich volume comes out at the underflow outlet. A simple mass bass balance formulation is used to model the inflow and outflow of the oil inside the volumes. Since the oil density is assumed constant, we write the mass balances as

$$\begin{aligned} \frac{dV_{O,o}}{dt} &= Q_{sep} - Q_{O,o} - Q_{Ex,o}, \\ \frac{dV_{U,o}}{dt} &= Q_{in,o} - Q_{sep} - Q_{U,o} + Q_{Ex,o}. \end{aligned} \tag{1}$$

where $V_{O,o}$ is the volume of oil in the oil-rich volume V_O ; $V_{U,o}$ is the volume of the oil in the water-rich volume V_U; Q_{sep} is the flowrate of the separated oil entering V_O; $Q_{O,o}$ is the flowrate of oil at the overflow; $Q_{Ex,o}$ is the excess flowrate of oil entering V_U (which is the case when the overflow opening is small and V_O is filled with oil); $Q_{in,o}$ is the inflow rate of oil; and $Q_{U,o}$ is the flowrate of oil at the underflow. Here all the volumes are expressed in [m^3] and flowrates in [m^3/h]. The parameters of hydrocyclone liners used in this paper is same as in Vallabhan et al. (2020).

The internal separation is expressed in terms of volumetric flow and given as $\frac{Q_{sep}}{Q_{in,o}}$. In Vallabhan et al. (2020), a droplet trajectory analysis is used to calculate the internal separation. Oil droplets of different size categories are tracked using their axial, tangential and radial velocity components. If the droplets cross the reverse-flow zone boundary (shown in red in Figure 1)) inside the hydrocyclone liner, they are assumed to be separated. The authors use a polynomial approximation to compute the internal separation $\frac{Q_{sep}}{Q_{in,o}}$. In this work, we use the same polynomial approximation model to calculate the internal separation under the assumption that we know the inflow rate and its value is between 1.5 m^3/h and 3.5 m^3/h. This approximation for internal separation is given as:

$$\frac{Q_{sep}}{Q_{in,o}} = p_2 Q_O^2 + p_1 Q_O + p_0. \tag{2}$$

where $p_2 = -9.447\text{e}7$, $p_1 = 9024$, $p_0 = 0.7648$. Here, the other factors, such as underflow rate Q_U, that affect the separation are kept constant and, hence,the separation is assumed to be only a function of overflow rate Q_O.

The excess oil entering V_U is computed as:

$$Q_{Ex,o} = \begin{cases} Q_{sep} - Q_O, & \text{if } Q_{sep} - Q_O > 0 \\ 0, & \text{otherwise} \end{cases}. \tag{3}$$

The volume fractions of oil in the two volumes V_O and V_U are defined as:

$$\beta_{O,o} = \frac{V_{O,o}}{V_O}, \quad \beta_{U,o} = \frac{V_{U,o}}{V_O}. \tag{4}$$

For simplicity, we assume that the internal volumes V_O and V_U are well mixed, which implies that the compositions in the outflows Q_O and Q_U are the same as the internal compositions. Then, we get from the definition of Eq. (4):

$$Q_{O,o} = \beta_{O,o} Q_O, \quad Q_{U,o} = \beta_{U,o} Q_U. \tag{5}$$

Re-writing (1) in terms of volume fractions gives

$$\begin{aligned} \frac{d\beta_{O,o}}{dt} &= \frac{1}{V_O}\Big(Q_{sep} - \beta_{O,o} Q_O - Q_{Ex,o}\Big), \\ \frac{d\beta_{U,o}}{dt} &= \frac{1}{V_F}\Big(Q_{in,o} - Q_{sep} - \beta_{U,o} Q_U + Q_{Ex,o}\Big). \end{aligned} \tag{6}$$

The two outflow Q_O and Q_U are calculated based on the simple valve equations given as:

$$\begin{aligned} Q_U &= C_{v1} Z_U \sqrt{\frac{2(P_3 - P_U)}{\rho_U}} \\ Q_O &= C_{v2} Z_O \sqrt{\frac{2(P_2 - P_O)}{\rho_O}}, \end{aligned}$$

where, C_{v1} and C_{v2} are the valve constants of the underflow and overflow valves, P_2 is the pressure at the overflow outlet, P_3 is the pressure at the underflow outlet, $Z_U \in [0,1]$ and $Z_O \in [0,1]$ are the valve positions, and ρ_U and ρ_O are the densities of liquid at the underflow and overflow outlets, respectively. P_O is the downstream pressure of the overflow valve, and P_U is the downstream pressure of the underflow valve . In this paper, we assume that P_O and P_U are known and equal to the atmospheric pressure. The pressure P_2 and P_3 are assumed to be either measured or can be calculated based on the pressure-flow model, as in Vallabhan et al. (2020).

3 Typical control strategy of hydrocyclones

The typical operational control of hydrocyclone consists of two control loops, the first one is flow rate control and the second one is flow split control Husveg et al. (2007). Figure 2 shows a simplified P&ID representing the two control loops.

The goal of the flow rate control loop is to maintain a certain level in the upstream tank separator and thereby maintaining the inflow rate of hydrocyclone between $Q_{in,min}$ and $Q_{in,max}$. This inlet flowrate range

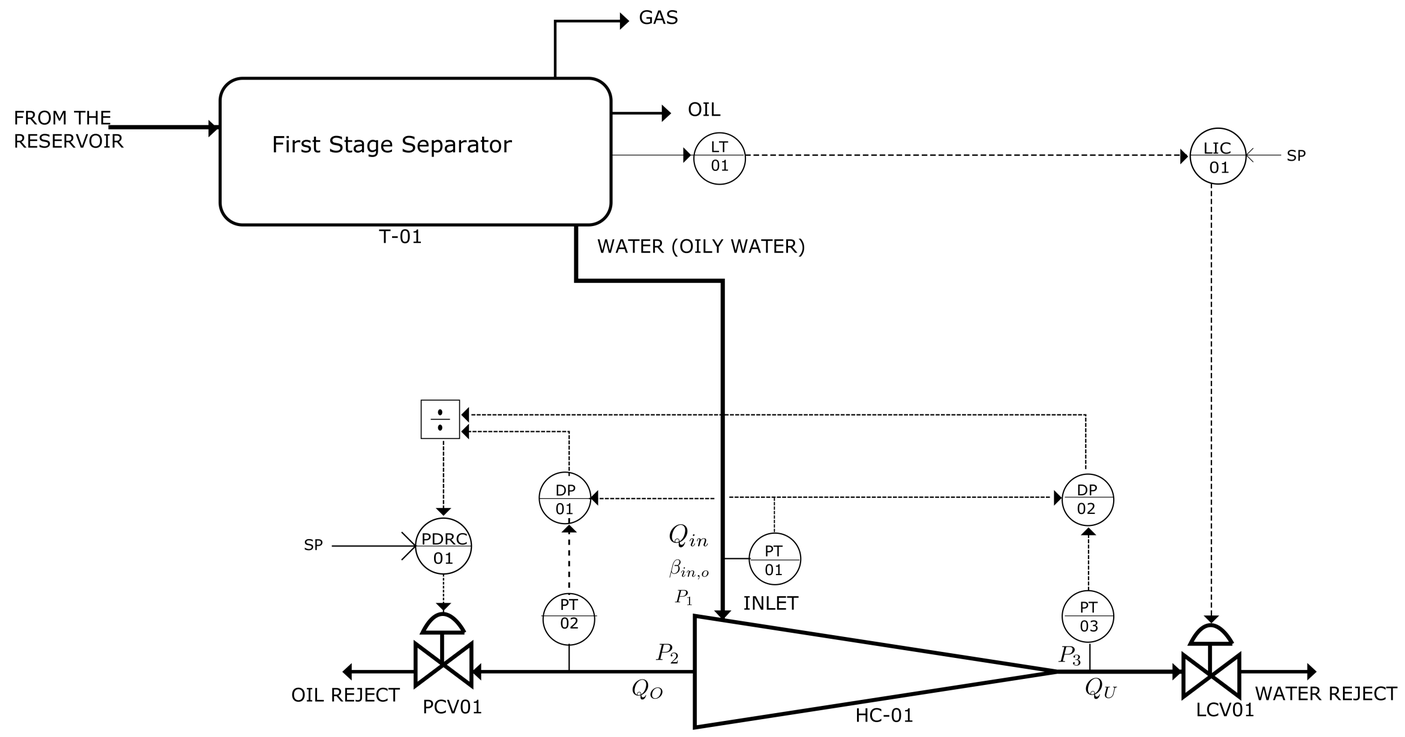

Figure 2: A typical control scheme of hydrocyclone representing flow rate and flow split control

characterizes an efficiency plateau, in which the oil-water separation is more effective (see Figure 3). This is achieved by manipulating the underflow control valve LCV01. In turn, the flow split control aims at maintaining a sufficient overflow rate in the hydrocyclone. The objective is to have good separation and maintain efficiency. The overflow control valve PCV01 is adjusted to keep a sufficient flow split ratio F_s, where $F_s = \frac{Q_O}{Q_{in}}$.

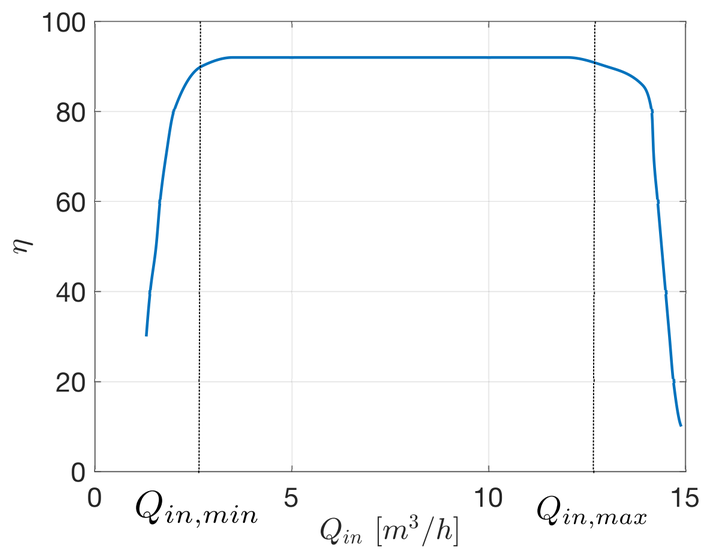

Figure 3: Relationship between efficiency and inflow rate of a hydrocyclone (Husveg et al., 2007). The efficiency of hydrocyclone is defined as $\eta = 1 - \frac{\beta_{U,o}}{\beta_{in,o}}$, where $\beta_{in,o}$ is the volume fraction of oil at the hydrocyclone inlet and $\beta_{U,o}$ is the volume fraction of the oil at the underflow outlet (water reject).

Since the the flow split has linear relationship with pressure drop ratio (PDR) and pressure sensors are cheaper and more reliable than flow sensors, PDR is given as the setpoint to controller PDRC01 instead of the flow split. The pressure difference at the inlet and the two outlets is used to calculate the pressure drop ratio (PDR), defined as:

$$\text{PDR} = \frac{P_1 - P_2}{P_1 - P_3} \tag{7}$$

where P_1, P_2, P_3 are the pressures at the inlet, overflow and underflow, respectively.

3.1 Issues with the typical control strategy

The experimental results in Meldrum (1988) show that PDR in the range 1.5 to 3 maintains the efficiency of the separation, if the inflow rate is kept at the efficiency plateau. However, keeping the setpoint of the PDR controller constant during plant disturbances (e.g., changes in the inlet oil concentration) can reduce the efficiency of hydrocyclones (Meldrum, 1988). Such changes may not be frequent in systems where first stage separators are gravity based with sufficient buffer volumes. On the other hand, if compact separators are used instead, frequent changes in the inlet oil concentrations for hydrocyclones are likely to happen.

In order to illustrate the effect of constant setpoint to the PDR controller of a hydrocyclone, we simulate the model described in the Section 2 with a simple PI controller (which acts as a PDR controller). Here, the process variable is PDR, which is calculated based on (7), and the manipulated variable is the overflow rate Q_O. We assume that the underflow valve is kept at a constant opening, which maintains the inflow rate

in the efficiency plateau. The simulation results are shown in Figure 4.

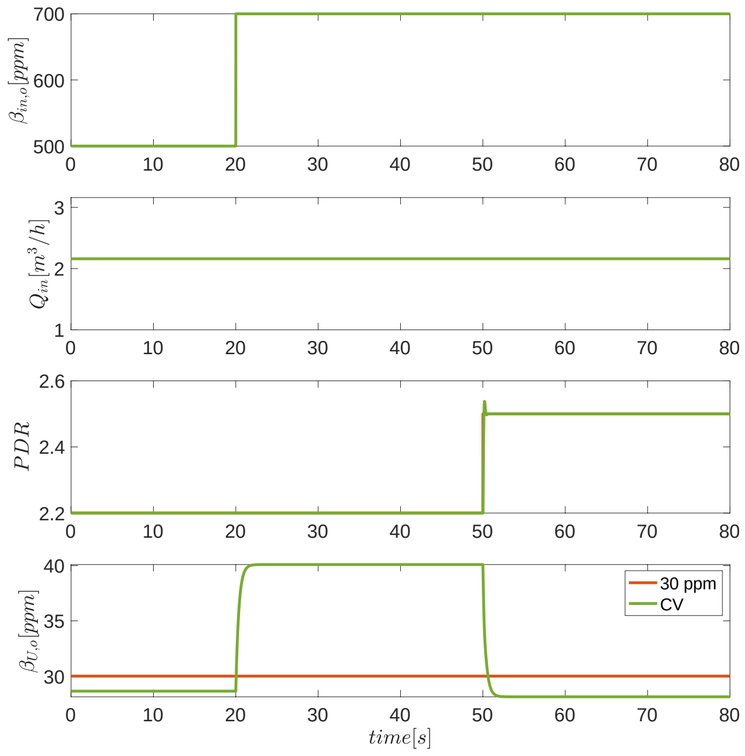

Figure 4: Simulation result showing increase in the $\beta_{U,o}$ with increase in β_{in} when fixed PDR setpoint. At 50 s, the PDR setpoint is manually adjusted to reduces $\beta_{U,o}$ below 30 ppm.

We start the simulation at steady-state with a PDR setpoint of 2.2, inlet oil concentration $\beta_{in,o}$ at 500 ppm and inflow rate of 2.2 m^3/h. With this operating condition, the PDR setpoint of 2.2 keeps the underflow oil concentration, $\beta_{U,o}$, below 30 ppm. At 20 s, $\beta_{in,o}$ is increased from 500 ppm to 700 ppm. The change in $\beta_{in,o}$ increases the underflow oil concentration, which decreases the efficiency of hydrocyclones. Since the inflow rate remains the same, the PDR does not change and the controller cannot react to the increase in the inlet oil concentration. At 50 s, the setpoint of the PDR controller is increased manually to bring the $\beta_{U,o}$ below 30 ppm. The simulation results indicate that the effect of changes in inlet oil concentration should be taken into consideration while designing control system for hydrocyclones.

We also did a laboratory experiment at a test rig to show the effect of constant PDR on increase in inlet oil concentration. The control loop implemented at the experimental setup is similar to the P&ID shown in Figure 2. The underflow valve is LCV01 is kept at 90 % and PCV01 is controlled by the PRDC01. The system is started with an inlet oil concentration of 350 ppm. In order to keep the underflow oil concentration below 30 ppm, the setpoint of the PDR controller is defined as 1.5. Later, the inlet oil concentration is increased to 800 ppm without changing the inflow rate. In Figure 5, we can see that the PDR is not changed and hence the controller PDRC01, does not take any action. However, we can see that the underflow oil concentration increases when the inlet oil concentration increases and this reduces the efficiency of hydrocyclone, confirming the simulation results. In order to deal with this problem, we propose three different control schemes. A feed-forward controller, a feedback/cascade controller, and also a model predictive controller. We compare their performance using the simulation scenario of Figure 4. After presenting the three methods, we discuss the advantages and challenges with their implementation.

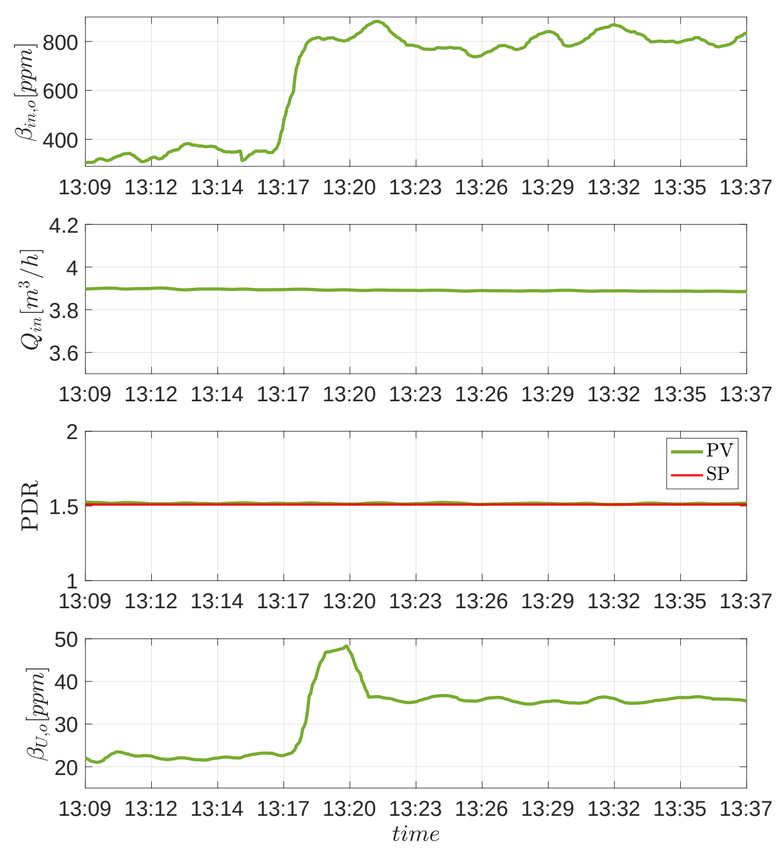

Figure 5: Laboratory experiment showing increase in the $\beta_{U,o}$ with increase in β_{in} when fixed PDR setpoint.

4 Feed-forward algorithm for hydrocyclones

If the disturbance can be measured before entering the system, then feed-forward control can be used for disturbance compensation. In this control scheme, a model is used to adjust the setpoints automatically based on the certain measurements. For example, in the system shown in Figure 4, we can use the measurements of the inlet-oil concentration $\beta_{in,o}$ and the inflow rate Q_{in} to adjust the PDR controller setpoint. By using this feed-forward scheme, we guarantee that the underflow oil concentration remains below 30 ppm without the need of a manual intervention. The block diagram of the implemented feed-forward control scheme

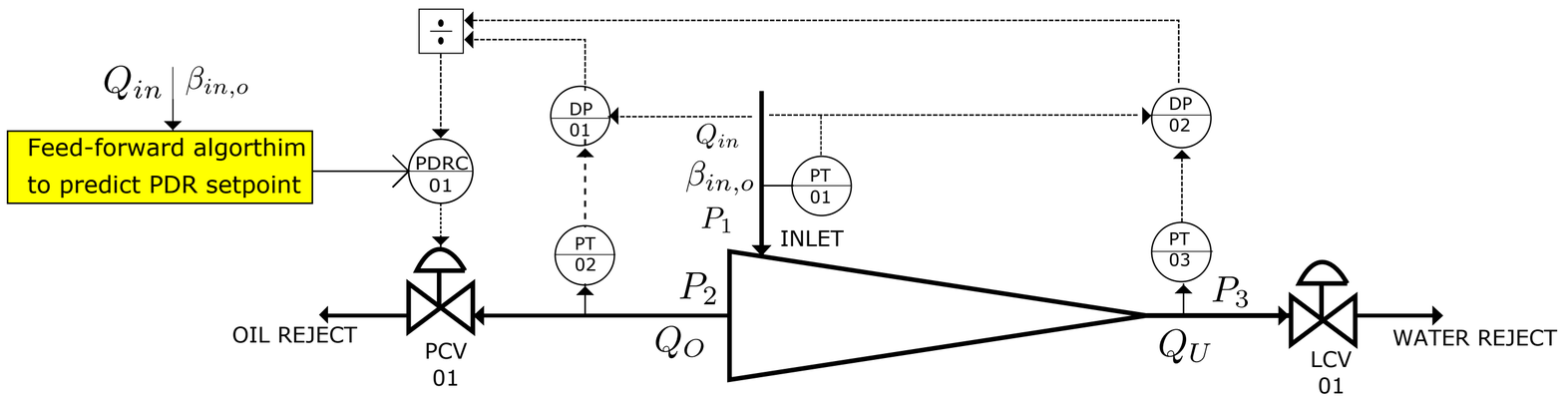

Figure 6: A diagrammatic representation of the feed-forward approach adjusting the PDR setpoint

is shown in Figure 6. For the feed-forward model, we use a Gaussian process regression (GPR) (MATLAB, 2021) model to predict the setpoints of the PDR controller based on the inflow rate and the inlet oil concentration. Hence, the GPR model has two input variables, Q_{in} and $\beta_{in,o}$, and one response variable, the desired PDR setpoint. We use GPR models because they are relatively easier to handle and interpret than conventional machine learning methods, such as neural networks (Williams and Rasmussen, 2006). However, one can use simple linear regression models for instance, given that they yield accurate predictions.

The training data for the GPR model identification is generated by simulating the model described in the Section 2 with a PDR controller. Then, inflow rates are varied from $1.8\,\mathrm{m}^3/\mathrm{h}$ to $2.8\,\mathrm{m}^3/\mathrm{h}$, inlet oil concentration is varied from 500 ppm to 1000 ppm, and PDR setpoint is manully varied from 2 to 3.5. Later, the PDR values that keep the $\beta_{U,o}$ below 30 ppm are filtered out. In an industrial setup, instead of using simulations, one can use historical data for inlet oil concentration, inflow rate and the changes in the PDR setpoint performed by the operator.

The data set is then fed to the MATLAB function *fitrgp*. The *fitrgp* function returns a GPR model.

Later, the model can be imported as a function in MATLAB and used as the feed-forward block in the control scheme shown in Fig. 6. Since this is a data-based model, its extrapolation capacity is poor. The model predictions are valid for the flow rate range $1.8\,\mathrm{m}^3/\mathrm{h}$ to $2.8\,\mathrm{m}^3/\mathrm{h}$ and the inlet oil concentration 500 ppm to 1000 ppm, which encloses the considered operating region. If a new regions is to be considered, a new GPR model needs to be generated.

4.1 Simulation results

Figure 7 shows the simulation results using the feed-forward model (GPR model) to predict the setpoint changes of the PDR controller. We plot the variations of inlet oil concentration $\beta_{in,o}$, PDR setpoint predicted by the feed-forward model, inflow rate Q_{in}, and concentration of the oil at the underflow outlet $\beta_{U,o}$. For representing the real system, we use the hydrocyclone model described in the Section 2. We start the simulation with inflow rate $2.2\,\mathrm{m}^3/\mathrm{h}$ and the inlet concentration of 500 ppm. Then at 50 s, we increase the inlet concentration to 700 ppm. The feed-forward model detects the change in the inlet oil concentration and predict the setpoint to be 2.8. Thus, the controller is able to maintain the underflow oil concentration below 30 ppm. As an additional check to the GPR model, we increase the inflow rate to $2.6\,\mathrm{m}^3/\mathrm{h}$ at 100 s. The feed-forward model changes the controller setpoint to 2.2, thereby keeping $\beta_{U,o}$ below 30 ppm. The PDR controller parameters are given in Table 2.

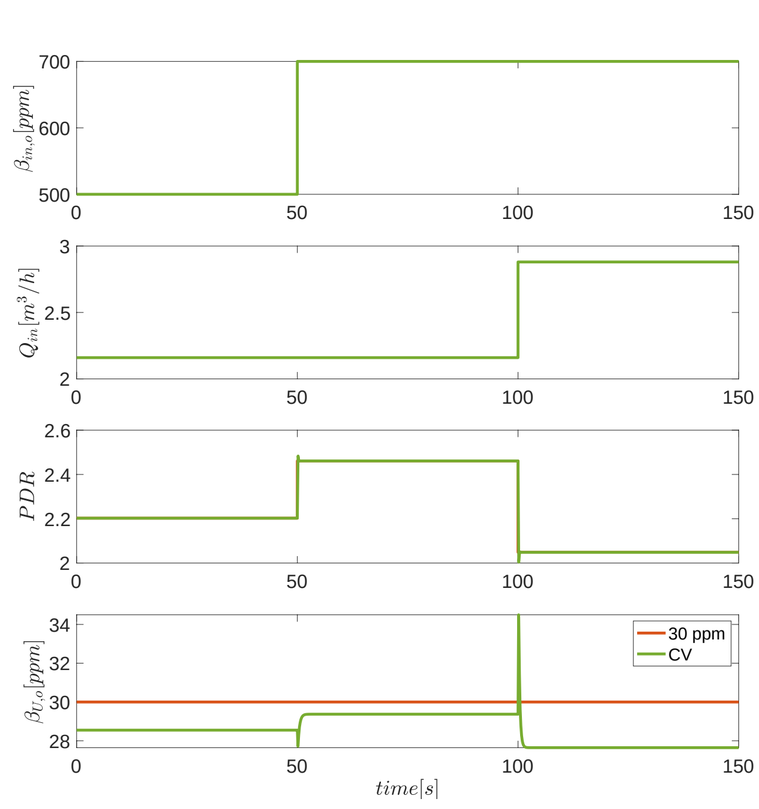

Figure 7: Simulation results showing the feed-forward control scheme. Here, the inlet oil concentration changes at 40 s and the inflow rate is changed at 100 s.

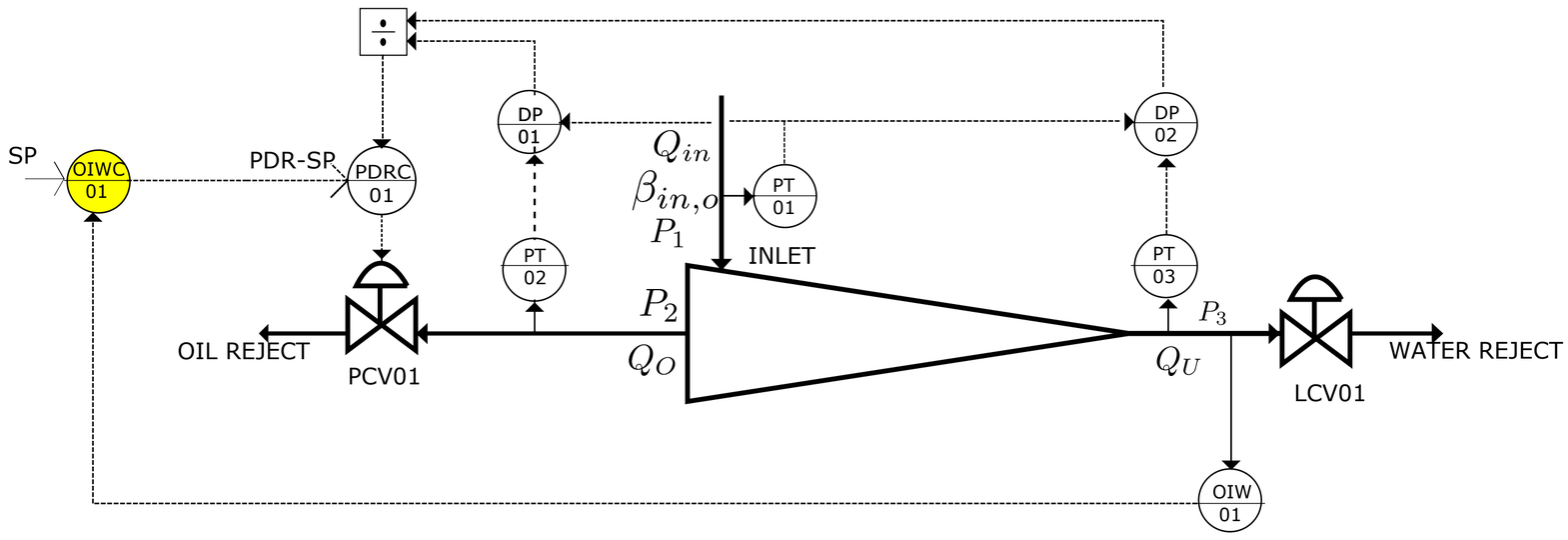

Figure 8: A diagrammatic representation of the cascade approach adjusting the PDR setpoint

5 Feedback/cascade control for hydrocyclones

As before, the goal of the feedback/cascade approach is to adjust the PDR controller setpoints automatically. For its implementation, the only pre-requisite is a sensor that measures the oil concentration at the underflow outlet with a sampling rate matching the control system. The diagrammatic representation of the feedback approach is shown in Figure 8. Here, a simple PI controller, OIWC01 acts as the primary controller. We can set the desired underflow concentration of oil as a setpoint to the primary controller. Later, this primary controller adjusts the setpoint of the secondary controller PDRC01 and maintains the underflow oil concentration $\beta_{U,o}$ to a desired level.

5.1 Simulation results

Again, the model of the Section 2 is used for representing the real system. Figure 9 shows the simulation results. We repeat the scenario from the feed-forward algorithm analysis. We start the simulation with inflow rate of $2.2\,\mathrm{m}^3/\mathrm{h}$ and the inlet oil concentration of 500 ppm. The setpoint of the primary controller is kept at 30 ppm. At 50 s, the inlet oil concentration is increased to 700 ppm, which increases $\beta_{U,o}$. The primary controller automatically adjusts the setpoint of PDRC01 to increase the separation and bring down $\beta_{U,o}$ to 30 ppm. Later, at 200 s, we increase the inflow rate to $2.6\,\mathrm{m}^3/\mathrm{h}$. Even though it improves the separation, the primary controller tracks the setpoint of 30 ppm and, hence, adjust the setpoint of PDRC01. The controller parameters of the primary and secondary controller are given in Table 2

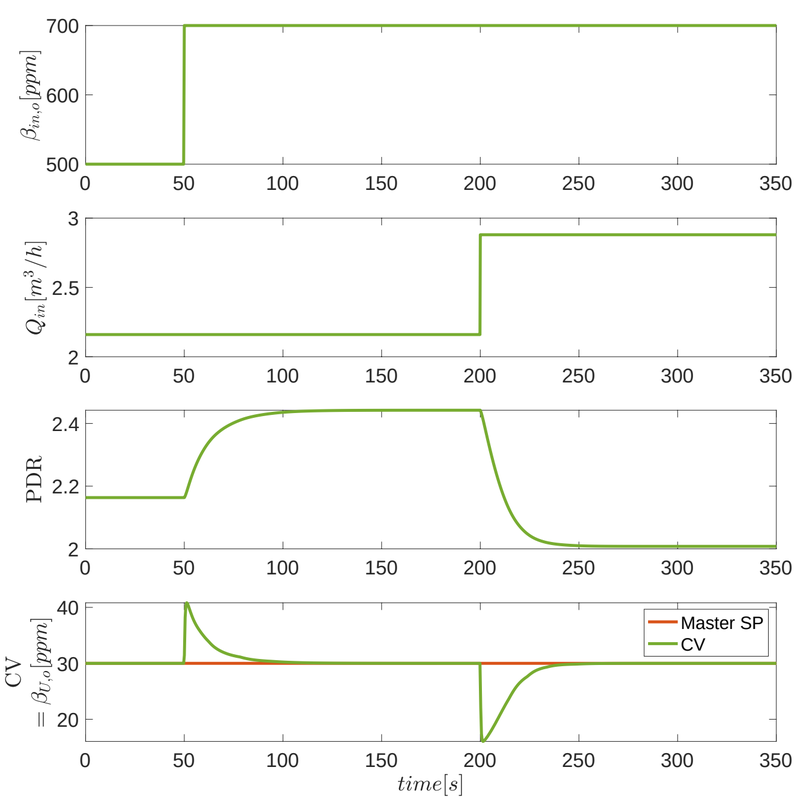

Figure 9: Simulation result showing the cascade control scheme. Here the inlet oil concentration is changed at 50 s and the inflow rate is changed at 200 s.

6 Model predictive control for hydrocyclones

In Model Predictive Control (MPC), we use a process dynamic model in combination with an optimization method for determining the manipulated variables' values. These values are chosen such that the deviation between the predicted controlled variables values and their reference is minimized; the MPC determines the optimal input by simulating its internal model (Seborg et al., 2010). Here, we implement a nonlinear MPC that regulates the fraction of oil at the underflow at a given setpoint by manipulating the flowrate of the

overflow by the use of the overflow control valve. In order to obtain a model suited for MPC applications, we rewrite the model of the Section 2 into a state-space form:

$$\begin{aligned}\dot{x}_1 &= \frac{1}{V_O}\Big(Q_{sep} - x_1 K u - Q_{Ex,o}\Big)\\ \dot{x}_2 &= \frac{1}{V_F}\Big(Q_{in,o} - Q_{sep} - x_2 Q_U + Q_{Ex,o}\Big)\ ,\end{aligned} \tag{8}$$

where the states x_1 and x_2 represent overflow oil fraction $\beta_{O,o}$ and, underflow oil fraction $\beta_{U,o}$. The control input u (system manipulated variable) is the overflow valve opening and $K = C_{v2}\sqrt{\frac{2(P_2-P_O)}{\rho_O}}$. In simulation, we assume P_2 to be constant during the integration interval.

The control problem can be formulated as:

$$\min_{\boldsymbol{x},u} \frac{1}{2}\int_{t_c}^{t_c+T_p} \Big((y(t)-y^{SP})^T Q(y(t)-y^{SP}) + \dot{u}(t)^T R\dot{u}(t)\Big)dt$$

s.t.

$$\begin{aligned}&\dot{\boldsymbol{x}}(t) = f(\boldsymbol{x}(t), u(t)), \quad t \in [t_c, t_c+T_p]\\ &y(t) = [0\ 1]\ \boldsymbol{x}(t), \quad t \in [t_c, t_c+T_p]\\ &\boldsymbol{x}(t_c) = \boldsymbol{x}_0,\\ &u_{min} \le u(t) \le u_{max}, \quad t \in [t_c, t_c+T_p]\\ &-\dot{u}_{max} \le \dot{u}(t) \le \dot{u}_{max}, \quad t \in [t_c, t_c+T_m]\\ &\dot{u}(t) = 0 \quad t \in [t_c+T_m, t_c+T_p] \cup [t, t+T_s]\ ,\end{aligned} \tag{9}$$

where, $\boldsymbol{x}$ are the states, u the control input, and f the system model, all described in (8); y is the measured output (fraction of oil at the underflow) and y^{SP} its setpoint; $\dot{u}$ is the control input change. The inequality constraints represent technical restrictions on the control inputs u; u_{min}, u_{max} are the input lower and upper bounds, and $\dot{u}_{max}$ is the maximum input change in one sampling time T_s (i.e $[t, t+T_s]$). t_c is the current time when the optimization problem is called. The prediction horizon T_p represents the control interval evaluated in the optimization problem, and the control horizon T_m is the horizon in which the manipulated variable can be optimized. Note that, after the control horizon T_m, the inputs are kept constant by setting $\dot{u} = 0$. The MPC is run every T_s seconds. Q is a matrix $n_y \times n_y$ that penalizes deviations of $y(t)$ from its setpoint y^{SP}, and R is a matrix $n_u \times n_u$ for penalizing manipulated variable movements.

6.1 Implementation

The plant model and the MPC algorithm were implemented in MATLAB using the CasADi framework (Andersson et al., 2019). The plant model f is integrated using CVodes from the Sundials suite in CasADi. A multiple shooting algorithm (Bock and Plitt, 1984) is used for computing the numerical solution of the optimal control problem in (9). This algorithm allows us to re-arrange the model dynamic equations in such a way that we can solve (9) using standard optimization nonlinear programming (NLP) solvers. Here we use IPOPT, which is an interior point NLP solver included in CasADi (Wächter and Biegler, 2006).

The MPC is implemented in a receding horizon framework, i.e. we compute the trajectory $\boldsymbol{u}^\star = [u_1^\star, u_2^\star, \ldots, u_{T_p}^\star]^T$ and apply only the first control move $u_1^\star$. The next time step, the process is repeated. This strategy is used for compensating unexpected system disturbances and plant-model mismatch (Rawlings et al., 2017). In the simulation, the plant model and the controller have the same sampling time of 0.01 s and the MPC is run every 0.01 s.

6.2 Simulation results

The simulation results with the model predictive controller are shown in Figure 10. We use the same scenario as in the previous case studies. We start the simulation with inflow rate of 2.2 m^3/h and the inlet oil concentration of 500 ppm. Then, at 40 s, the inlet oil concentration is increased to 700 ppm, while the outlet setpoint for the outlet oil concentration is kept at 30 ppm. We see that the MPC automatically adjusts the overflow valve opening Z_o to reject the disturbance in the feed. Since we added a maximum input change constraint to account for the system inertia (constraint on $\dot{u}$), the Z_o profile is smooth, which is important for practical implementation. Next, we increase the inflow rate to 2.6 m^3/h. The MPC is also able to track the setpoint of $\beta_{U,o}$ for this disturbance. Note that we assume full state feedback, i.e. the states (overflow and underflow oil fractions) are measured at every sampling time. The MPC parameters are given in Table 2.

7 Comparing the control scheme alternatives

We compare the three proposed approaches in terms of necessary measurements, as well as model and solver requirements. Note, we do not focus on performance criteria such as integral squared error, integral absolute error, etc. Since these are highly dependent on the tuning of the approach, poorly chosen parameters could influence the comparison. Therefore, we focus on qualitative criteria that will help the practitioner/engineer decided which strategy should be used based on the available resources. The characteristics of the three methods are summed up in Table 1.

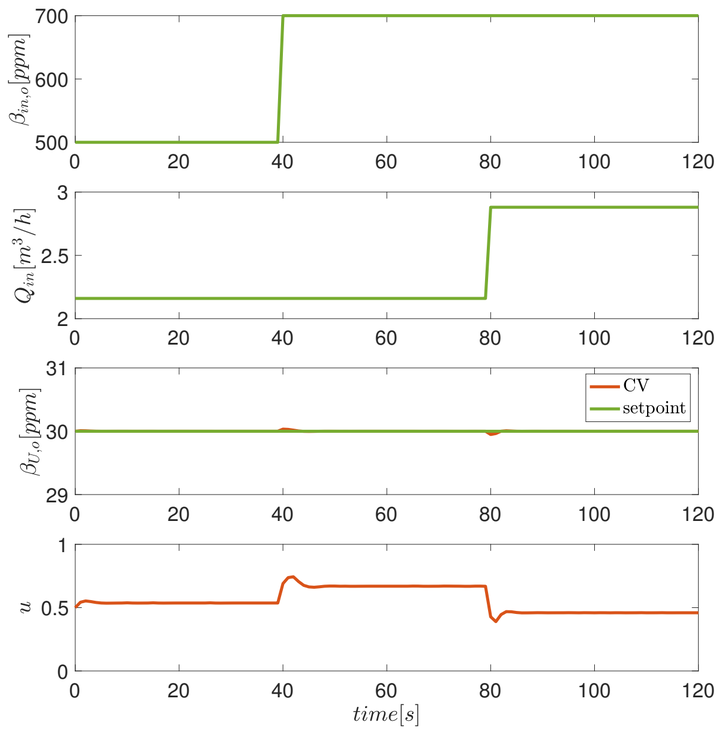

Figure 10: Simulation result of the MPC implementation. The controller first tracks the underflow oil fraction setpoint. Disturbances enters the system at 40 s and 80 s, represented by a change in the inlet oil concentration and the inflow rate respectively. The controller rejects both the disturbance maintaining $\beta_{U,o}$ at its setpoint.

The implementation of the feed-forward approach requires online measurements of the inlet oil-concentration and inflow rate. They are used in combination with the feed-forward model to update the PDR setpoints according to the system disturbances. To obtain this model, we need historical data of the two previously mentioned measurements, as well as a specific values of the PDR setpoints. These values are chosen such that, given an inlet condition, the underflow concentration stays under a threshold, e.g., lower than 30 ppm. The setpoints can be obtained via simulations or based on process knowledge. Ideally, we need data from a large operation envelope to ensure that the feed-forward strategy works in different plant conditions. This feed-forward approach has the disadvantage that, in scenarios such as slugging where the inlet-oil concentration increases rapidly, the changes in the PDR setpoint aiming at improving separation can cause more water at the overflow outlet (oil-rich stream).

In comparison to the feed-forward approach, the feedback/cascade control requires measurement only of the underflow oil concentration. This method is a direct way of controlling the efficiency of hydrocyclones. The secondary PDR controller responds to changes in the inflow rates and maintains the PDR at a given setpoint. However, if a disturbance occurs in the inlet oil concentration and/or in the inlet oil-droplet distribution, the separation efficiency of the hydrocyclone changes, and this will not be reflected in the PDR setpoint. Then, the primary controller can detect these disturbances by measuring the underflow oil concentration, and adjust the PDR setpoint to improve the efficiency. Note that there is an upper bound in the PDR beyond which the separation cannot be improved. In this case, if the primary controller tries to increase the PDR setpoint to maintain the separation efficiency, more water goes out through the overflow outlet. Hence, it is important to know the limitation of the system in use and deactivate the primary controller at the right time, which can turn out to be a major disadvantage of this approach.

This deficiency can be mitigated by the model-predictive control approach. By using MPC, we can explicitly take into account operating constraint while dealing with the feed disturbances. Moreover, MPC has the potential to increase the separation regularity since it considers the interaction among multiple system variables, whereas PI controllers act based on single-input, single output relationships (Qin and Badgwell, 2003). The main disadvantage of the MPC formulation is that it requires a fairly accurate model. Also, in the model formulation proposed in this paper, we assume that underflow and overflow oil concentration are measured. It is not common to have a oil in water sensor at the overflow outlet of the hydrocyclones. As an alternative, we could use soft-sensors such as Kalman filters to estimate the overflow oil concentration. Another possibility of future work is to re-formulate the optimisation problem to minimize the underflow $\beta_{U,o}$ (instead of tracking a setpoint) and also maximize the total throughput of the hydrocyclones by adjusting the underflow valve.

Conclusions

In this paper, we propose three new control schemes for de-oiling hydrocyclones and study the effectiveness of these controllers when subjected to different plant disturbances. The schemes were designed in order to address issues with the standard hydrocyclone control strategy. Typically, a PDR controller is used to keep the underflow oil concentration at a given setpoint. However, if the inlet oil concentration and/or in the inlet oil-droplet distribution change, the PDR setpoint needs to be updated or the outlet purity requirements will not met.

The first scheme uses a feed-forward model to update the setpoint of a typical PDR controller. The

Table 1: Comparison of the three approaches used for controlling the underflow oil fraction of a hydrocyclone.

Approach	**Required measurements**	**Model**	**Optimization solver**	**Possible disadvantages**
Feed-forward	∘ Inlet oil fraction ∘ Inflow rate	Feed-forward model to predict PDR setpoint changes	No	∘ Fast inlet oscillations may lead to high concentrations of water at the overflow outlet
Feed-back/cascade	Underflow oil fraction	No	No	∘ Primary controller may need to be deactivated if upper bound in the PDR is violated, which causes high water concentration at the overflow outlet
Model Predictive Control	∘ Overflow oil fraction ∘ Underflow oil fraction	Yes. State-space model of Eq. (8) can be used	Yes	∘ Fairly accurate model needed ∘ Oil in water sensor is necessary (or a soft sensor needs to be developed)

Table 2: Tuning parameters

Description	Variable	Value
Feed-forward		
PDR control prop. gain	K_c	0.67
PDR control int. gain	τ_I	0.047
Feed-back/cascade		
Primary control prop. gain	K_c	0.5
Primary control int. gain	τ_I	0.5
Secondary control prop. gain	K_c	−542.16
Secondary control int. gain	τ_I	0.2598
Model Predictive Control		
Setpoint weighting matrix	Q	5e8
Input weighting matrix	R	0.01
Prediction horizon	T_p	15
Control horizon	T_m	10
Input upper bounds	$u_{\max}$	0.01
Input lower bounds	$u_{\min}$	1
Max input change	$\dot{u}_{\max}$	0.5

second scheme is a feedback/cascade approach, where the primary controller takes measurements of oil concentration at the underflow outlet and updates the setpoint of the secondary controller (PDR controller) to maintain the underflow oil concentration at a required level. The third control scheme is a model predictive controller. Here, the control objective is to minimize the variation of the underflow oil concentration from a reference point while taking into account operating constraints, such as max water-in-oil concentrations.

In the simulations, we see that all the control schemes meet the requirement to keep the underflow oil concentration below 30 ppm other than briefly during transients. We also present guidelines for choosing the appropriate scheme based on the available resources at the industrial site (such as measurements, hardware and software at hand). As an extension of this work feed-forward and cascade control schemes are implemented at a newly constructed experimental rig at NTNU and result are being finalised.

Acknowledgements

This project is supported by the Norwegian Research Council, industrial partners and NTNU under the Subsea Production and Processing (SUBPRO) SFI program.

References

Andersson, J. A. E., Gillis, J., Horn, G., Rawlings, J. B., and Diehl, M. CasADi – A software framework for nonlinear optimization and optimal control. *Mathematical Programming Computation*, 2019. 11(1):1–36.

Beyer, J., Bakke, T. H., Lichtenthaler, R., and Klungsøyr, J. Environmental effects of offshore produced water discharges evaluated for the barents sea. *NIVA-rapport*, 2019.

Bock, H. G. and Plitt, K.-J. A multiple shooting algorithm for direct solution of optimal control problems. *IFAC Proceedings Volumes*, 1984. 17(2):1603–1608.

Bram, M. V., Hansen, L., Hansen, D. S., and Yang, Z. Hydrocyclone separation efficiency modeled by

flow resistances and droplet trajectories. *3rd IFAC Workshop on Automatic Control in Offshore Oil and Gas Production*, 2018. 51(8):132–137.

Bram, M. V., Jespersen, S., Hansen, D. S., and Yang, Z. Control-oriented modeling and experimental validation of a deoiling hydrocyclone system. *Processes*, 2020. 8(9):1010.

Das, T. and Jäschke, J. Modeling and control of an inline deoiling hydrocyclone. *3rd IFAC Workshop on Automatic Control in Offshore Oil and Gas Production OOGP*, 2018. 51(8):138–143.

Durdevic, P., Pedersen, S., Bram, M., Hansen, D., Hassan, A., and Yang, Z. Control oriented modeling of a de-oiling hydrocyclone. *17th IFAC Symposium on System Identification SYSID*, 2015. 48(28):291–296.

Durdevic, P. and Yang, Z. Application of hinf robust control on a scaled offshore oil and gas de-oiling facility. *Energies*, 2018. 11(2):287.

Hansen, L., Durdevic, P., Jepsen, K. L., and Yang, Z. Plant-wide optimal control of an offshore de-oiling process using mpc technique. *Ifac-papersonline*, 2018. 51(8):144–150.

Husveg, T., Rambeau, O., Drengstig, T., and Bilstad, T. Performance of a deoiling hydrocyclone during variable flow rates. *Minerals Engineering*, 2007. 20(4):368–379.

MATLAB. Gaussian process regression models. `https://se.mathworks.com/help/stats/gaussian-process-regression-models.html`, 2021. (accessed 1 March 2021).

Meldrum, N. Hydrocyclones: A solution to produced-water treatment. *SPE Production Engineering*, 1988. 3(04):669–676. URL `https://doi.org/10.2118/16642-PA`.

Orlowski, R., Euphemio, M. L. L., Euphemio, M. L., Andrade, C. A., Guedes, F., Tosta da Silva, L. C., Pestana, R. G., de Cerqueira, G., Lourenço, I., and Pivari, A. Marlim 3 phase subsea separation system-challenges and solutions for the subsea separation station to cope with process requirements. In *Offshore Technology Conference*. Offshore Technology Conference, page n/a, 2012.

Pereira, R. M., Campos, M. C. M. M. d., de Oliveira, D. A., de Souza, R. d. S. A., Filho, M. M. C., Orlowski, R., Duarte, D. G., Raposo, G. M., Lillebrekke, C., Ljungquist, D., Carvalho, A., and Fares, M. Ss: Marlim 3 phase subsea separation system: Controls design incorporating dynamic simulation work. In *Offshore Technology Conference*. Offshore Technology Conference, Houston, Texas, USA, page 13, 2012. URL `https://doi.org/10.4043/23564-MS`.

Qin, S. J. and Badgwell, T. A. A survey of industrial model predictive control technology. *Control engineering practice*, 2003. 11(7):733–764.

Rawlings, J. B., Mayne, D. Q., and Diehl, M. *Model predictive control: theory, computation, and design*, volume 2. Nob Hill Publishing Madison, WI, 2017.

Seborg, D. E., Mellichamp, D. A., Edgar, T. F., and Doyle III, F. J. *Process dynamics and control*. John Wiley & Sons, 2010.

Vallabhan, M. and Holden, C. Non-linear control algorithms for de-oiling hydrocyclones. In *2020 28th Mediterranean Conference on Control and Automation (MED)*. IEEE, pages 85–90, 2020.

Vallabhan, M., Holden, C., and Skogestad, S. A first-principles approach for control-oriented modeling of de-oiling hydrocyclones. *Industrial & Engineering Chemistry Research*, 2020. 59(42):18937–18950. URL `https://doi.org/10.1021/acs.iecr.0c02859`.

Wächter, A. and Biegler, L. T. On the implementation of an interior-point filter line-search algorithm for large-scale nonlinear programming. *Mathematical programming*, 2006. 106(1):25–57.

Williams, C. K. and Rasmussen, C. E. *Gaussian processes for machine learning*, volume 2. MIT press Cambridge, MA, 2006.

4.2 Non-linear control algorithms for de-oiling hydrocyclones

The citation of the published article is given below:

M. Vallabhan and C. Holden, *Non-linear control algorithms for de-oiling hydrocyclones*, 2020 28th Mediterranean Conference on Control and Automation (MED), 2020, pp. 85-90, doi: 10.1109/MED48518.2020.9183115.

The postprint version of the paper follows.

Non-linear control algorithms for de-oiling hydrocyclones

Mishiga Vallabhan[1] and Christian Holden[2]

***Abstract*— Reduction in environmental footprint has become one of the key performance indicators in the oil and gas industry. As per the OSPAR commission, produced water containing more than 30 ppm of oil cannot be discharged to sea. This clearly indicates the importance of advanced control systems in produced-water system equipment like hydrocyclones and compact flotation units. It is expected that the control algorithms handle all the plant disturbances and meet the performance specifications. This paper investigates non-linear control algorithms for controlling the efficiency of hydrocyclones. Here, two well-known non-linear control design techniques– feedback linearization control and sliding mode control are used for the control of a hydrocyclone.**

I. INTRODUCTION

More the oil and gas one takes out from the reservoir, the more cautious one has to be in reducing the environmental footprint. The produced water treatment system plays an important role in cleaning the oily-water in on-shore and offshore platforms. In order to meet the environmental regulations [1] it is important to maintain the efficiency of produced water treatment equipment.

One of the most common component in a produced water treatment system is a hydrocyclone. The possibility of hydrocyclones for liquid-liquid separation was investigated in [2] and Bardeley's conventional cyclone was redesigned for de-oiling by extending the cylindrical portion of the cyclone to give adequate residence time. The first full scale commercial hydrocyclone concept was used in Conoco's Murchison platform in the year 1985 [3]. Modelling of hydrocyclones have been an extensive topic of research, and most of the models are CFD-based, which use Navier-Stokes equations to simulate the flow. In [4], a model based on the droplet trajectories was presented, and this was used to predict the cyclone efficiency. Later, [5] developed a model based on the droplet trajectories by considering the swirl intensity, and also discuss the pressure drop across the hydrocyclone.

In [6], a first-order transfer function model was proposed for studying the hydrocyclones. A control-oriented model for an inline hydrocyclone with a swirl element was developed by [7]. A grey-box of modelling of a hydrocyclone was developed by [6] where model parameters were estimated using the experimental data.

A hydrocyclone, or more specifically a 'hydrocyclone liner', has a tangential inlet through which oily water enters. It has two outlets, one is called the overflow outlet where the purified oil comes out and the other is called the underflow outlet where the cleaned water comes out. The specially designed tangential inlets of liners generate a centrifugal force which aids in the separation of oil from water. The lighter oil particles move towards the center, and the denser water moves towards the walls of the hydrocyclone liners. The geometrical structure of a liner comprises of a cylindrical section, followed by two conical sections of reduced diameters and another cylindrical section much longer than rest of the three sections. The last cylindrical section gives more residence time for the oil droplets and this enhances the separation. Fig. 1 shows a rough sketch of a hydrocyclone liner.

Industrial-scale hydrocyclone consists of many liners stacked together inside a big casing. The oily water coming from the upstream separator is connected to this hydrocyclone casing, and the fluid moves to the tangential inlets of individual liners. The outlet of the individual liners are are connected to two outlet chambers. Since the liners are parallel, an industrial hydrocyclone with many liners has the same behaviour as a single liner. Here the whole analysis is on a single hydrocyclone liner.

There has not been much research on improving the control aspects of hydrocyclones. In [8], an H_∞ robust controller using a black box model was developed. Advanced nonlinear algorithms can help in improving the separation efficiency in the presence of unforeseen plant disturbances. In this paper, a state-space model for a de-oiling hydrocyclone is derived. Owing to the nonlinear nature of the model nonlinear control algorithms can be a better option to handle plant disturbances. Hence, a feedback linearization control algorithm and a sliding mode control algorithm is developed for de-oiling hydrocyclones.

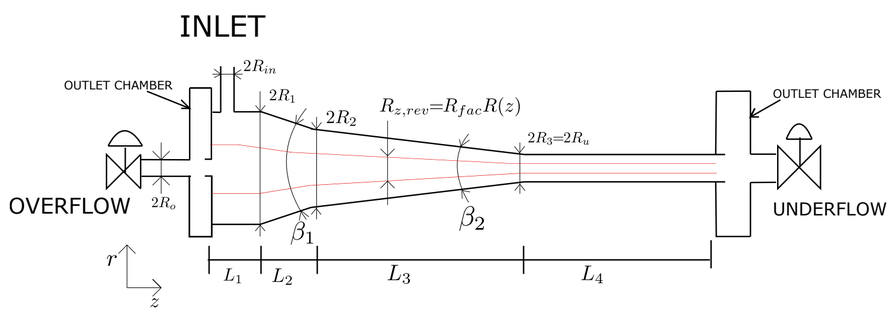

Fig. 1. A hydrocyclone liner.

II. DYNAMIC MODEL

This section gives a brief description of a dynamic model of a de-oiling hydrocyclone. The physical volume of a

[1]Department of Mechanical and Industrial Engineering, Norwegian University of Science and Technology (NTNU),Trondheim, Norway mishiga.vallabhan@ntnu.no

[2]Department of Mechanical and Industrial Engineering, Norwegian University of Science and Technology (NTNU),Trondheim, Norway christian.holden@ntnu.no

978-1-7281-5742-9/20/$31.00 ©2020 IEEE

hydrocyclone liner, denoted as V_{HC}, is divided into two sub-volumes: the volume of liquid that leaves the hydrocyclone overflow flow V_R, and the volume that will leave the underflow V_F. The volume inside the blue dotted lines in Fig. 2 is V_R and the volume outside it is V_F. All the liquid in V_R travels in the reverse direction, as does some of the fluid in V_F. Most of the fluid in V_F flows in the forward direction. V_R is 'oil-rich' with potentially some water, V_F is 'water-rich' with very little oil (a thin yellow line in Fig. 2 represents the oil droplets in V_F).

There exists a reverse-flow zone for a hydrocyclone, and this has the same shape as the hydrocyclone itself [4]; the radius of the reverse-flow zone (marked as red colour in Fig. 1 and 2) is a factor of hydrocyclone radius given as

$$R_{z,rev} = R_{fac} R(z) \,, \tag{1}$$

where $R(z)$ is the radius of the hydrocyclone at different axial positions z and $R_{z,rev}$ is the radius of reverse-flow zone at the respective axial positions. In [4] and [5] some formula for calculating the value of R_{fac} is given. This paper considers this a tuning parameter where $R_{fac} \in [0.3, 0.4]$.

It is to be noted that volume V_R is fixed and that, $V_F = V_{HC} - V_R$. We consider only the oil inside V_F and V_R for the mass-balance analysis.

Let Q_{in} be the total known inflow rate (oil and water) entering the hydrocyclone. We also assume that the inlet mass fraction of oil (β_{in}) to be a known parameter. Then, the inflow rate of the oil is given by $Q_{ino} = \beta_{in} Q_{in}$.

The oil-water mixture entering V_F starts separating, and the separated oil droplets move towards V_R. Oil droplets which are not separated remains in V_F and later comes out as underflow. V_R starts filling up with oil during the separation. The oil core in V_R is assumed to have the same shape (but smaller) than the hydrocyclone.

The flow rate of the separated oil is denoted as Q_{sep}. The separation depends on the separation efficiency of a hydrocyclone. One way to calculate the separation efficiency is by droplet trajectory analysis [4], where the oil droplets entering the hydrocyclone are tracked to determine if they enters reverse-flow zone, get separated and thereby comes out as overflow or they leave the cyclone as a part of underflow.

In [9], an internal separation ε is defined for hydrocyclones, which gives the percentage of oil separated out of the total oil coming into the hydrocyclone. Hence, if we know the inflow rate of the oil Q_{ino} then flow rate of the separated oil (Q_{sep}) is given by $Q_{sep} = \varepsilon Q_{ino}$. Also, [9] approximated a relation between the internal separation ε and the overflow rate Q_o using droplet trajectory analysis given as

$$\varepsilon = p_2 Q_o^2 + p_1 Q_o + p_0 \,, \tag{2}$$

where $Q_o \in [0, 6.5\text{E}-5] \text{m}^3/\text{s}$ and the polynomial coefficients are $p_2 = -5.332\text{E}7$, $p_1 = 5519$, $p_0 = 0.84099$. In this paper, we use this same relation for the mass-balance equation given later in this section.

As the separation increases the volume V_R gets filled up with the oil. When V_R is completely filled up by oil, we assume that the excess oil flows back into V_F. This is termed as back-flow Q_b. A simple mass-balance formulation of the volume of oil in the oil-rich volume (V_{Or}) and volume of oil in the water-rich volume (V_{Of}) are given by,

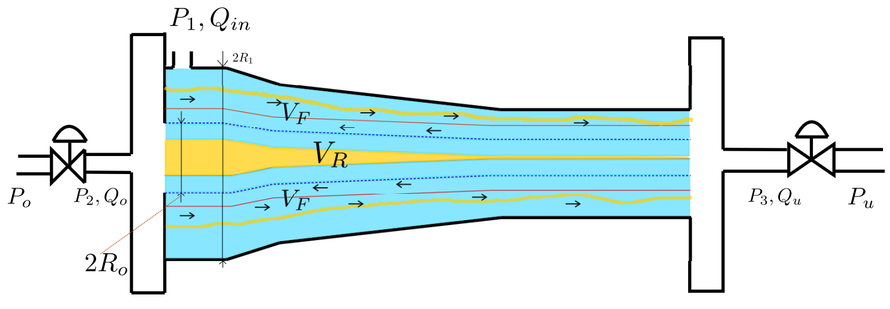

Fig. 2. Pictorial representation of hydrocyclone volumes used for modelling, with oil-rich volume and water-rich volume.

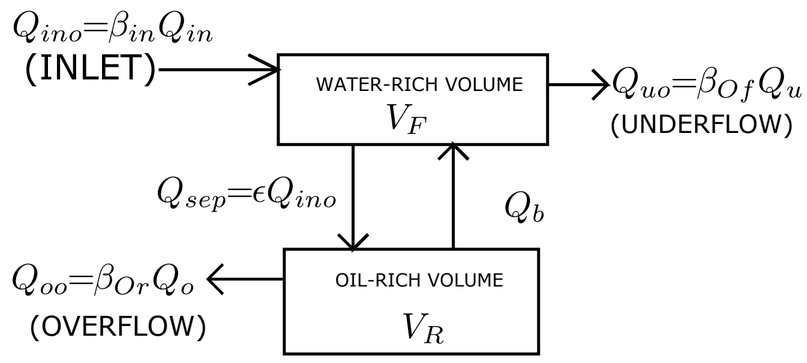

Fig. 3. Block diagram representation of the model.

$$\dot{V}_{Or} = Q_{sep} - Q_{oo} - Q_b \tag{3}$$
$$\dot{V}_{Of} = Q_{ino} - Q_{sep} - Q_{uo} + Q_b \,. \tag{4}$$

Here, Q_{oo} flow rate of the oil through the overflow outlet, Q_{uo} flow rate of the oil through the underflow outlet. These two flow rates can be calculated if we know the fraction of oil insides V_R and V_F. The oil fraction inside oil-rich volume (β_{Or}) is

$$\beta_{Or} = \frac{V_{Or}}{V_R} \,,$$

and the oil fraction inside the water-rich volume (β_{Of}) is

$$\beta_{Of} = \frac{V_{Of}}{V_F} \,.$$

Then $Q_{oo} = \beta_{Or} Q_o$ and $Q_{uo} = \beta_{Of} Q_u$, where Q_o and Q_u are total (oil and water) overflow and underflow rate of the hydrocyclone.

The back-flow entering V_F is given by,

$$Q_b = \begin{cases} Q_{sep} - Q_o, & \text{if } Q_{sep} - Q_o > 0 \\ 0, & \text{otherwise} \,. \end{cases} \tag{5}$$

A block diagram representation of the model is shown in Fig. 3.

The rate of change of oil volumes can be represented in terms of oil fractions as

$$\dot{V}_{Or} = V_R \dot{\beta}_{Or} \tag{6}$$
$$\dot{V}_{Of} = V_F \dot{\beta}_{Of} \,. \tag{7}$$

For ease of analysis in state-space form (3) and (4) is written in terms of oil-fraction, as

$$\dot{\beta}_{Or} = \frac{1}{V_R}\Big(\varepsilon Q_{ino} - \beta_{Or} Q_o - Q_b)\Big) \tag{8}$$

$$\dot{\beta}_{Of} = \frac{1}{V_F}\Big(Q_{ino}(1-\varepsilon) - \beta_{Of} Q_u + Q_b)\Big)\,. \tag{9}$$

The two outlet flows are modelled using,

$$Q_u = Cv_1 z_u \sqrt{\frac{2(P_3 - P_u)}{\rho_u}} \tag{10}$$

$$Q_o = Cv_2 z_o \sqrt{\frac{2(P_2 - P_o)}{\rho_o}}\,, \tag{11}$$

where Cv_1 and Cv_2 are valve constants of the underflow and overflow valves, P_2 is the pressure at the overflow outlet, P_3 is the pressure at the underflow outlet, $z_u \in [0,1]$ and $z_o \in [0,1]$ control signals to the valves, ρ_u and ρ_o are the density of liquid at the underflow and overflow outlets, and P_o is the downstream pressure of the overflow valve, and P_u is the downstream pressure of the underflow valve. The pressure P_2 and P_3 used in this paper are calculated based on the steady state pressure-flow model given in [9]. The underflow valve is kept at fixed percentage opening (50 %). The dynamic model of a hydrocyclone represented by (8)–(11) are used for deriving the model-based controllers in Sections III and IV.

III. FEEDBACK LINEARIZATION

A mathematical model should satisfy the property of uniqueness and existence in order to solve for an initial value problem. This can be guaranteed if the model is continuous and the first derivative exists and is continuous [10, Lemma 3.2]. For the model (8)–(9), we introduce two states $\varphi = \beta_{Or}$ and $\psi = \beta_{Of}$. From (5), its is clear that the Q_b does not have a continuous derivative at $Q_b = Q_{sep} - Q_o$.

Consider a C^1 Heaviside approximation $f_2(x)$ of the form

$$f_2(x) = \begin{cases} 1 & \text{if } x > \mu \\ -\frac{2}{\mu^3}x^3 + \frac{3}{\mu^2}x^2 & \text{if } 0 \le x \le \mu \\ 0 & \text{if } x < 0 \end{cases}$$

where $\mu \neq 0$. A shifted version of this i.e., $f_2(Q_{sep} - Q_o)$ is multiplied by $Q_{sep} - Q_o$ (refer (5)) and we have

$$F(t) = (Q_{sep} - Q_o) f_2(Q_{sep} - Q_o) \approx Q_b\,. \tag{12}$$

The derivative of the function $F(t)$ is clearly continuous. We re-write the model (8)–(9) as

$$\dot{\varphi} = K_1 D_1 - K_1 Q_o \varphi - K_1 F(t) \tag{13}$$

$$\dot{\psi} = u - K_2 Q_u \psi + K_2 F(t) \tag{14}$$

$$y = \psi\,. \tag{15}$$

Here, $K_1 = \frac{1}{V_R}$, $K_2 = \frac{1}{V_F}$, $D_1 = \varepsilon Q_{ino}$, $D_2 = Q_{ino}(1-\varepsilon)$, $K_2 D_2 = u$ and state ψ is considered as the output.

Here u is considered as the virtual control input. The physical control input is the control valve opening z_o which control the flow Q_o. Later in this section we are deriving the conversion of u to z_o. The design of feedback linearizing control (FBLC) in this section is based on [10, Ch. 15].

Note that $K_1(D_1 - F(t))$ in (13) is also dependent on Q_o (recall that ε is a function of Q_o in (2)), however, to simplify the analysis, we consider it as a time-varying disturbance to this subsystem and $K_1(D_1 - F(t)) > 0$ as Q_o and Q_{ino} are the flow rates, which are strictly non-negative.

The relative degree of the system (13)–(15) is $\rho = 1$ and is well defined in $\mathbb{R}^2$. Following the nomenclature in [10], the internal dynamics of the system is given by (13) and the external dynamics of the system is given by (14) and clearly the system is in normal form. Comparing [10, equation 13.17] and (14) we have $A_c = 0$, $B_c = 1$, $\gamma(x) = 1$, and $u - \alpha(x) = u - K_2 Q_u \psi + K_2 F(t)$.

A controller $u = v + \alpha(x)$ is chosen to track the given set-point, hence a variable $\tilde{\psi} = \psi - \psi_{ref}$ is defined. The external dynamics can re-written as $\dot{\tilde{\psi}} = v$, and this external dynamics is made exponentially stable by designing a controller of the form

$$v = K_c \tilde{\psi} + K_I \int_0^t \tilde{\psi} d\tau\,, \tag{16}$$

where $K_c > 0$ and $K_I \ge 0$.

From (13), the internal dynamics φ is independent of the external dynamics ψ and the internal dynamics is analysed independently for the boundedness criteria.

Consider a Lyapunov function candidate $\mathbb{V} = \frac{1}{2}\varphi^2$. Its clear that this candidate function satisfies, $g_1(\|\varphi\|) \le \mathbb{V} \le g_2(\|\varphi\|)$, where $g_1(\|\varphi\|) = g_2(\|\varphi\|) = \frac{\varphi^2}{2}$ and belongs to class K_∞. The derivative of $\mathbb{V}$ along the trajectory of (13) is given by

$$\dot{\mathbb{V}} = \varphi K_1(D_1 - F(t)) - K_1 Q_o \varphi^2\,.$$

It is also assumed that there exists a minimum overflow such that $Q_o \ge Q_{o,min} > 0$, which can be related to the physical condition where the overflow valve is never closed fully. Hence,

$$\dot{\mathbb{V}} \le \varphi K_1(D_1 - F(t)) - K_1 Q_{o,min} \varphi^2\,.$$

To analyse the stability properties of the internal dynamics in the presence of the disturbance term $K_1(D_1 - F(t))$, we consider this term as a virtual input in the analysis. Rewriting the derivative of the Lyapunov function candidate

$$\begin{aligned}\dot{\mathbb{V}} &= \varphi U - K_1 Q_{o,min}\varphi^2 \\ &= -(1-\theta)K_1 Q_{o,min}\varphi^2 - \theta K_1 Q_{o,min}\varphi^2 + \varphi U \\ &\le -(1-\theta)K_1 Q_{o,min}\varphi^2, \forall |\varphi| \ge \frac{|U|}{\theta Q_{o,min} K_1} = g_3(|U|)\end{aligned}$$

where $0 < \theta < 1$ and g_3 is a class $\mathscr{K}$ function and $(1-\theta)K_1 Q_{o,min}\varphi^2$ is a continuous positive definite function on $\mathbb{R}$. Hence, according to [10, Theorem 4.19] system (13) is input-to-state stable with $\gamma = g_1^{-1} \circ g_2 \circ g_3$ or $\gamma(r) = \frac{r}{\theta Q_{o,min} K_1}$. From the definition of input-to-state stability [10, Definition 4.7], for any bounded input $U(t)$, the state $\varphi(t)$ is bounded. Thus, we conclude that the internal dynamics of the system (13) is uniformly bounded.

To summarise, as the system (13)–(15) has a well-defined relative degree and the feedback linearising control law u can ensure that $\tilde{\psi}(t) \to 0$ and the internal dynamics are bounded, if $\tilde{\psi}(0)$ and $\varphi(0)$ are sufficiently small and the inlet condition $K_1 D_1$ of the hydrocyclone is bounded.

The aim of the controller is to minimise the oil content in the water-rich volume V_F and thereby reducing the oil ppm at the underflow outlet. The desired oil ppm at the underflow is given as a setpoint to the controller. The overflow rate Q_o is controlled to achieve the desired oil ppm at the underflow. As mentioned earlier, the physical control input is z_o and hence, to derive a relation between z_o and the virtual control input u, we have to calculate the desired flow rate to satisfy $K_2 D_2 - u = 0$. This can be done by substituting the values of internal separation (polynomial approximation) and formulating a quadratic problem as shown below,

$$K_2 Q_{ino}(1-\varepsilon) - u = 0 \tag{17}$$
$$\implies K_2 Q_{ino}(1 - p_2 Q_o^2 - p_1 Q_o - p_0) - u = 0 \tag{18}$$
$$\implies A Q_o^2 + B Q_o + C = 0\,, \tag{19}$$

where $A = -p_2 K_2 Q_{ino}$, $B = -p_1 K_2 Q_{ino}$ and $C = Q_{ino} K_2 - p_0 Q_{ino} K_2 - u$. The positive solution of (19) is taken as the desired overflow Q_{des}.

For this desired flow rate we can calculate the percentage opening of the valve using (11) and hence,

$$z_o = \frac{Q_{des}}{C v_2 \sqrt{\frac{2(P_2 - P_o)}{\rho_o}}}\,.$$

IV. SLIDING MODEL CONTROL WITH INTEGRAL ACTION

The sliding mode controller (SMC) design discussed in this section is based on [10, Ch. 14]. Here the system is augmented with an integral state, the integral of the regulation error $y - y_{ref}$ and a feedback controller is designed to stabilise the augmented system at the equilibrium point. The normal form of the system (13)–(14), derived in Section III is used for the design of the SMC.

Augmenting the system with an integrator gives

$$\begin{aligned}\dot{\varphi} &= K_1 D_1 - K_1 Q_o \varphi - K_1 F(t)\\ \dot{e}_0 &= e_1\\ \dot{e}_1 &= u - K_2 Q_u \psi + K_2 F(t)\,,\end{aligned}$$

where $e_1 = \dot{e}_o = y - y_{ref}$, which will be used for the integral term.

A sliding surface of the form $s = k_0 e_0 + e_1$, where $k_0 < 0$ is chosen. The derivative of the sliding surface is given as

$$\dot{s} = k_0 e_1 + u - K_2 Q_u \psi + K_2 F(t)\,.$$

Next step is to choose a controller u of the form

$$\begin{aligned}u &= -(k_0 e_1 - K_2 Q_u \psi + K_2 F(t)) + w\\ \dot{s} &= w\,.\end{aligned}$$

In general $w = -\beta_0 \mathrm{sat}(\frac{s}{\vartheta})$, where $\beta_0 > 0$ is a constant and ϑ is a positive constant such that $1/\vartheta$ is slope of the linear portion of the saturation $\mathrm{sat}(s/\vartheta)$.

Rewriting the system in terms of the sliding surface,

$$\dot{\varphi} = K_1 D_1 - K_1 Q_o \varphi - K_1 F(t) \tag{20}$$
$$\dot{e}_0 = -k_0 e_0 + s \tag{21}$$
$$\dot{s} = -\beta_0 \mathrm{sat}(\frac{s}{\vartheta})\,. \tag{22}$$

We consider a Lyapunov function candidate $\mathrm{V}_1 = \frac{1}{2}s^2$, for analysing the reaching phase of the sliding mode controller,

$$\begin{aligned}\dot{\mathrm{V}}_1 &= s(-\beta_0 \mathrm{sat}(\frac{s}{\vartheta}))\\ &\leq -\beta_0 |s| \quad, \forall |s| \geq \vartheta\,.\end{aligned}$$

Therefore, whenever $|s(0)| > \vartheta$, $|s(t)|$ will be strictly decreasing, until it reaches the set $\{|s| \leq \vartheta\}$ in finite time and remains inside thereafter. Now for analysing the sliding phase, another Lyapunov candidate function is taken $\mathrm{V}_2 = \frac{1}{2}e_0^2$,

$$\begin{aligned}\dot{\mathrm{V}}_2 &= -k_0 e_0^2 + e_0 s\\ &\leq -k_0 e_0^2 + |e_0|\,\vartheta\\ &\leq -(1-\theta_1) k_0 e_0^2,\ \forall |e_o| \geq \frac{\vartheta}{k_0 \theta_1}\,,\end{aligned}$$

where $0 < \theta_1 < 1$. Thus the trajectory converges to the set $\Omega_\vartheta = \{|e_o| \leq \frac{\vartheta}{k_0 \theta_1}, |s| \leq \vartheta\}$. The dynamics described by (20) does not contain e_o and hence it cannot be influenced by the sliding surface. It is similar to the internal dynamics in the feedback linearization control and same arguments discussed in Section III applies for (20) and the solutions are bounded as the system is input-to-state stable.

V. SIMULATION AND RESULTS

Simulation results are used for studying the effectiveness of nonlinear control algorithms (designed in Sections III and IV) for hydrocyclones. The control objective is to keep the oil fraction of the underflow outlet of a hydrocyclone at 30 ppm (OSPAR criteria). During the simulation, the inlet pressure P_1 is kept at 6 bar and other model parameters used in the simulation are given in Table I. Here, the hydrocyclone liner considered is Colman and Thew type [4]. We assume that we can measure oil fraction at the underflow (e.g [11]). Also, the results from [12] are promising in terms of using the oil-in-water sensor for control purposes. As a baseline for non-linear control, we choose the feedback linearization algorithm because of its good performance under ideal conditions. The sliding mode controller is a good option to compare against the base-line controller as it is robust to modelling uncertainties. Optimised tuning of non-linear controllers could change their performance. Hence, the result discussed further in this section is part of a preliminary study and it is to understand the behaviour of the hydrocyclone model to non-linear controllers.

In the first case study we analyse the system without considering measurement noise or model errors. The first external disturbance (a step change from 1000 ppm to 1500 ppm of inlet oil fraction β_{in}) is introduced to the plant at 20 s. The second disturbance is introduced at 60 s where the underflow opening is increased from 50 % to 57 %. The

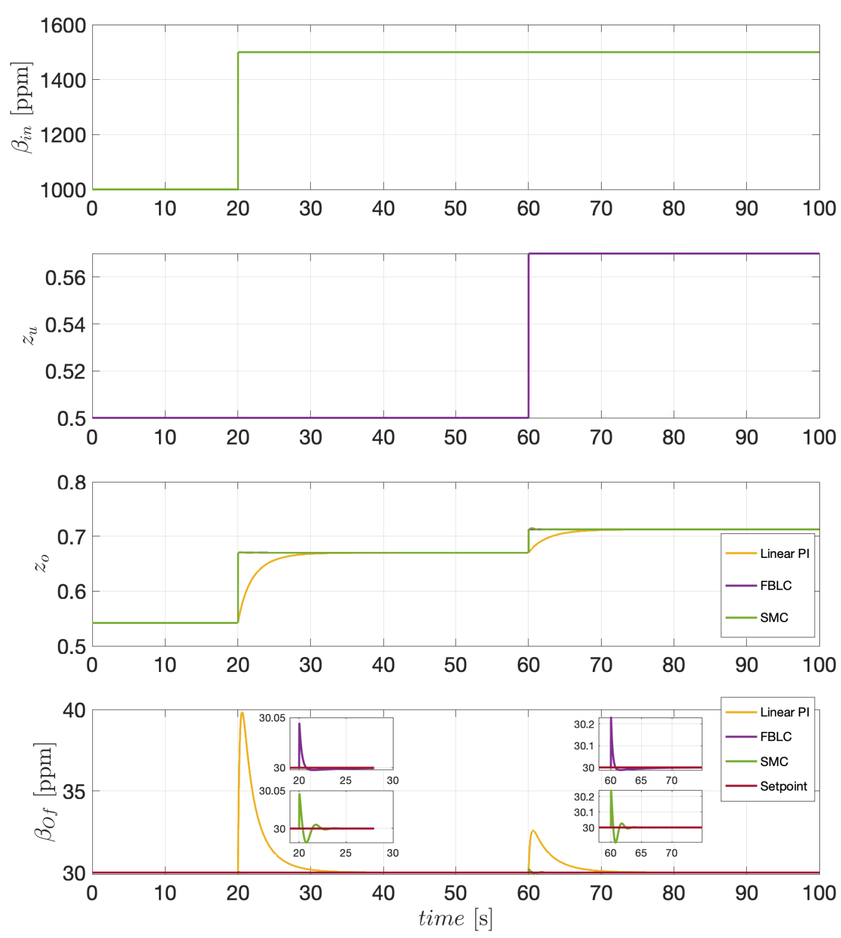

Fig. 4. Simulation result showing the response of a feedback linearization controller, a sliding mode controller and a linear PI controller subjected to plant disturbance.

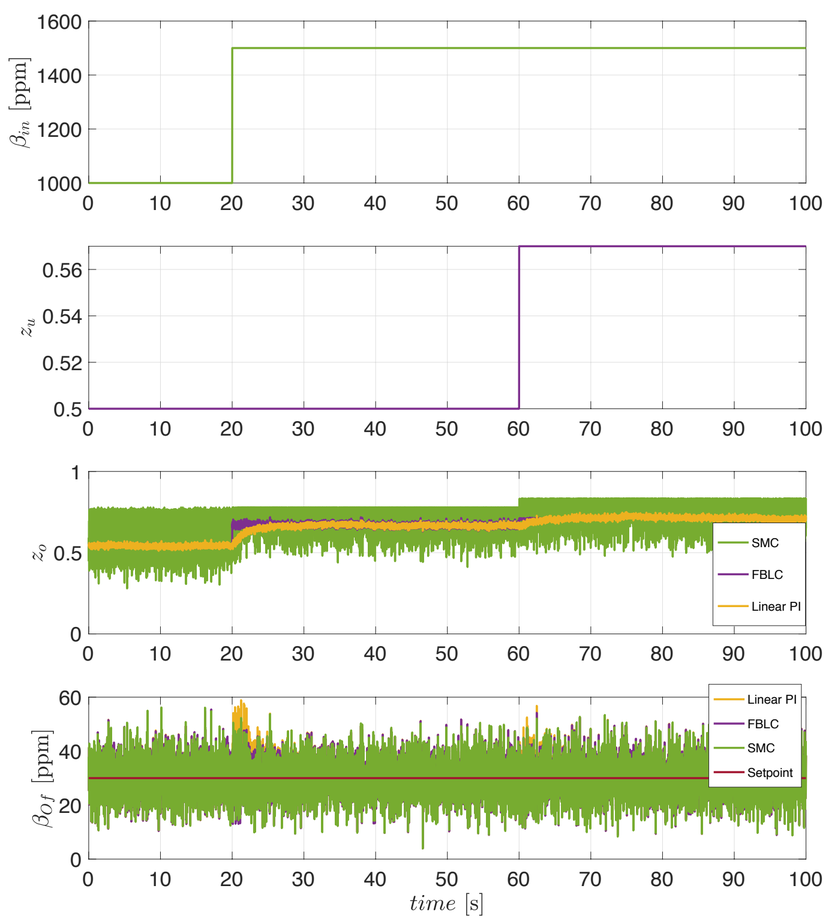

Fig. 5. Simulation result showing the response of a feedback linearization controller, a sliding mode controller and a linear PI controller with measurement noise of 5 %.

response of a feedback linearization controller ($K_c = 4$, $K_I = 1$), a sliding mode controller ($k_o = -2$, $\beta_o = 1$, $\vartheta = 0.1$) and a linear PI controller ($P = -13.96$, $I = -49.865$ [13]) were simulated. All the three controllers tracked the desired setpoint of 30 ppm even in the presence of plant disturbances. As expected, the linear PI controller was not efficient in handling the transients. The root mean square error (RMSE) values (given in Table II) indicate that feedback linearization controller had the best performance and the linear PI controller had the worst. The simulation results are shown in Fig. 4. The values of the inlet oil fraction β_{in}, the percentage opening of the underflow valve z_u, the physical control output z_o and the oil fraction at the underflow β_{Of} are shown in the simulation results.

In the second case study we analyse the system with measurement noise and without any modelling errors. All the tuning parameters for the controllers remain the same as in the first case study. We use 5 % multiplicative Gaussian white noise on β_{Of} throughout the simulation. The simulation results are shown in Fig. 5. Two external disturbances similar to the first case study are introduced to the plant during the simulation to test the performance and robustness of the controllers. All three controllers managed to keep the controlled variable within the limits during the external disturbances. The RMSE for the three controllers are given in Table II. The feedback linearizing controller shows slightly better performance than sliding mode controller.

In the third case study we analyse the system with measurement noise and modelling errors. We introduce an error in the plant model (8) and (9) by increasing the model parameter $K_2 = 6K_2$. The simulation results are shown in Fig. 6. The external disturbances introduced are similar to the first and the second case studies. The sliding mode controller and the linear PI controller keep the controlled variable within the limits during the external disturbances. A small box included inside the β_{Of} shows the same simulation done without measurement noise. This figure indicates that the feedback linearization controller is not able to track the setpoint and has a bias in the output. However, the sliding mode controller and the linear PI track the setpoint asymptotically even in the presence of external disturbances. The RMSE values in Table II indicated that the sliding mode controller has the best performance. It can also be noted that the linear PI controller has better performance than the feedback linearizing controller.

In the fourth case study, we consider a random disturbance to the underflow valve opening (this emulates slugging behaviour in a tank separator upstream of a hydrocyclone.) at 20 s. The inlet oil concentration is kept at 1000 ppm. The simulation results are shown in Fig. 7 and all the three controllers managed to keep the controlled variable within the reasonable limits during the random changes in the underflow valve opening.

VI. CONCLUSIONS

This paper gives a state-space representation of a dynamic mass-balance model of a hydrocyclone. Later, this representation of the model is utilised for deriving two model-based nonlinear control algorithms. A feedback linearizing controller and a sliding mode controller are derived in this paper. The response of the two derived nonlinear control

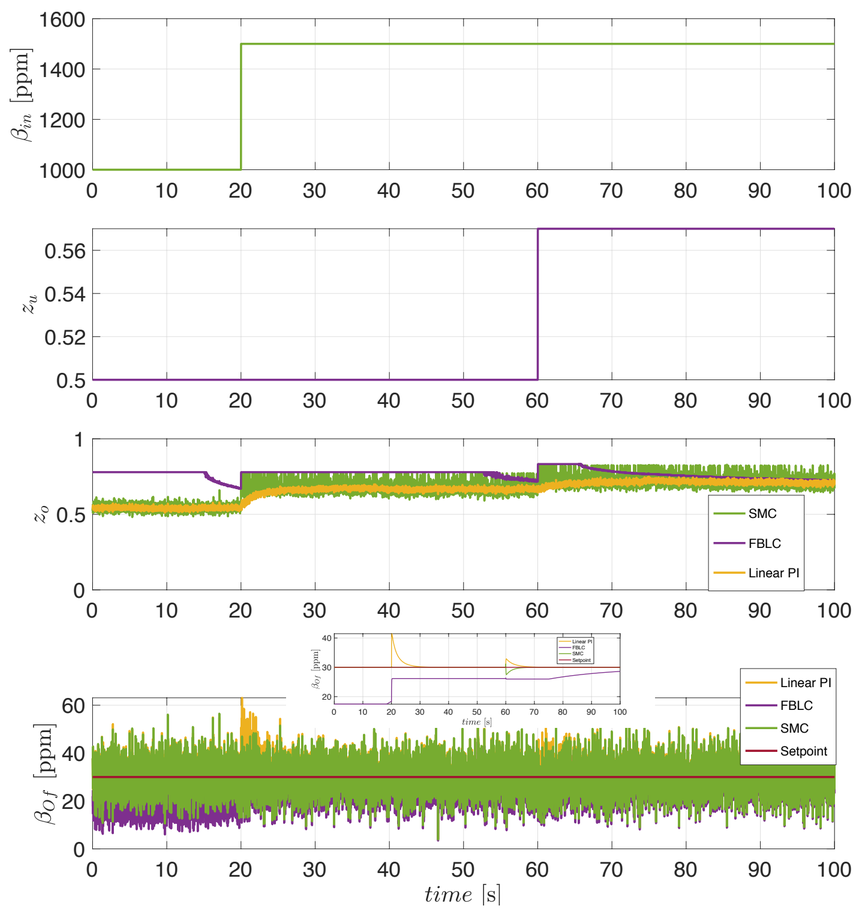

Fig. 6. Simulation result showing the response of a feedback linearization controller, a sliding mode controller and a linear PI controller with measurement noise of 5 % and modelling error.

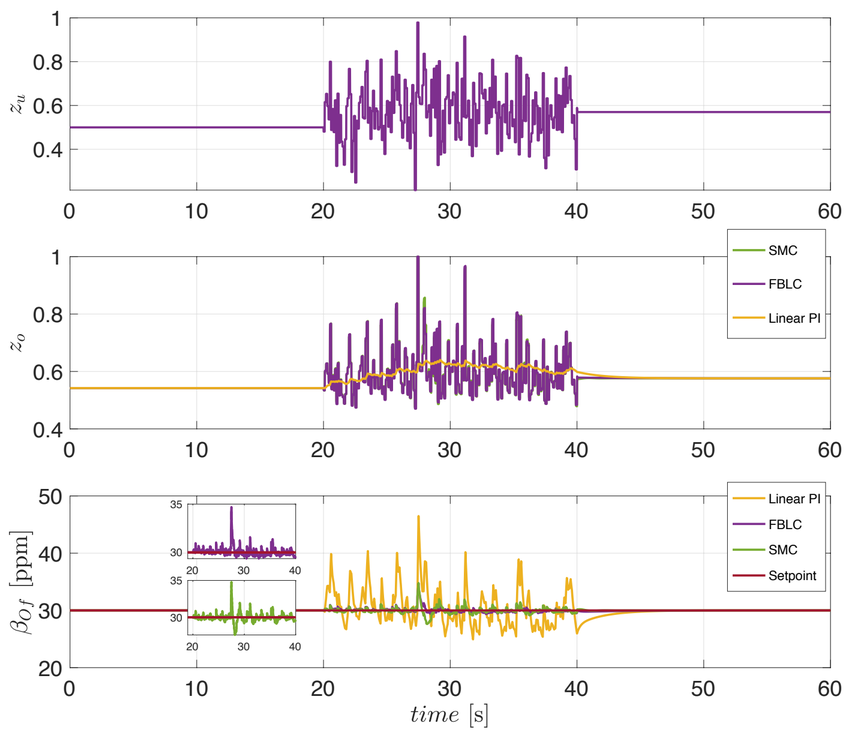

Fig. 7. Simulation result showing the response of a feedback linearization controller, a sliding mode controller and a linear PI controller when random changes are introduced to the underflow valve emulating slugging behaviour.

algorithms and a simple linear PI controller is studied. The simulation results show that all three control algorithms have good performance in the presence of disturbances without considering measurement noise and modelling errors. In the presence of measurement noise, the feedback linearizing controller has better performance than the other two controllers. Further, introducing modelling errors, the feedback linearizing controller fails to track the setpoint in the presence of external plant disturbances. The sliding mode controller and the linear PI controller are robust to the presence of modelling errors.

TABLE I

PARAMETERS USED FOR SIMULATION

Parameter	Value	Unit
$P_u = P_o$	1.01325	bar
ρ_o	910	kg/m^3
ρ_u	1000	kg/m^3
V_{HC}	$2.0896\text{E}-4$	m^3
V_R	$2.00071\text{E}-6$	m^3
Cv_1	$5.0671\text{E}-5$	m^2
Cv_2	$2.5335\text{E}-6$	m^2
μ	0.001	-

TABLE II

RMSE VALUE ($\beta_{Of} - Set point$)

RMSE Value ppm	Linear PI	FBLC	SMC
Case 1	1.2540	0.0088	0.0114
Case 2	6.9652	6.7543	6.8325
Case 3	6.9741	8.4482	6.7629
Case 4	2.027	0.3770	0.3038

Future work is to validate the state-space model of hydrocyclone using experimental data and also investigate more robust controllers like gain scheduling or H_∞ algorithms. The state-space model presented in this paper can be used to develop state estimators and the estimator model for the oil fraction could be a replacement for expensive oil-in-water sensors.

ACKNOWLEDGMENTS

This project is supported by the Norwegian Research Council, industrial partners and NTNU under the Subsea Production and Processing (SUBPRO) SFI program.

REFERENCES

[1] [Online]. Available: https://www.ospar.org/work-areas/oic
[2] M. Thew, "Hydrocyclone redesign for liquid-liquid separation." *Chemical Engineering Journal*, pp. 17–19, 21, 23, 07 1986.
[3] N. Meldrum *et al.*, "Hydrocyclones: A solution to produced water treatment," in *Offshore Technology Conference*. Offshore Technology Conference, 1987.
[4] D. Wolbert, B.-F. Ma, Y. Aurelle, and J. Seureau, "Efficiency estimation of liquid-liquid hydrocyclones using trajectory analysis," *AIChE Journal*, vol. 41, no. 6, pp. 1395–1402, 1995.
[5] C. Gomez, J. Caldentey, S. Wang, L. Gomez, R. Mohan, O. Shoham *et al.*, "Oil-water separation in liquid-liquid hydrocyclones (llhc)-experiment and modeling," in *SPE Annual Technical Conference and Exhibition*. Society of Petroleum Engineers, 2001.
[6] P. Durdevic, S. Pedersen, M. Bram, D. Hansen, A. Hassan, and Z. Yang, "Control oriented modeling of a de-oiling hydrocyclone," *IFAC-PapersOnLine*, vol. 48, no. 28, pp. 291–296, 2015.
[7] T. Das and J. Jäschke, "Modeling and control of an inline deoiling hydrocyclone," *IFAC-PapersOnLine*, vol. 51, no. 8, pp. 138–143, 2018.
[8] P. Durdevic and Z. Yang, "Application of h robust control on a scaled offshore oil and gas de-oiling facility," *Energies*, vol. 11, no. 2, p. 287, 2018.
[9] M. Vallabhan, C. Holden, and S. Skogestad, "A first principles approach for control-oriented modelling of de-oiling hydrocyclones," *Submitted to MIC*, 2020.
[10] H. K. Khalil, *Nonlinear Systems*, 3rd ed. Prentice Hall, 2002.
[11] [Online]. Available: https://mirmorax.com/oil-in-water-analyzer/
[12] P. Durdevic, C. Raju, M. Bram, D. Hansen, and Z. Yang, "Dynamic oil-in-water concentration acquisition on a pilot-scaled offshore water-oil separation facility," *Sensors*, vol. 17, no. 1, p. 124, 2017.
[13] S. Skogestad, "Simple analytic rules for model reduction and pid controller tuning," *Journal of process control*, vol. 13, no. 4, pp. 291–309, 2003.

Chapter 5

Experimental test rig for hydrocyclones

As a part of the experimental study, a text-rig consisting of industrial-scale hydrocyclones was built at the Department of Mechanical Engineering, NTNU. The rig was constructed in two phases. The first phase was the construction and commissioning of hydrocyclone skid and this was done as a part of master project [22]. The second phase was the pump system for feeding the hydrocyclone skid. This was constructed and commissioned during this PhD study. Appendix A.3 gives the P&ID of the pump system with details of the instruments and devices. Some modifications such as installation of oil-in-water analysers were made to the hydrocyclone skid during this PhD study. Appendix A.1 highlights those modifications and give the P&ID of the hydrocyclone skid.

Appendix A.2 gives date sheet of the oil-in-water sensor used in the test rig. Modbus is used for communication of the sensor values into the control system.

This chapter presents an article briefly describing the construction of the experimental rig. The flow-loop calibration of the online oil-in-water analysers done using offline Mastersizer 3000 is explained in this article. Furthermore, experiments to shows the ineffectiveness of the PDR control scheme is given in this article.

5.1 Experimental test setup for de-oiling hydrocyclones using conventional PDR control

The citation of the published article is given below:

Vallabhan K. G., Mishiga, Dudek, Marcin, and Holden, Christian. *Experimental Test Setup for Deoiling Hydrocyclones Using Conventional Pressure Drop Ratio Control.* SPE Prod & Oper (2022;): https://doi.org/10.2118/208608-PA.

The preprint version follows.

Chapter 6

Experimental results

This chapter gives the experimental results of three novel control schemes for de-oiling hydrocyclones. A cascade, a feed-forward and a direct control scheme are implemented at the test rig. The main performance criteria for the new control schemes is to maintain the oil concentration at water reject at 30 ppm.

6.1 De-oiling hydrocyclones: an experimental study of new control schemes

The citation for the published article is given below:

Vallabhan K G, Mishiga, Holden, Christian, and Skogestad, Sigurd. *Deoiling Hydrocyclones: An Experimental Study of Novel Control Schemes.* SPE Prod & Oper (2022): https://doi.org/10.2118/209576-PA.

The preprint version of the article follows.

Chapter 7

Conclusion and future work

This chapter draws an overall conclusion of this thesis work, highlighting the research questions answered during this endeavour. Some limitations of the theoretical study done in this thesis are discussed here. Furthermore, some future work which can be implemented at the test rig are also discussed here.

7.1 Conclusion

This thesis focuses on control aspects of the produced-water treatment system using hydrocyclones. Chapter 3 and Chapter 4 discussed the theoretical analysis of this research work.

Chapter 3 presented a control-oriented model for de-oiling hydrocyclones. Here, a relationship between the overflow rate and the separation inside the hydrocyclones were derived based on the droplet trajectory model. The model and its control properties were verified using a simple PID-based oil concentration controller. This model was useful in analysing the behaviour of hydrocyclones for changes in inflow rate and the inlet oil concentration. Section 4.1 discusses the drawbacks of the traditional PDR control scheme using the hydrocyclone model. Additionally, it proposes three new control schemes to mitigate the PDR control scheme's ineffectiveness: a cascade scheme, a feedforward scheme, and a model predictive controller. Section 4.2 discusses two more model-based controllers: a feedback linearization controller and a sliding mode controller. Both of the model-based controllers have similar performance in the presence of disturbances without considering modelling errors and measurement noise. However, in the presence of modelling errors, the sliding mode controller has better disturbance rejection than the feedback linearization controller.

There are some limitation on the theoretical analysis done in this thesis. The first limitation is that the proposed model requires the knowledge of the probability distribution of the oil droplets at the inlet of the hydrocyclones. In this model, the separation

is approximated using a polynomial considering a plausible droplet distribution. However, more generalised representation of separation incorporating all the possible droplet distributions needs to be developed. The second limitation is that all the model based controllers discussed in Chapter 4 assume that the oil concentration at the water reject and the oil reject can be measured, thereby making it expensive to implement.

Chapter 5 gives the details of the experimental setup constructed for the analysis and testing of new control schemes. The test-rig can emulate the first-stage gravity separator and generates disturbances at the inlet of the hydrocyclones. Chapter 5 also describes the operational procedure, details of flow loop calibration of online oil-in-water analysers, and methods used for generating disturbances in inlet oil concentration and droplet distribution. The detailed description of test procedures ensures, in principle, the reproducibilty of the results. The ineffectiveness of the PDR control schemes was also tested at the rig.

Three new control schemes: cascade, feedforward and direct oil concentration were verified at the test rig. It was noted that all three control schemes were able to meet the performance criteria of 30 ppm of oil concentration at the water-reject. Among the three control schemes, cascade control scheme has some advantages because the secondary controller provides the linearization effect and the slower primary controller makes it robust to measurement noise. The feedforward control scheme needs a static map of the inlet oil concentration, droplet distribution and the corresponding PDR to keep the oil concentration at the water reject below 30 ppm. The data required for this mapping was collected using separate experiments where PDR values were adjusted manually to bring the oil concentration at the water reject below 30 ppm for different inlet oil concentrations and droplet distributions. So, in a real-time system, these static mapping needs to be provided by the cyclone vendors based on their test data. Direct oil concentration control needs a deadband to keep prevent an oscillating response. Providing a set point much lower than 30 ppm can eliminate the need for a deadband.

To summarise the contributions of this thesis:

- A control-oriented mathematical model was developed to study the behaviour of the hydrocyclones to different disturbances and to develop new controllers.
- The drawbacks of traditional PDR control schemes was analysed theoretically and experimentally.
- New control schemes to overcome the limitations of the exiting control schemes were verified theoretically and experimentally.
- A pump and tank system module (Appendix A.3) capable of emulating the first stage gravity separator, was constructed and commissioned during this PhD study. This test setup can be used as an input system to any produced water treatment equipment.

7.2 Future work

In order to make use of the hydrocyclone model as part of a bigger system, the model needs to be validated and model parameters need to updated using real-time or experimental data. Relationships between the percentage of separated oil and the overflow rate is an important factor that needs to be validated based on the experimental data. A preliminary approximation of this is given in Appendix B.

An optimized control strategy to maximise the water removal capacity of the hydrocyclone while keeping the oil-in-water concentration at the limit prescribed by the environmental agencies is another possibility of future work. For this, the interaction of hydrocyclones with upstream separators such as a gravity separator or a pipe separator needs to be considered.

The test-setup at NTNU is also equipped with hydrocyclones in series. Appendix A.1 shows the P&ID of this experimental setup. As a future work, new control schemes proposed in this thesis can be tested for series hydrocyclones.

References

[1] Discharges to the sea, https://www.norskpetroleum.no/en/environment-and-technology/discharges-to-the-sea/. URL https://www.norskpetroleum.no/en/environment-and-technology/discharges-to-the-sea/. (accessed May 4, 2021).

[2] Invisible platforms, https://www.equinor.com/en/magazine/the-final-frontier.html. URL https://www.equinor.com/en/magazine/the-final-frontier.html. (accessed May 4, 2021).

[3] Foundation Fieldbus. URL https://www.fieldcommgroup.org/technologies/foundation-fieldbus. (accessed Sepetembet 4, 2021).

[4] HART. URL https://www.fieldcommgroup.org/technologies/hart/hart-technology. (accessed Sepetembet 4, 2021).

[5] MODBUS. URL https://modbus.org. (accessed Sepetembet 4, 2021).

[6] Ormen lange overview, https://www.shell.com/about-us/major-projects/ormen-lange/ormen-lange-overview.html. URL https://www.shell.com/about-us/major-projects/ormen-lange/ormen-lange-overview.html. (accessed May 4, 2021).

[7] PROFIBUS. URL https://www.profibus.com. (accessed Sepetembet 4, 2021).

[8] Challenges in reusing produced water, https://www.spe.org/en/industry/challenges-in-reusing-produced-water/, 2010. URL https://www.spe.org/en/industry/challenges-in-reusing-produced-water/. (accessed Apr 27, 2021).

[9] Deoiling hydrocyclones, https://eprocess-tech.com/products/oil-water-separation/deoiling-hydrocyclones/, 2021. URL https://eprocess-tech.com/products/oil-water-separation/deoiling-hydrocyclones/. (accessed Sept 4, 2021).

[10] Y. Bai and Q. Bai. *Chapter 2 - Subsea Field Development*, pages 27–62. Gulf Professional Publishing, Boston, 2010. ISBN 978-1-85617-689-7. doi: https://doi.org/10.1016/B978-1-85617-689-7.10002-0. URL https://www.sciencedirect.com/science/article/pii/B9781856176897100020.

[11] J. Beyer, T. H. Bakke, R. Lichtenthaler, and J. Klungsøyr. Environmental effects of offshore produced water discharges evaluated for the barents sea. *NIVA-rapport*, 2019.

[12] M. V. Bram, L. Hansen, D. S. Hansen, and Z. Yang. Hydrocyclone separation efficiency modeled by flow resistances and droplet trajectories. *3rd IFAC Workshop on Automatic Control in Offshore Oil and Gas Production*, 51(8):132–137, 2018.

[13] M. V. Bram, S. Jespersen, D. S. Hansen, and Z. Yang. Control-oriented modeling and experimental validation of a deoiling hydrocyclone system. *Processes*, 8(9):1010, 2020.

[14] J. Caldentey, C. Gomez, S. Wang, L. Gomez, R. Mohan, and O. Shoham. Oil/water separation in liquid/liquid hydrocyclones (llhc): Part 2-mechanistic modeling. *SPE Journal*, 7(4):362–372, 2002.

[15] O. G. Dahlhaug. A study of swirl flow in draft tubes. 1997.

[16] T. Das and J. Jäschke. Modeling and control of an inline deoiling hydrocyclone. *3rd IFAC Workshop on Automatic Control in Offshore Oil and Gas Production OOGP*, 51(8):138–143, 2018.

[17] P. Durdevic and Z. Yang. Application of h-infinity robust control on a scaled offshore oil and gas de-oiling facility. *Energies*, 11(2):287, 2018.

[18] P. Durdevic and Z. Yang. Dynamic efficiency analysis of an off-shore hydrocyclone system, subjected to a conventional pid-and robust-control-solution. *Energies*, 11 (9):2379, 2018.

[19] W. J. Georgie. Effective and holistic approach to produced water management for offshore operation. In *Offshore Technology Conference*, page 13, Houston, Texas, 2002. Offshore Technology Conference. ISBN 978-1-55563-249-6. doi: 10.4043/14286-MS. URL https://doi.org/10.4043/14286-MS.

[20] C. Gomez, J. Caldentey, S. Wang, L. Gomez, R. Mohan, and O. Shoham. Oil/water separation in liquid/liquid hydrocyclones (llhc): Part 1-experimental investigation. *Spe Journal*, 7(04):353–372, 2002.

[21] J. Hargreaves and R. Silvster. Computational fluid dynamics applied to the analysis of deoiling hydrocyclone performance. *Chemical Engineering Research and Design;(UK)*, 68(A4), 1990.

[22] M. Hellem and J. Djupvik. Completion of compact separator laboratory. Master's thesis, NTNU, 2017.

[23] T. Husveg, O. Rambeau, T. Drengstig, and T. Bilstad. Performance of a deoiling hydrocyclone during variable flow rates. *Minerals Engineering*, 20(4):368–379, 2007.

[24] E. T. Igunnu and G. Z. Chen. Produced water treatment technologies. *International Journal of Low-Carbon Technologies*, 9(3):157–177, 2012.

[25] N. Meldrum. Hydrocyclones: A solution to produced-water treatment. *SPE Production Engineering*, 3(04):669–676, 1988. doi: 10.2118/16642-PA. URL https://doi.org/10.2118/16642-PA.

[26] Mirmorax. Oil-in-water analyzer, 2020. URL https://mirmorax.com/oil-in-water-analyzer/. (accessed Sep 23, 2021).

[27] A. Motin. *Theoretical and numerical study of swirling flow separation devices for oil-water mixtures*. PhD thesis, Michigan State University, 2015.

[28] R. Orlowski, M. L. L. Euphemio, M. L. Euphemio, C. A. Andrade, F. Guedes, L. C. Tosta da Silva, R. G. Pestana, G. de Cerqueira, I. Lourenço, A. Pivari, A. Witka, H. Folhadella, L. Pacheco, S. Kronemberger, and J. Vilela. Marlim 3 phase subsea separation system - challenges and solutions for the subsea separation station to cope with process requirements. In *Offshore Technology Conference*, page 11, Houston, Texas, USA, 2012. Offshore Technology Conference. ISBN 978-1-61399-200-5. doi: 10.4043/23552-MS. URL https://doi.org/10.4043/23552-MS.

[29] OSPAR. Discharges, ospar convention https://www.ospar.org/work-areas/oic/discharges, 2001. URL https://www.ospar.org/work-areas/oic/discharges. (accessed May 4, 2021).

[30] ProAnalysis. Unique oil in water monitors, 2020. URL https://oilinwater.com. (accessed Sep 23, 2021).

[31] M. Saidi, R. Maddahian, B. Farhanieh, and H. Afshin. Modeling of flow field and separation efficiency of a deoiling hydrocyclone using large eddy simulation. *International Journal of Mineral Processing*, 112:84–93, 2012.

[32] H. S. Skjefstad and M. Stanko. Experimental performance evaluation and design optimization of a horizontal multi-pipe separator for subsea oil-water bulk separation. *Journal of Petroleum Science and Engineering*, 176:203–219, 2019.

[33] L. Svarovsky and M. Thew. *Hydrocyclones: analysis and applications*, volume 12. Springer Science & Business Media, 1992.

[34] M. Thew. Hydrocyclone redesign for liquid-liquid separation. *Chemical Engineer (London)*, (427):17–23, 1986.

[35] D. Wolbert, B.-F. Ma, Y. Aurelle, and J. Seureau. Efficiency estimation of liquid-liquid hydrocyclones using trajectory analysis. *AIChE Journal*, 41(6):1395–1402, 1995.

[36] G. Young, W. Wakley, D. Taggart, S. Andrews, and J. Worrell. Oil-water separation using hydrocyclones: An experimental search for optimum dimensions. *Journal of petroleum science and engineering*, 11(1):37–50, 1994.

Appendices

Appendix A

Experimental test setup

A.1 Hydrocyclone test skid

The hydrocyclone test-skid was build as a part of a master thesis. The details of the hardware can be found on the thesis [22]. The P&ID of the test skid is given in Figure A.1. Some modifications were made for the test skid during this thesis work. The pink markings in the P&ID shows those modifications. A bypass line with a manual valve was installed to isolate the hydrocyclone HC-100 from the other two cyclones HC-200 and HC-300. This was done for testing new control schemes with a single hydrocyclone before testing it with cyclones in series. A special cross-section arrangement was made at the inlet, the water reject outlet of HC-100 and at the water return line for installing the online oil-in-water anlayser probes. In the future, the inlet probe will be placed at the water outlet while testing the series operation of hydrocyclones and the final oil concentration after the series operation can be measured.

A.2 Oil-in-Water Analyser

The online oil-in-water analysers used in the test-setup are ultrasound- based analysers. It can give the oil concentration in mg/l and in ppm, and the Dv50 values of of oil droplets which gives a rough estimate of the droplet distribution. They can also give the number distribution of the droplets, but need data of over 20 mins for the stochastic calculation of the distribution. Figure A.2 shows an oil-in-water analyser probe placed in the flow loop. The data sheet of the probes used in this test setup is in Figure A.3.

A.3 Pump System

The pump module in the test rig is a newly constructed unit during the PhD work. The P&ID was developed by SINTEF Industry. This pump module is expected to emulate

A. Experimental test setup

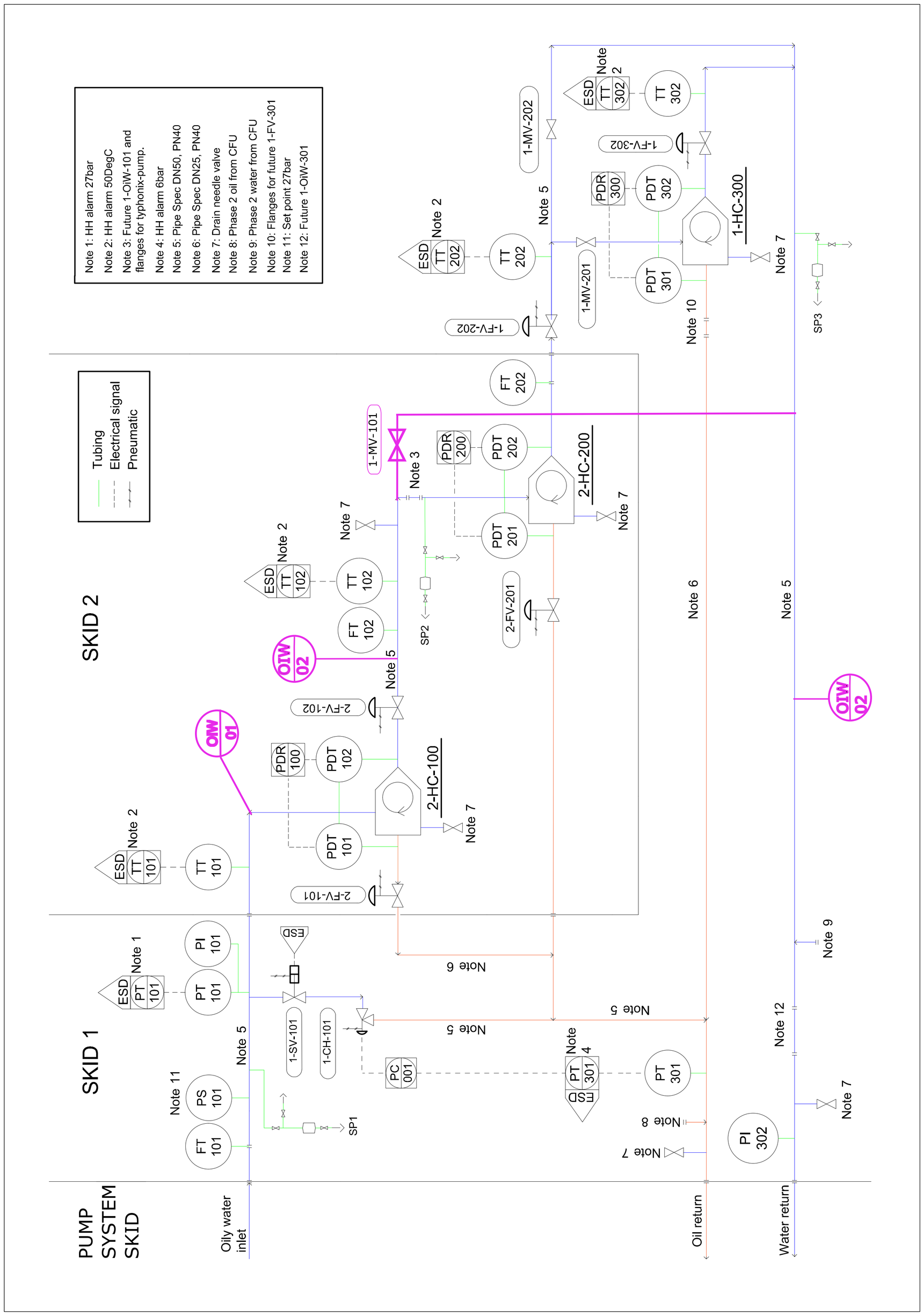

Figure A.1: P&ID for hydrocyclone test-setup.

Figure A.2: Mirmorax online oil-in-water analyser installed at the test-rig.

the first-stage gravity separator.

Figure A.4 shows the P&ID for the pump system. Here, tank 4-TX-804 stores the pure oil. This oil is directly injected into the water stream after pump 4-PA-806. The oil reject from the hydrocyclone is sent to tank 4-TX-803 and the water reject from the hydrocyclone is send to tank 4-TX-801. An auxiliary pump 4-PG-101 is used to take out the water from oil reject tank 4-TX-803 and move it to the water reject tank 4-TX-801. After removing the water from the bottom of 4-TX-803, the pure oil is pumped back to oil reservoir 4-TX-804 using auxiliary pump 4-PG-102.

Another auxiliary pump 4-PG-104 pumps back the water from the water reject tank 4-TX-801 to water reservoir 4-TX-802 and the remaining oil present in water reject tank is pumped back to oil reservoir 4-TX-804 using auxiliary pump 4-PG-103. A throttle valve 4-PV-013 is used to simulate the level control valve downstream of the first-stage separator and can be used to introduce rapid changes in the operation conditions of hydrocyclones. Also, this valve is used to adjust the oil droplet size. A pressure-limiting valve 4-PSV-025 is placed at the oil discharge line and its activated when the pressure goes above 40 bar. The oil coming out of the valve is routed back to oil reservoir 4-TX-801. Table A.1 gives the details of the instruments connected to control system. Figure

A. Experimental test setup

NORSOK	INSTRUMENT DATASHEET **Oil in Water Analyser**	MIRMORAX

Tag number	:	OIW-1070-19-PE	Process data sheet	:	NA
		OIW-1072-19-PE	Flow range (process)	:	0.5-3.5 m/s
Service description	:	Produced water line	Range	:	0 -2500 ppm (Oil & particles)
P&ID	:		Calibrated range	:	0-2500 ppm
Area	:		P.O. Number	:	N1937025

	GENERAL			Note
1	Type	:	Oil In Water Monitor	
2	Complete assembly	:	Yes	
3	Manufacturer	:	Mirmorax	
4	Manufacturer model no	:	LR2500 Titan	
	INSTRUMENTAL CHARACTERISTICS			
5	Characteristic	:	Ultrasonic measurements	
6	Accuracy	:	< 1% relative	
7	Repeatability	:	<1%	
8	Stability	:	<1%	
9	Stabilization time	:	1 sec	1
10	Adjustable range	:	0-2500 (oil & particles)	
11	Zero adjustment	:	yes	
12	Operating limits	:	0 -2500 ppm	
	PROBE			
13	Type	:	OIW ultrasound probe	
14	Manufacturer	:	Mirmorax	
15	Manufacturer model no	:	LR2500 Titan w/auto clean	2
16	Mounting	:	In-line (horizontal)	
17	Conn. size/type proc.	:	2" 150# RF Flanged	
18	Conn. size/type sign.	:	See electrical data	
19	Conn. size/type aux.	:	See hook-up dwg	
20	Rating	:	20 bar (Test Pressure 30 bar)	
21	Sour service spec.	:	MR0175 / ISO15156	
22	Material body	:	Titan gr. 2	
23	Material stab	:	SS316	
24	Wetted parts	:	Titan gr. 2	
25	Material 2" flange	:	Duplex	
26	Material conn. lines	:	NA	
27	Protective coating	:	Xylan coating	
28	Ex. Classification probe	:	II 2 G Ex d IIB T4 Gb	
29	Weight probe	:	19 kg	
	ELEMENT			
30	Type	:	Ultrasonic transducer	
31	Dimension	:	50 mm	
32	Material, element	:	PEI, Titanium gr.2	

	Field Unit		
33	Mounting	:	Vertical
34	Dimension	:	406x587x255
35	Material	:	SS316
36	Enclosure protection	:	IP66
37	Hazardous area	:	Zone 1
38	Ex. Classification	:	Ex db IIB T5 Gb
39	Signal gland type/size	:	M20
40	Power gland type/size	:	M20
41	Protective coating	:	NA
42	Local LCD display	:	NA
43	Auto Clean Syst. mod.	:	NA
44	ACS pump	:	NA
45	ACS acc. Vol./ set P	:	NA
46	ACS PSV cal. 2.5 bar	:	NA
47	ACS heater	:	NA
48	Weight enclosure	:	70 kg
	ELECTRICAL DATA		
49	Function	:	On line
50	Output signal	:	RS485 Modbus RTU
51	Output action	:	Continous
52	Supply voltage	:	230 VAC
53	Consumtion	:	36W (50W start-up)
54	Load limitation	:	min. 0.25A
	MISCELLANIOUS		
55	Max distance between probe and Field Unit, 6 mtr		
56	Operational temp.	:	0 - 90 °C
57	Ambient temp.	:	-20 to 40 °C
58	Particle size oil	:	2 - 70 µM
59	Particle size sand	:	2 - 60 µM
60	Flow regime	:	Turbulent, Reynolds no > 5000
61	Water salinity	:	0 - 350 g/l NaCl
62	Output	:	Oil & particle concentration Mean particle size, D50 Oil and particle size distribution Salinity and Temperature

NOTES

1. 1 min. stabilization after power on,
   thereafter measurements every 1 second

Rev	Date	Issue/description	Prepared	Checked	Approved	Datasheet no	Page
1	28.08.2019	Re-Issued for approval	ECB	EG	OV		
0	11.06.2019	Issued for approval	ECB	EG	OV	MAX-TD-7044-03209	

Figure A.3: OIW Datasheet.

A.5 shows a picture of the pump system installed at the test-rig and Figure A.6 shows a picture of the entire experimental rig.

Table A.1: Tag name and description of the IOs in the pump module.

Field Tag	System Tag	Description	Type of IO	Min	Max	Unit
3-PG-806	-	Water pump	-	-		
-	3-SX-101	Motor speed-water pump	AI	0	2900	RPM
-	3-XU-101	Motor start-water pump	DO	0	1	–
3-PG-805	-	Oil pump	-	-	-	
-	3-SX-101	Motor speed-oil pump	AI	0	2900	RPM
-	3-XU-101	Motor start-oil pump	DO	0	1	RPM
4-PV-013	3-FV-101	Flow control valve	AO	0	100	%
PT-101	3-PT-101	Water pump discharge pressure	AI	0	70	bar
PT-201	3-PT-102	Oil pump discharge pressure	AI	0	70	bar
PT-301	4-PT-101	Oil reservoir pressure	AI	0	10	bar
PT-401	4-PT-102	Water reservoir pressure	AI	0	10	bar
FT-201	3-FT-102	Oil flow rate	AI	0	5	l /min

A. Experimental test setup

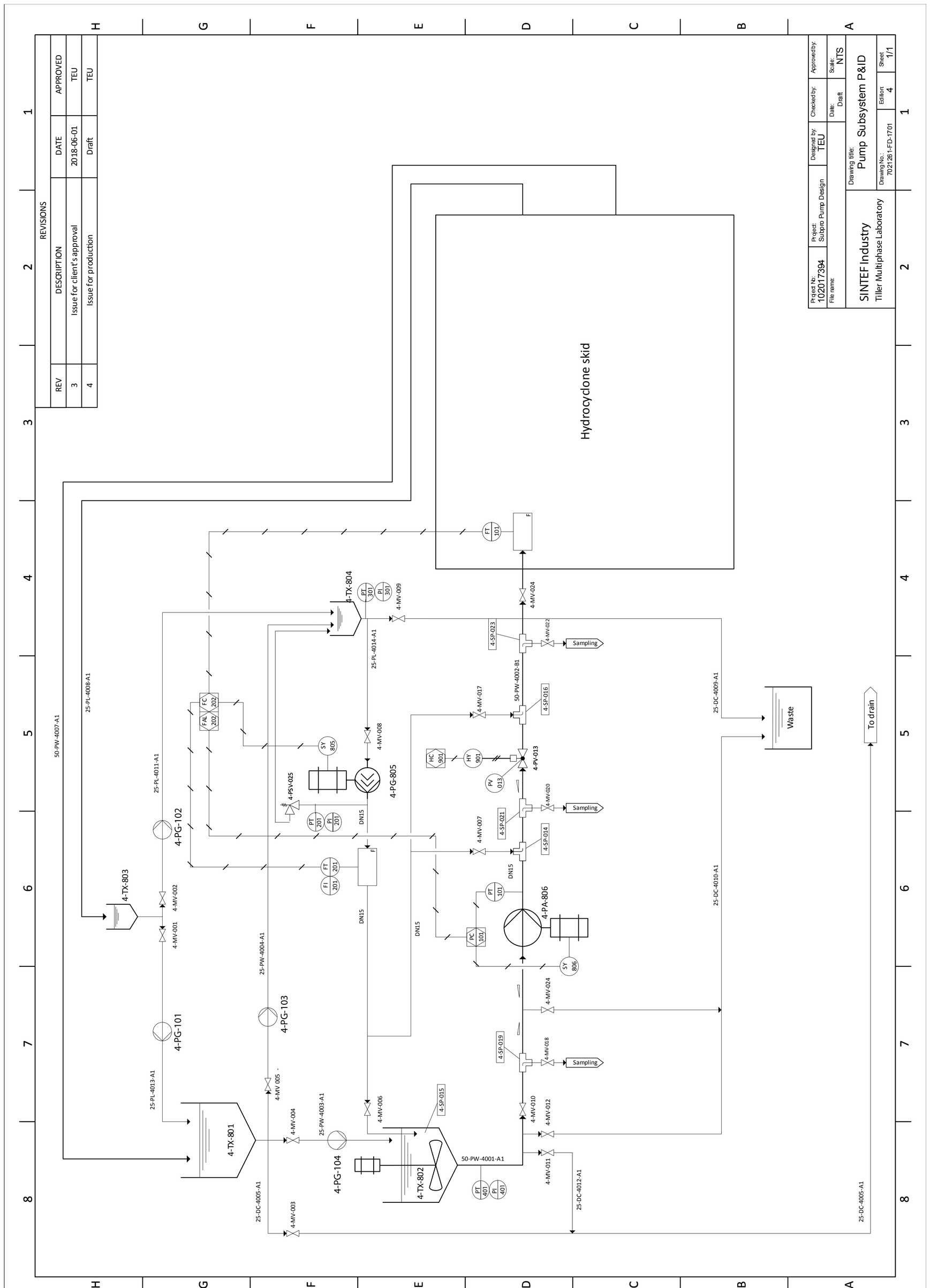

Figure A.4: P&ID for pump system.

Figure A.5: A picture of the pump system installed at the test-rig.

A. Experimental test setup

Figure A.6: A picture of the entire experimental setup.

Appendix B

Preliminary data for internal separation

This section gives a preliminary analysis that can be used to find the relationship between the internal separation and the overflow rate using experimental data. In Chapter 3, we expressed internal separation in terms of the ratio of volumetric flows as $\frac{Q_{sep}}{Q_{in,o}}$. Here, Q_{sep} is the volumetric flow of the separated oil which comes out of the oil reject and $Q_{in,o}$ is the volumetric flow of the oil coming into the hydrocyclone. In the mathematical model, the relationship between internal separation and the overflow rate was derived based on the droplet trajectory analysis.

Another way to get this relationship is to get data points from experiments. The combination of three disturbances (inflow rate, inlet oil concentration and droplet distribution) needs to be considered while generating the data points. An example, we fix the inflow rate to $3.9\,\mathrm{m}^3/\mathrm{h}$ and the inlet oil concentration to $300\,\mathrm{ppm}$ and take three plausible droplet distributions at our test-rig which corresponds to Dv50$= 11 \pm 1.5$ μm, Dv50$= 8.6 \pm 1.5$ μm and Dv50$= 6.81 \pm 1.5$ μm, then vary the overflow rate by changing the position of the oil reject valve and calculate the internal separation by measuring oil concentration at the inlet and the water reject. Figure B.1 shows the data points generated in this experiment.

More data points need to generated by varying inflow rate and inlet oil concentration independently. Then, combining all these data points a suitable data-driven model can be generated for calculating the internal separation.

B. *Preliminary data for internal separation*

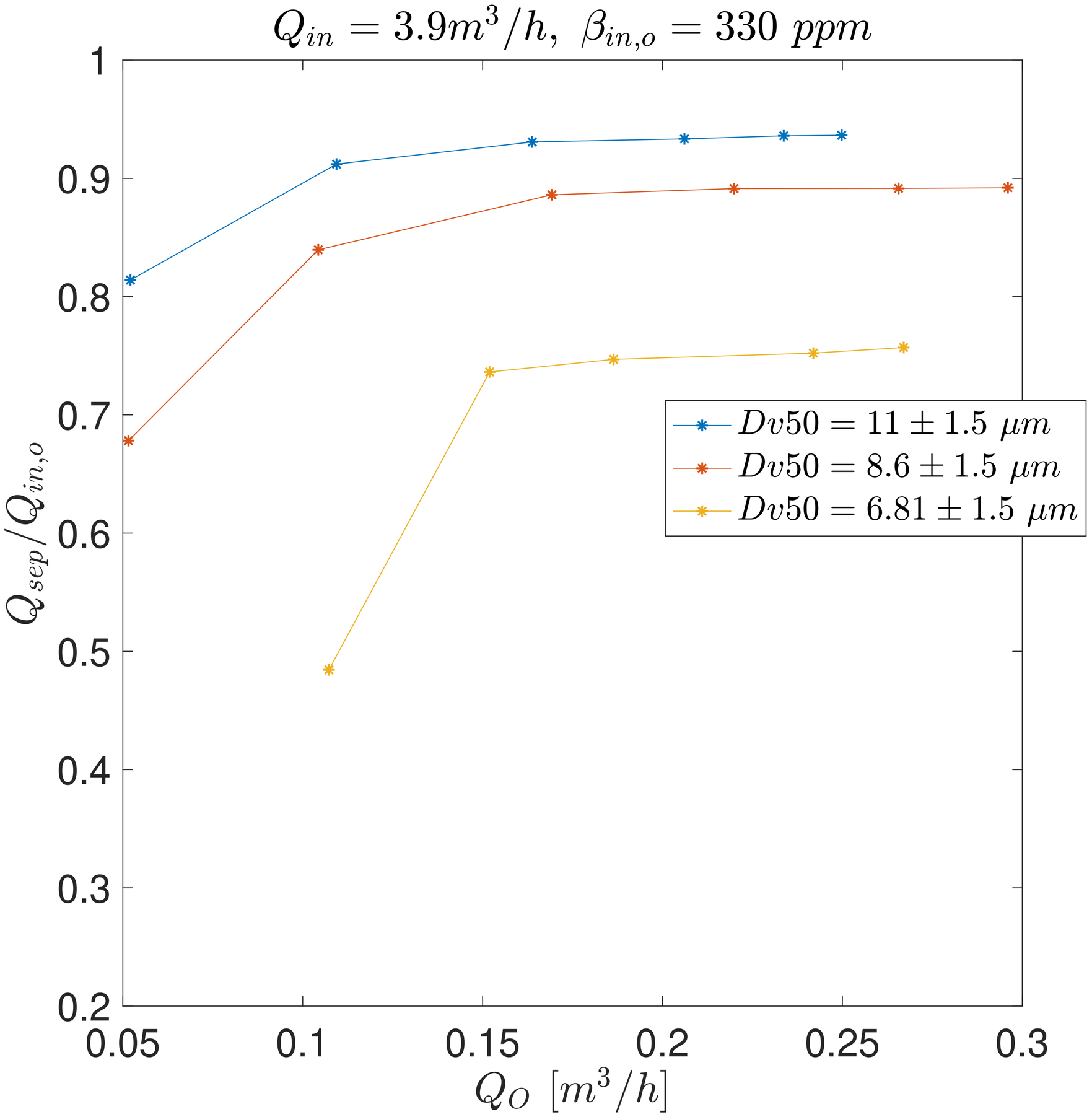

Figure B.1: Data points showing the relationship between internal separation and over-flow rate.

Appendix C

Process control and automation

This section explains the practical implementation of a process control system and individual function blocks. Later, a control loop associated with a de-oiling hydrocyclone, is taken as an example, and its practical implementation at our laboratory is described. Figure C.1 shows the basic block diagram representation of a process control loop.

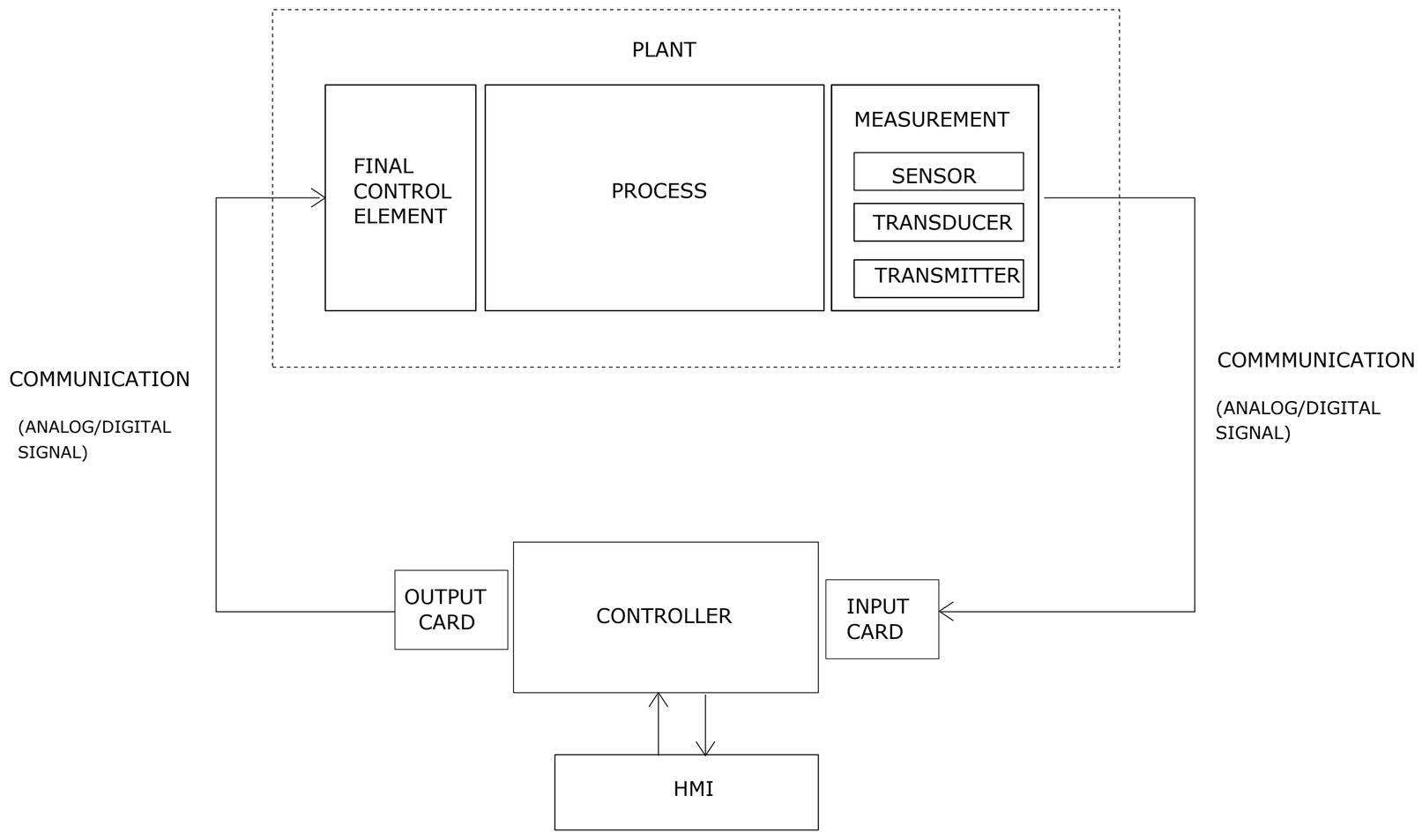

Figure C.1: Block diagram representation of a process control system.

The definition of each block follows

- The *process* can be an entire process plant, or part of a process plant that needs some control action. For example, it can refer to flow control in a pipe section, or complete control of the distillation column.

- The *measurement* block has three components: the first, a sensing element, where the physical variable in a process such as pressure or flow is initially sensed. The second, a transducer, which converts the sensed physical signal into an analog or digital electrical information. The third, a transmitter, which amplifies and puts signals into a format, signals suitable for transmission over long distances with zero or minimal information loss.

- The *final control element* is a physical device that carries out the decision made by the controller. For example, a pump's variable speed drive adjusts the pump speed according to the control signal received from the controller. A pneumatic control valve controlling the flow through a pipe is another example of a final control element. The electrical signal from the controller is given to I/P (current to pressure) converter, which adjusts the pressure, to open or close the valve, according to the control signal.

- The process, measurement and final control element are together called the *plant*.

- *Analog communication*: The electrical information is transmitted either as a current signal which is in the range of 4 mA to 20 mA or a voltage signal which is in the range of 0 V to 10 V. Electrical signals are transmitted through a multi-core cable, where each pair of wires carry one sensor's signal. Then the analog to digital (ADC) converters at the controller end converts this analog information to a digital form used in control algorithms. One of the main disadvantages of electrical communication is the extensive use of wires, as each sensor uses a pair of wires.

- *Digital communication*: In digital communication, a network forms the base of transmission. Commonly used network configurations are star, ring and bus. There are many digital communication protocols available in the market. All these protocols are based on the OSI model, which standardises these protocols and makes them inter operable. These types of digital communications are commonly referred to as *fieldbus*. Some of the commonly used Fieldbus protocols are MODBUS [5], FOUNDATION Fieldbus [3] and Profibus [7]. Wireless communication of sensor signals is an upcoming technology in the industry. A popular wireless communication protocol is wireless HART [4].

- The *Controller* represents the part of a process control where a decision is made based on the measured signals. Physically, industrial controllers are microprocessor-based hardware units, where control algorithms written in IEC61131 are downloaded using dedicated software. A standard PC can also act as a controller, where control algorithms are implemented in a programming environment such as LABVIEW. Error detection is also a part of the controller, which checks the deviation of the measured signal from the reference value (setpoint) and takes control action accordingly.

Data acquisition cards are auxiliary parts of the controllers, where the measured variables, in the form of analog or digital signals, are received. They are also used to send out control signals to the final control element from the controller. These input/output cards have many channels, enabling them to handle multiple transmitters and final control elements simultaneously. The human-machine interface (HMI) enables the operators to give setpoints to the controllers, monitor various process values, alarms, and events occurring during the operation.

Consider the flow-split control loop of a de-oiling hydrocyclone in Figure 2.8. A physical implementation of this control loop can be explained using the functional blocks shown in Figure C.1. Figure C.2 marks the different elements of a process control system for flow-split control, and their implementation at our test rig. Definitions of each process-control system with respect to flow-split control is as follows:

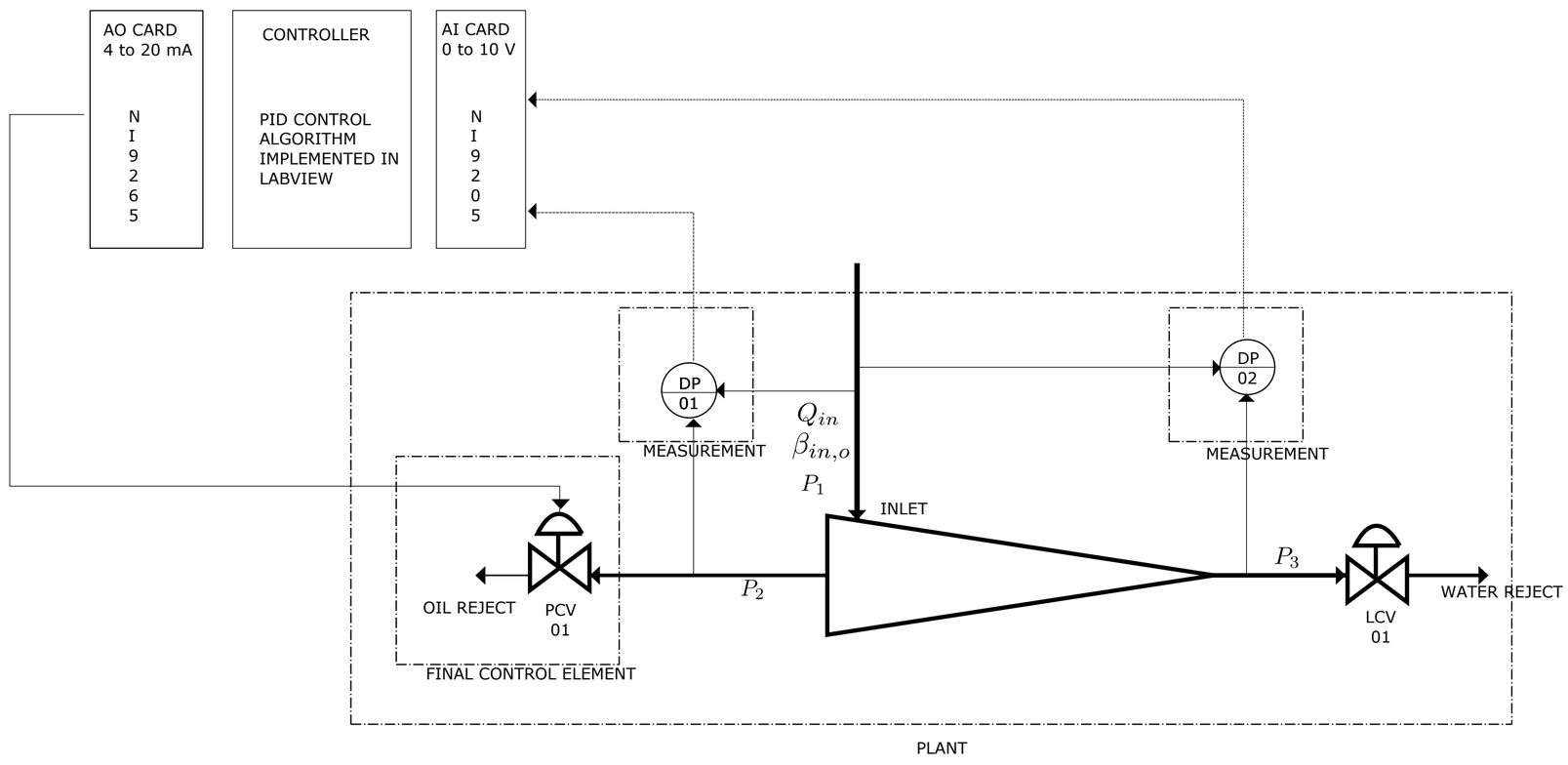

Figure C.2: Process control functional blocks in flow split control.

- The *process* here is the oil-water separation inside the de-oiling hydrocyclone. The pressure drop ratio across the inlet to oil-reject and inlet to water-reject is controlled to maintain the separation.
- *Measurement*: Here pressure drop across the inlet and the two outlets are measured using two differential pressure transmitters DP01 and DP01. The initial sensing element of this transmitter is a piezoresistive diaphragm. Change in pressure is reflected as a change in resistance (transducer), which is further converted to a 4 to 20 mA analog signal.
- *Final control element*: Here, the pressure control valve PCV01 is the final control element of the flow split control system. PCV01 is a pneumatic valve with a current to pressure converter (I/P). The I/P gives the correct pressure signal to the valve's actuator, corresponding to the control signal from the controller.

- *Communication*: Analog signals of 4 to 20 mA is used as communication signal between the transmitter to controller, and also from controller to final control element
- *Controller and I/O cards*: Here we use an NI9205 from National Instruments as an input card. The card is a 32-channel single-ended/16-channel differential analog input module with input range ± 200 mV to 10 V. The 4 to 20 mA signal from the transmitters DP01 and DP02 are converted to voltage signals using 500 Ω resistor circuits. NI9265 is a 4 channel analog output module with output range 0 to 20 mA. The control signal from the controller is converted into a mA signal in the software, and sent to the card. The controller here is normal PC, and the control algorithms are implemented using LABVIEW. The communication between the controller and the cards is through Ethernet and a compactDAQ NI9188 Ethernet chassis.

ISBN 978-82-326-6495-5 (printed ver.)
ISBN 978-82-326-6670-6 (electronic ver.)
ISSN 1503-8181 (printed ver.)
ISSN 2703-8084 (online ver.)

NTNU
Norwegian University of
Science and Technology